INDUSTRIAL NUCLEONICS CORPORATION

Federal Systems Division
Columbus, Ohio

FINAL REPORT

13 April, 1967

to

NATIONAL AERONAUTICS AND SPACE ADMINISTRATION

George C. Marshall Space Flight Center
Huntsville, Alabama

on

"Performance of Studies to Determine the Feasibility of Various Techniques for Measuring Propellant Mass Aboard Orbiting Space Vehicle"

Contract No. NAS8-21014

TABLE OF CONTENTS

LIST OF ILLUSTRATIONS

FORWARD

There have been a number of nucleonic studies made on mass propellant measurements in which it was implied that a suggested source-detector configuration would provide measurement accuracies of the order of one per cent of full tank capacity. In some cases, experimental tests have been run with tanks with different fill levels and different orientations. The bulk of these studies to date have not supplied sufficient analytical and/or experimental data to permit the optimization of a design to meet a desired accuracy nor have they given sufficient confidence data on the accuracy predicated.

The study described herein summarizing data from 200,000 cases removes the objections heretofore made and provides:

(a) Design specifications for source-detector configurations for accuracies up to 2% for liquid hydrogen tanks ranging in length from 8 to 60 feet.

(b) Confidence limits on each configuration presented and permits the customer to choose the simplest configuration which will meet his accuracy needs.

(c) An analytical and experimental method which may be used in ground simulation tests. These ground tests permit the development of an acceptable low g mass propellant testing system which may be tested both analytically and experimentally under full g ground conditions, thus removing the need for huge space costs for this development. Scaled down or full-size

tanks can be implemented. The full-size tanks would need to be filled with LH_2. Water can be used in the scaled down tanks. Foam for voids can be used in both cases. The analytical and experimental approach taken is not restricted to nucleonic measuring techniques but may also be used on R. F. techniques.

(d) An approach which with further study would permit X-ray sources to supplant the nuclear sources for tanks whose lengths do not exceed 25 feet.

(e) Line sensing techniques which may be used in either hydrogen or oxygen for any size tank. The techniques do have the disadvantage that they require the incorporation of internal structures within the fuel tanks.

The value of this report lies in:

(a) Its approach to the solution of a space need. The approach has combined basic principles from the realms of basic nuclear laws in the interaction between radiation and matter, similitude (not just scaling), energy discrimination and detection, statistical weighting and information processing. Full use of computer techniques were made to optimize each configuration, thus reducing experimental efforts to the role of confirmation of predicted results.

(b) Quantitative results on what can be done.

1.0 INTRODUCTION

1.1 Work Statement

The following requirements, as established by the contract work statement, have been met:

A. The tank configuration shown in Figure 1 shall be simulated in the feasibility study. The size of the tank will range from a length (L) of 60 ft. to 8 ft. The ratio of length to radius (L/R) will be 4 for all tank sizes.

The propellants to be considered are liquid oxygen and liquid hydrogen.

B. The study shall consist of the following tasks.

1. Determine which radiation techniques are feasible for measuring the mass of LOX and LH_2 in the tank size range shown in Figure 2. (The shadow techniques discussed in Section 3.2.1 and 4.2 are applicable to oxygen tanks of arbitrary size; in addition to the shadow techniques, the gamma transmission technique discussed in Sections 3.1.1 and 4.1 is applicable to hydrogen tanks up to 60 feet in length.)
2. Determine the scaling laws and scaling limitations for each technique. (The scaling laws and limitations with respect to experimental systems are discussed in Section 3.1.1.4.)

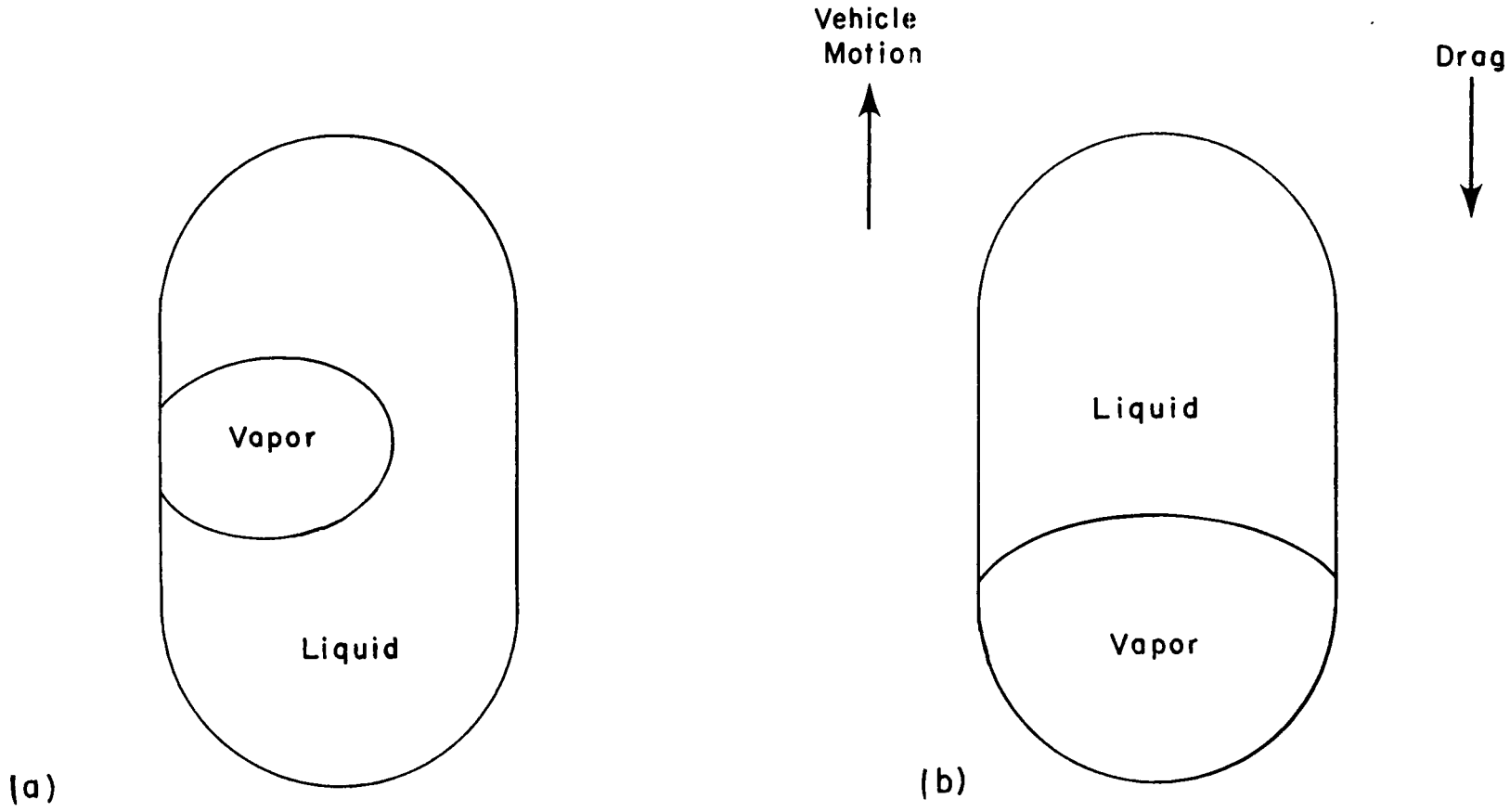

Steady State Propellant Location for a) Planetary Coast (Zero Gravity), b) 100 NM Orbit (Low to High Gravity).

Figure 1

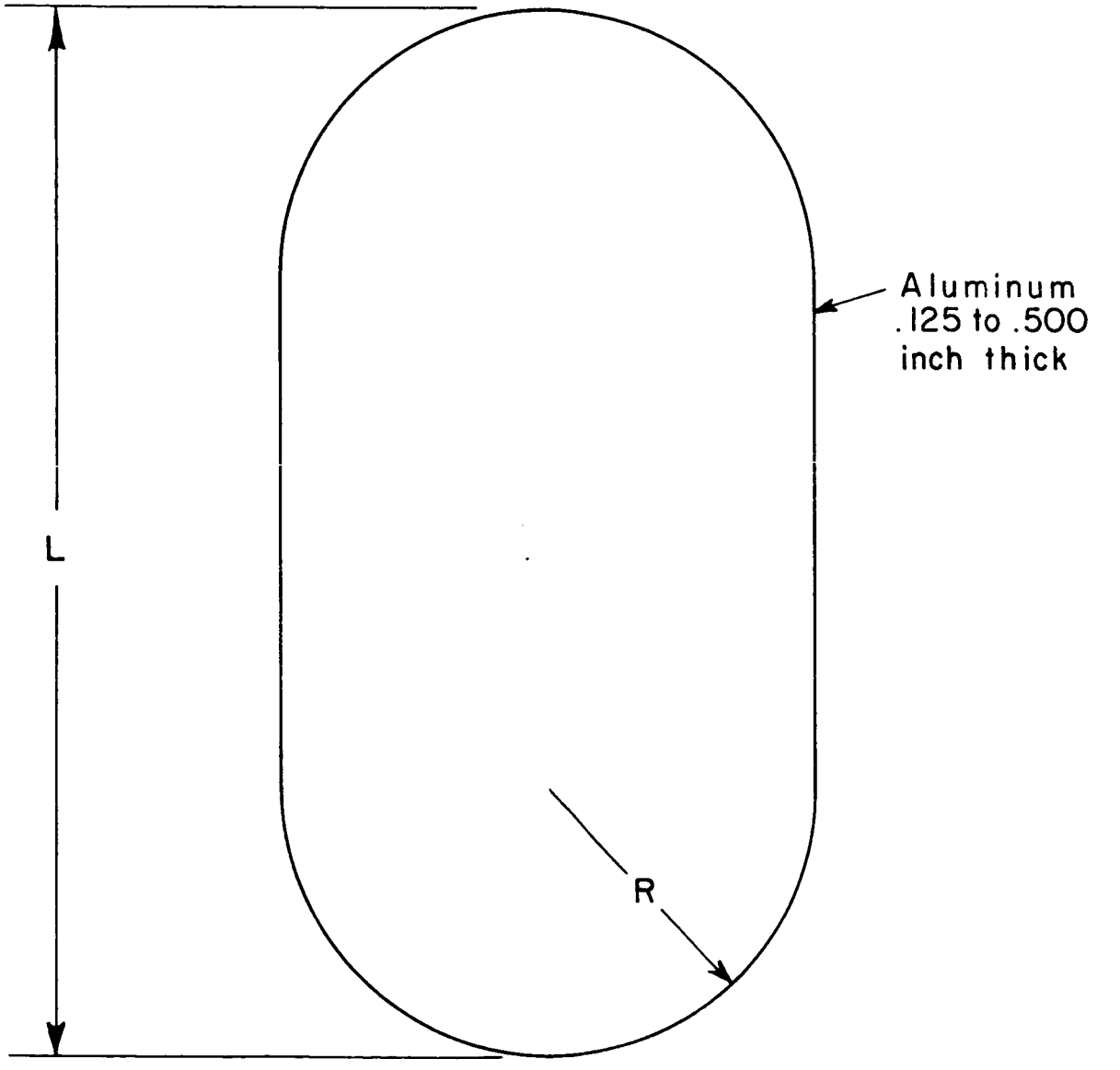

Tank Geometry

Figure 2

3. Determine general hardware requirements, including the number of sources and detectors required, the optimum type source and detectors, and general signal conditioning requirements. (General hardware requirements are set forth in Section 4.0.)

4. Determine general design parameters for each technique which is feasible, including source and detector locations, power, weight and size requirements for source, detectors, and signal conditioning. (Source-detector locations are considered in Section 3.1.1.3; other design parameters are given in Section 4.0.)

5. Determine the effects of internal components on the performance of the propellant gauge. The general internal component configuration shown on the S-IVB Hydrogen tank drawing will be used for the purpose of this study. (The effects of internal structures are mentioned in Section 3.1.1.6.)

C. The following requirements for the propellant mass gauge shall be used as design goals for the feasibility study.

1. The propellant mass gauge shall measure the total propellant mass in the tanks to an accuracy of ±2% of full scale or better. (Accuracy requirements are mentioned in detail in Sections 2.1, 3.1.1.3, 3.1.1.4, 3.1.1.5, and 4.0.)

2. The response time of the propellant mass gauge shall be 0.5 seconds or less. (Response time requirements are discussed in Sections 2.1 and 4.0.)

3. Radiation hazards to personnel anywhere outside the tanks shall be minimized. A dose ratio of 5 mr/hr is considered acceptable. (Radiation safety requirements are discussed in Sections 2.1, 3.1.1.5, and 4.0.)

4. The propellant mass gauge will be required to perform to all requirements herein only when the general orientation of the propellant is as shown in Figure 1. (The relationship between the propellant configuration of Figure 1 and various acceleration environments is discussed in Section 2.3.)

1.2 Summary of Recommended Systems

Two basic systems are recommended for application to the measurement of oxygen and hydrogen mass in the general configurations of Figure 1. The recommended systems are evaluated on the basis of their ability to measure propellant mass in a tank in which the vapor phase exists as a spherical bubble. Both systems are based on techniques whereby the mass of propellant located along a number of lines parallel to the tank axis is sampled; over 200,000 computer simulations involving spherical bubbles of random sizes and locations were examined in the optimization and

evaluation of the various arrays of sampling locations. An array of twelve sampling locations was optimized and evaluated to be capable of less than 0.7% average absolute error, an error consistent with a 2% of tank capacity system accuracy. Arrays of seven, ten, and fifteen sampling locations were also optimized and evaluated. Computer evaluation of the optimal array of fifteen indicated an average absolute error of about 0.6% and a maximum absolute error of less than 2% of tank capacity.

A gamma transmission technique is recommended for the measurement of mass in hydrogen tanks. Consisting of mated, collimated sources and detectors located at the twelve optimal sampling locations at the tank top and bottom, the transmission technique using Co^{60} is capable of meeting the accuracy, safety, and response time specifications for tanks up to 30 feet in length. If the sources are located within the tank, in a plane perpendicular to the tank axis, the required measurement can be made for tanks up to 60 feet in length.

A low energy gamma backscatter technique, in which sources and detectors are located along twelve sampling lines positioned at the optimal sampling locations, is recommended for the measurement of oxygen in tanks. The backscatter technique is volume sensitive in nature, as the backscattered radiation intensity detected by the sources is dependent upon the presence or absence of the liquid phase adjacent to the sampling lines and upon the geometrical extent of the liquid phase. The technique is appropriate for tanks of arbitrary sizes; additionally, it may be applied to hydrogen tanks.

X-ray sources may have applicability to transmission systems. However, since the energy of X-ray radiation generated by reasonably compact X-ray devices is low in comparison with high energy nucleonic gamma radiation, the penetrating power of the X-ray systems is about one-half that of the nucleonic systems; hence, the technique is applicable to tanks of about 13 feet in length without internal structures and to about 25 feet in length with a single plane of centrally-located X-ray sources positioned internally. The primary advantage of the X-ray systems lies in the ability to switch them on and off; their capability of producing a large number of photons is somewhat wasted since the radiation safety requirements limit the number of photons emanating from the tank walls at any time. Further studies of X-ray techniques for tanks whose lengths are less than 30 feet are recommended to determine (1) the appropriate means of high energy X-ray generation, (2) the extent to which collimation, energy discrimination, and commutation of mated X-ray sources and detectors is required to assure a unique correspondence between propellant mass and an appropriate function of detector outputs, (3) the penetration capability, (4) the extent to which feedback control of the emission is required to restrict radiation levels at the tank surface to less than 5 mr/hr, and (5) experimental system accuracy capabilities.

2.0 DESIGN CONSIDERATIONS

2.1 General Specifications

The investigation required by Contract NAS8-21014 involves a feasibility study of high energy radiation methods for the measurement of liquid oxygen and liquid hydrogen in tanks when the general orientation of the propellant is as shown in Figure 1. The study includes tanks from 8 to 60 feet in length with length to radius ratio of 4 (Figure 2). Three critical specifications established in the work statement are:

1. System accuracy (± 2% of capacity),
2. Response time (0.5 seconds),
3. Radiation safety requirements (5 mr/hr at the external tank surface).

The 2% system accuracy requirement imposes stringent accuracy requirements on the various system functions. Primarily, three sources of error exist in the radiation mass measurement system: measurement technique error, statistical counting error, and calibration error. Measurement technique error, intrinsic to the method by which the mass measurement is made, is reflected in variations in the mass measurement encountered as a constant mass of propellant assumes various orientations within a tank, other sources of error remaining constant. Statistical counting error arises from the random processes of photon emission, interaction with matter, and detection. Calibration error is inherent in the correlation of data (typically, radiation count rate) with the mass in the tank,

a correlation made through a predetermined one-to-one correspondence between the data and the propellant mass. Factors which influence calibration error are typically electronic drift, tank geometry variations, and similar effects. Since the three sources of error are essentially independent, the standard deviation of the system error is related to the individual standard deviations of error by

$$\sigma = \sqrt{\sigma_T^2 + \sigma_N^2 + \sigma_C^2} \quad , \qquad (2\text{-}1)$$

where σ_T, σ_N, and σ_C are, respectively, the standard deviations of the measurement technique error, the statistical counting error, and the calibration error. As Equation (2-1) dictates, to achieve a one-standard deviation system error of 2%, it is necessary to hold the other sources of error to about 1%.

The response time of 0.5 seconds places a lower limit on source size. In order to constrain the statistical counting error (σ_N) to the 1% level, the number of photons or particles detected and analyzed within 0.5 seconds must exceed a minimum value. In opposition, the radiation safety requirement imposes a restriction on the maximum number of photons or particles that can be emitted by the source. In general, the conflict between statistical counting requirements and radiation safety requirements imposes the limit on tank size for which the radiation mass measurement system is feasible.

Another limiting factor is the dynamic range of the detector. For systems in which digital counting is required so that energy discrimination can be employed to eliminate unwanted counts, count loss becomes a severe problem for high count rate. Switching to analog processing of counts results in a loss of the energy discrimination capability. Therefore, detector counting requirements impose an upper limit on the number of photons that can be processed accurately and thus restrict the tank size for which the radiation mass measurement is applicable.

2.2 Pertinent Propellant Characteristics

A list of propellant properties is given in Table 1, the properties listed being pertinent to this study. Extreme accuracy of the physical constants is rarely required; the number of significant figures given is compatible with a system error of 2%.

The following physical constants of water, employed in various simulation systems, are pertinent:

Parameters	Value
Liquid Density, gm/cm^3 (at 20° C)	1.00
Molecular Weight	18.016
Gamma-Ray Attenuation (at 662 keV)	
Cross Section, cm^2/gm	0.086
Liquid Half-thickness, cm	8.0

TABLE 1. Pertinent Physical Constants of Liquid Hydrogen and Oxygen

Parameter	Hydrogen	Oxygen
Normal Boiling Point (NBP) at 1 atmosphere	-252.7° C 20.4° K	-183.0° C 90.2° K
Melting Point	-259.1° C 13.0° K	-218.4° C 54.7° K
Vapor Density, grams/cc (at 1 atm, NBP)	1.33×10^{-3}	4.74×10^{-3}
Liquid Density, grams/cc (at NBP)	0.071	1.14
Surface Tension, dynes/cm (liquid against its vapor)	1.9 at 20° K	13.2 at 90° K
Molecular Weight	2.016	32.000
Gamma-Ray Attenuation (at 662 keV)		
Cross Section, cm^2/gm	0.154	0.077
Liquid Half-thickness, cm	63	7.8
Beta Particle Attenuation (Half-thickness at 2.24 MeV)		
Liquid, mm	6.5	.81
Vapor (at NBP), cm	35	20
Alpha Particle Attenuation, mm (liquid penetration at 5 MeV)	0.1	0.1

2.3 Propellant Behavior in an Orbiting Vehicle

The general propellant orientation indicated in Figure 1 was given by NASA for this study as representative to first-order of zero gravity fluid behavior. More accurately (since gravitational gradients exist throughout space), the propellant orientation in space corresponds to low Bond number behavior, where the Bond number provides a comparison between gravitational and capillary effects:

$$B_o = \frac{\rho g L^2}{T} , \qquad (2\text{-}2)$$

where ρ is the fluid density, g the acceleration, L a characteristic dimension of the system, and T the surface tension. For low Bond number systems, capillary forces dominate the hydrostatic propellant behavior, while for high Bond number systems, acceleration forces dominate the behavior. Therefore, even in extremely low acceleration environments, forces exist which prevent the propellant from assuming random orientations. Figure 3 indicates the acceleration dominant and the capillary dominant regimes in liquid oxygen (90° K) and liquid hydrogen (20° K), the regimes being separated by unity Bond number lines.[1]

Theoretical studies indicate that, in capillary dominant regimes, the minimum energy propellant configuration is one in which the vapor phase is present in spherical bubbles. Energy considerations further indicate that total surface energy is minimized if the vapor bubbles coalesce into a single large bubble, and additionally, that the bubbles tend to attach themselves

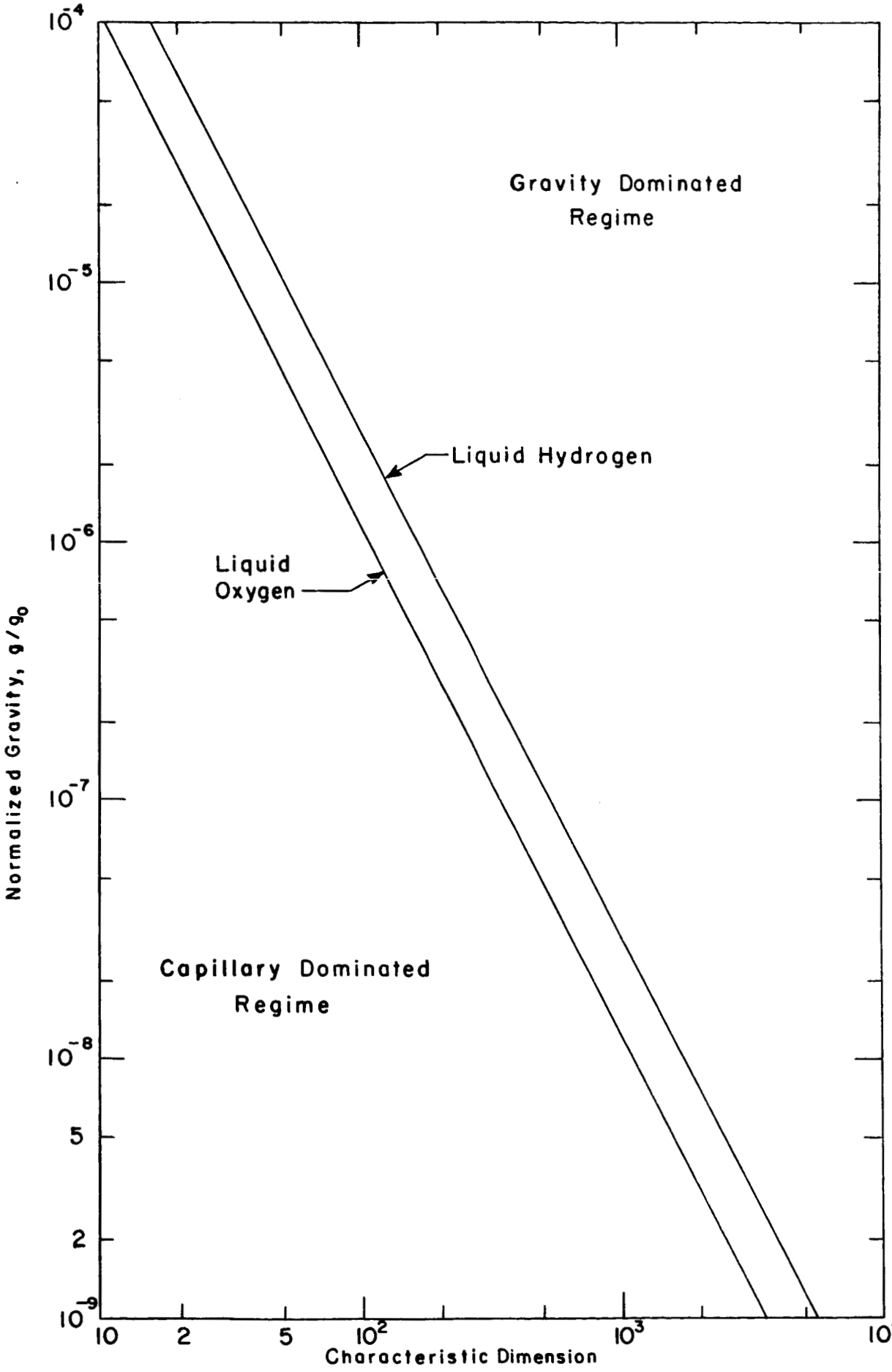

Normalized Gravity as a Function of Characteristic Dimension for Unity Bond Number.

Figure 3

to the wall. Low acceleration experiments generally verify that such minimum energy configurations occur, though some experiments indicate that metastable equilibrium situations occur in which small bubbles group around and attach themselves to a larger bubble, much like a bunch of grapes.[1, 2]

Thus, completely random orientations of propellant within a tank are statically unstable. For low Bond number situations, capillary forces cause the formation of a spherical bubble or a cluster of bubbles. For high Bond number situations, acceleration forces, although small, tend to orient the propellant so that a single relatively flat liquid-vapor interface exists. Such propellant behavior is of fundamental importance with regard to the design of propellant mass measurement systems.

2.4 Radiation and Interactions

The radiation sources available for the measurement of propellant mass are limited to alpha, beta (including positron), gamma, and neutron sources, and machine-generated X-ray and proton sources. More exotic sources of fundamental particles are generally inappropriate for engineering applications. The charged particles and neutrons are restricted to limited application to a mass measurement system from an information transmittal viewpoint; their range is too short for them to carry information concerning the existence of mass more than a few centimeters from their origin.

2. 4. 1 Gamma Radiation

Nuclear sources of high energy photons may be divided into two groups: (1) isotopic gamma emitters, and (2) isotopic beta emitters which generate significant bremsstrahlung. Usually the gamma emission is monoenergetic; that is, particular nuclear transitions are accompanied by the emission of gamma-rays with constant, quantized energy values. In addition, the interaction of emitted beta particles with matter results in the generation of high energy photons characterized by a continuous energy spectrum; the radiation is known as bremsstrahlung or "braking radiation".

Bremsstrahlung, basically electromagnetic radiation which is emitted when an electron is accelerated or decelerated in the coulomb field of the nucleus, has been investigated quantum mechanically and relativistically. The approximate fraction of beta energy which is converted to external gamma radiation is

$$\frac{E_{brem}}{E_{beta\ ave}} \simeq \frac{Z}{3000} E_{max} , \qquad (2-3)$$

where E_{brem} is the average bremsstrahlung energy, $E_{beta\ ave}$ is the average beta energy, E_{max} represents the maximum beta energy in MeV, and Z is the atomic number of the target material. A typical bremsstrahlung spectrum is indicated in Figure 4.[3]

High energy photon radiation can also be generated by man-made high energy electron sources such as X-ray tubes. The difference between nuclear β ray sources and X-ray sources lies in the energy spread of the electrons

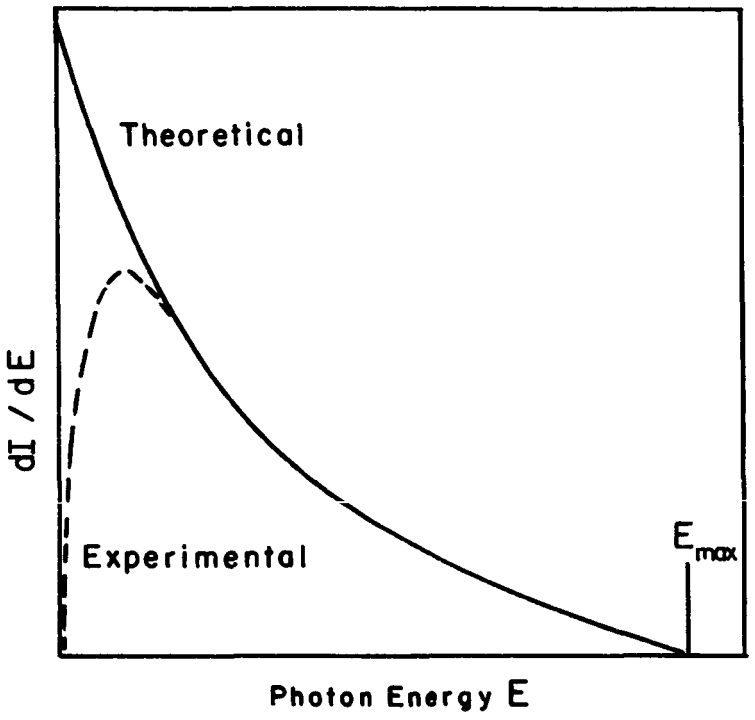

Typical External Bremsstrahlung Spectrum, Intensity of Photons Emitted per Unit Energy Increment as a Function of Photon Energy.

Figure 4

striking the target. X-ray sources produce a monoenergetic source of electrons while the nuclear β source produces a continuum of energies below E_{max}. Both sources produce bremsstrahlung and characteristic radiation. The highest characteristic radiation of natural materials is the 99 keV $K_{\alpha 1}$ radiation of uranium. The ratio of the bremsstrahlung produced to that of the characteristic radiation produced increases as energy of the impinging electrons is increased. As the energy of the incident electrons is increased above the K-edge energy (115 keV for U), the intensity of the bremsstrahlung increases while the intensity of the characteristic radiation falls. The X-ray spectrum produced by the complex interaction of monoenergetic electrons and a thick target exhibits a linear dependence of the number of photons per energy increment upon energy, as indicated in Figure 5.[3]

An atomic mechanism is fundamental to the production of characteristic gamma-rays. In the characteristic spectra, radiation is produced by the interaction of machine-generated or nuclear-produced electrons with the bound electrons of the target material. The incident electrons effect the ejection of electrons from various atomic shells of the target; photon emission results when other atomic electrons re-occupy the various vacancies. Due to the quantized energy levels of the atomic electrons, the emitted radiation produced by the atomic interaction is also quantized so that only various characteristic energies occur. The atomic interactions may occur as emissions or absorptions, but the quantized energy levels are characteristic.

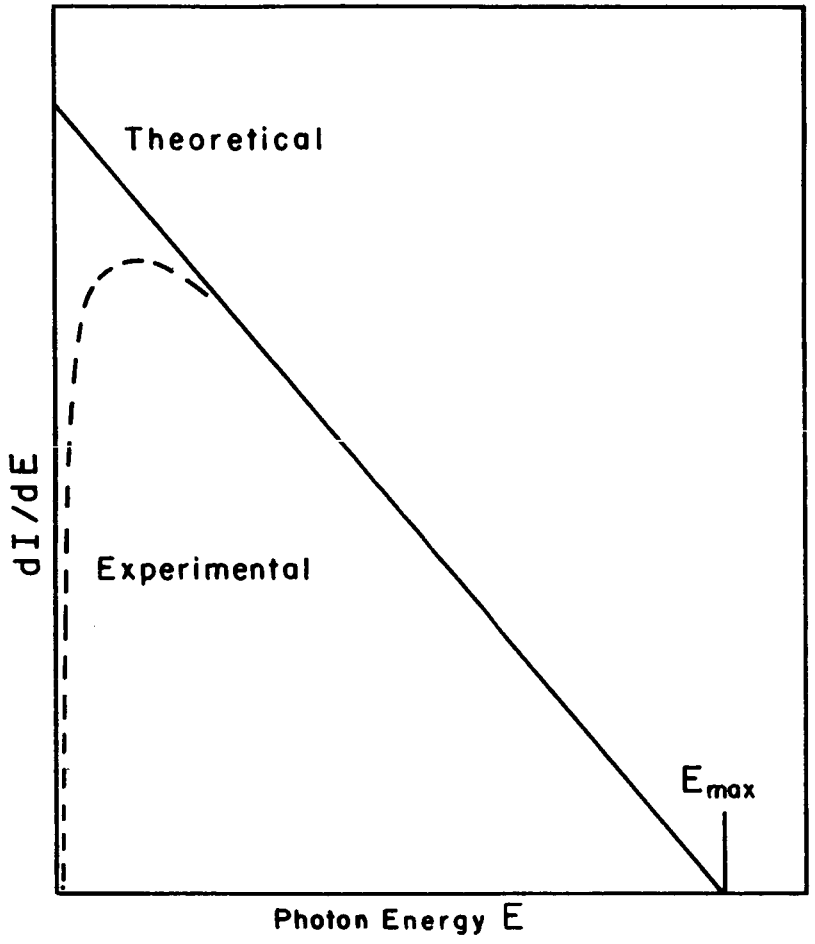

Typical X-Ray Spectrum, Intensity of Photons Emitted Per Unit Energy Increment as a Function of Photon Energy.

Figure 5

The characteristic X-ray spectrum is superimposed upon the continuous spectrum in Figure 6, a typical X-ray spectrum in which the derivative of intensity (I) with respect to photon wavelength (λ) is plotted as a function of photon wavelength. The continuous spectrum of the figure can be presented as depicted in Figure 5 through a transformation of variables. The minimum wavelength, λ_{min} of Figure 6, is related to E_{max} of Figure 5 by

$$E_{max} = hc/\lambda_{min} , \qquad (2-4)$$

where h is Planck's constant and c is the velocity of light. As Figure 6 indicates, most X-radiation occurs in the continuous spectrum; relatively little energy is radiated in the characteristic spectrum.[4]

2.4.2 Penetration and Absorption of Gamma-Rays

For the case in which the interaction between the transmitted radiation and the surrounding medium is negligible, the flux at a distance R from a point source is

$$\phi = \frac{S}{4 \pi R^2} , \qquad (2-5)$$

where ϕ is the flux in number of radiation particles or photons second^{-1} centimeter^{-2} and S is the source strength in number of emissions/second. However, in general, radiation interacts with the surrounding medium so that absorption and degradation of the radiation occurs.

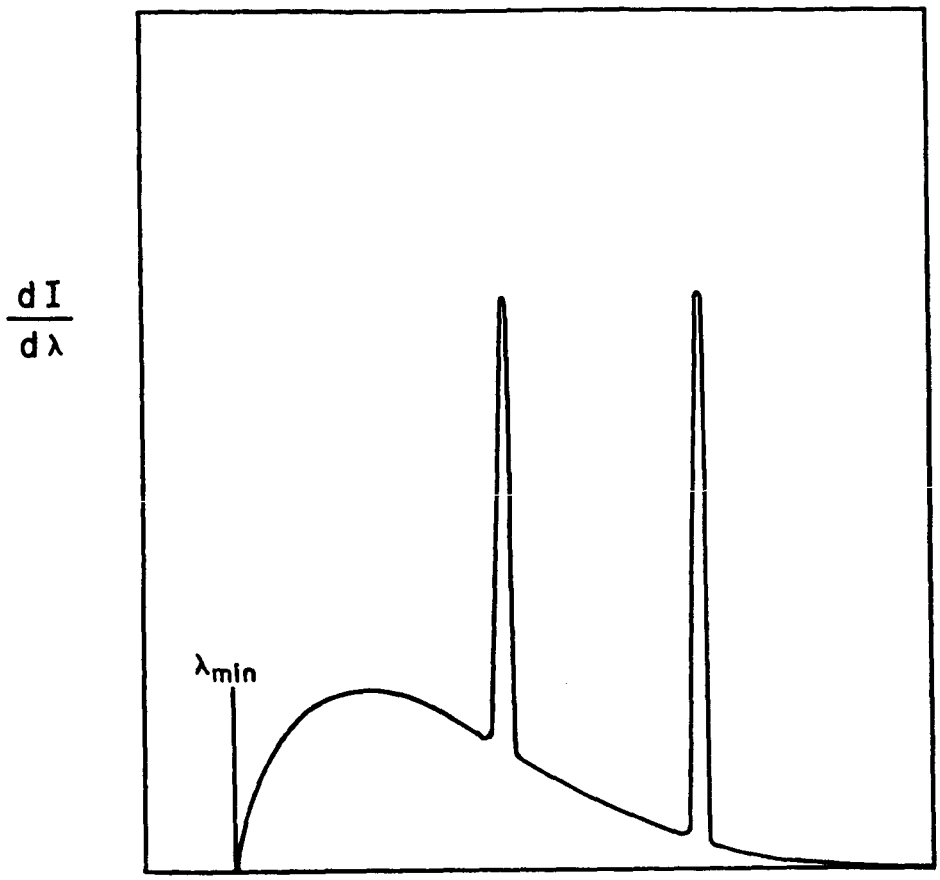

Typical X-Ray Spectrum, $dI/d\lambda$ as a Function of λ.

Figure 6

High energy electromagnetic radiation interacts with matter in a number of fashions, the following four of which are most common: (1) through the production of photoelectrons, (2) through Compton scattering, (3) through Thompson and Raleigh scattering, and (4) through pair production in the atomic or nuclear field. In the first and fourth interactions, the incident radiation is completely absorbed; in the second interaction, the incident photon transfers some energy to an electron; in the third interaction, the photon is elastically scattered. For photon energies between about 30 keV and 3 MeV, the dominant interaction in liquid hydrogen and liquid oxygen is the Compton interaction.

The macroscopic representation of the multiple interactions of numerous photons is effectively made in terms of an exponential attenuation model. A theoretical model based on the interaction cross sections of individual collisions and verified by experiment indicates that the attenuation of primary gamma photons is described by

$$\phi_p = \frac{S}{4 \pi R^2} e^{-\mu \rho x}, \qquad (2\text{-}6)$$

where ϕ_p is the flux of primary photons which do not interact during passage through matter, ρ is the material density, x is the thickness of attenuating medium through which the radiation passes (not necessarily equal to R), μ is the mass attenuation coefficient in cm^2/gm (equal to the sums of the various interaction cross sections), and S is the source strength in emissions/second. The quantity $(\mu \rho)^{-1} = \lambda$ is defined to

be the characteristic length of the radiation in the particular medium; that is, the length of absorber for which a parallel, collimated beam is attenuated to e^{-1} of its initial value. Thus, ϕ_p gives the flux of photons that have experienced neither energy degradation nor directional change during propagation through the medium.

3.0 EVALUATION OF MEASUREMENT TECHNIQUES

The interactions of radiation with matter are fundamental to nucleonic propellant mass measurement techniques of two generic types: mass sensitive measurements and volume sensitive measurements. Although the fundamental interactions are dependent on mass, count data may be processed on a geometrical basis so that the volume of propellant liquid is sensed rather than its mass. The volume sensitive measurement types must be supplemented by pressure and temperature measurements so that mass can be inferred.

Screening of measurement techniques is concerned with the answer to one fundamental question: Can the measurement system produce a one-to-one correspondence between some function of the detector signals and the mass within the tank consistent with the NASA specifications listed in Section 2.1?

3.1 Mass Sensitive Measurement Schemes

Three fundamental radiation techniques are mass sensitive in nature. These techniques are based on the transmission, diffusion, and scattering of radiation.

Transmission techniques comprise those mass measurement techniques in which propellant mass is inferred from the attenuation of radiation transmitted across a significant expanse of the tank volume. Range considerations indicate that only gamma radiation is appropriate for the transmission measurements. Due to physical limitations on source and detector areas,

sampling techniques are generally required. Two types of radiation sources are of fundamental interest with respect to transmission measurements: monoenergetic gamma sources (as typified by Cs^{137} and Co^{60}) and continuous radiation sources (as typified by X-ray and bremsstrahlung sources).

Diffusion and scattering techniques comprise measurement techniques in which the amount of radiation detected, regardless of the radiation path from source to detector, is used as an index of propellant mass. Again, only high energy electromagnetic radiation is appropriate.

3.1.1 Monoenergetic Gamma Transmission Technique

3.1.1.1 General Description and Applicability

The monoenergetic gamma transmission technique is based on the exponential attenuation of primary radiation (that radiation which has not interacted with matter) from a monoenergetic gamma-ray beam according to the model

$$N = N_o e^{-x/\lambda} \quad , \qquad (3\text{-}1)$$

where N is the photon count at the detector, N_o the count with the tank evacuated, x the absorber thickness, and λ the characteristic length. The inverse R^2 dependence (Equation 2-6) is eliminated since the source and the detector are assumed to be fixed relative to one another. Through a sampling network of n parallel, collimated radiation beams normally directed either through the tank parallel to the tank axis or across the tank

perpendicular to the tank axis, the mass within the tank is inferred from the mass of absorbing material located in each beam. (The two transmission types are depicted in Figure 7.) The count at the i^{th} detector is

$$N_i = N_{o_i} e^{-\mu(\rho_L \ell_i + \rho_g t_i)} , \qquad (3-2)$$

where μ is the attenuation coefficient, ρ_L and ρ_g are the liquid and gas densities, and ℓ_i and t_i are the thicknesses of liquid and gas within the i^{th} radiation beam. The mass sampled by the i^{th} beam is approximately

$$M_i = A_i W_i (\rho_L \ell_i + \rho_g t_i) = \frac{A_i W_i}{\mu} \ln \frac{N_{o_i}}{N_i} , \qquad (3-3)$$

where A_i is an appropriate area and W_i an appropriate weighting factor. Typically, for a system in which radiation beams are directed parallel to the tank axis,

$$A_i = \frac{A_c}{n} , \quad W_i = 1 \text{ for all } i , \qquad (3-4)$$

where A_c is the cross sectional area of the tank. Then the total mass in the tank is

$$M = \sum_{i=1}^{n} M_i . \qquad (3-5)$$

Thus, the mass in the tank is approximated by the summation of the mass in n cylinders of liquid and gas, the amount of liquid and vapor contained in the cylinders being inferred from the radiation attenuation.

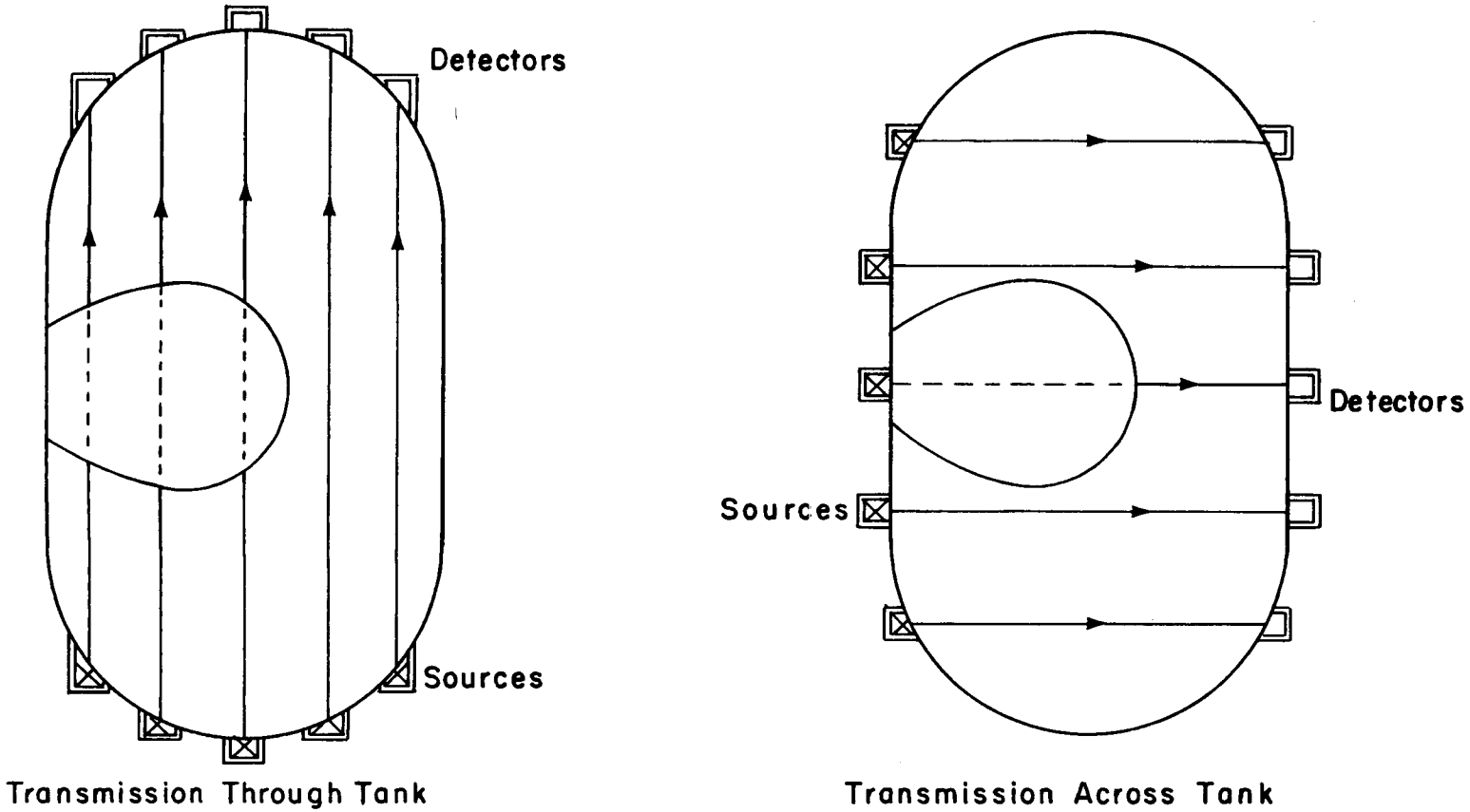

Fundamental Transmission Configuration (No Internal Structure)

Figure 7

Two precautions must be taken to insure that Equation (3-2) is valid; that is, to insure that the count is exponentially dependent on the mass interposed between source and detector. First, both source and detector must be tightly collimated so that no crosstalk exists; that is, so that no photons emanating from a source strike any detector other than the one directly opposite to that source. Second, in order to insure that no scattered photons are detected, the incident photons must be discriminated energetically so that only primary photons, those which have not interacted with matter and lost energy, are detected.

Thus, a one-to-one correspondence between mass and a function of the detector outputs can be established so that the monoenergetic gamma transmission technique is capable of providing the required mass measurement. A detailed description of a monoenergetic gamma transmission system is given in Section 4; evaluation of system accuracy capabilities is presented in this section.

3.1.1.2 Sampling and Weighting Considerations

Measurement technique error for the monoenergetic gamma transmission system is determined by the validity of the sampling method employed. Essential to the sampling technique is the information processing scheme by which the data acquired by each sampling beam is manipulated to yield a final measurement of propellant mass. Knowledge of the fluid behavior in the particular gravity environment may be incorporated in the data processing, but that knowledge must be precise or gross errors

may result. For example, in a low Bond number environment in which a single vapor bubble of spherical shape is expected to be present, only four degrees of freedom exist (the sphere radius and the three coordinates of the sphere center) so that the sampling of the bubble thickness in four separate positions through a known geometrical array uniquely determines its volume and, hence, the total propellant mass--if and only if the bubble is indeed solitary and spherical. If the bubble is not spherical or if a bubble cluster exists, the mass determination based on four thicknesses can be grossly erroneous. Thus, data processing systems which depend on four independent measurements of bubble thickness (or on linear programming methods for more than four independent measurements) are extremely sensitive to the exact fluid behavior and are of limited value, at least until actual space missions determine the precise nature of bubble configurations. More general sampling methods are desired.

Fundamental to the required measurement system is the feature that all volume increments within the tank must be weighted equally; that is, the presence of mass in any of the volume increments within the tank must render a constant contribution to the proper function of the outputs of the detectors. Since source and detector sizes are limited, sampling techniques are required. By its very nature, sampling implies that only selected volume increments are interrogated concerning the amount of mass present so that the presence of mass in many volume increments produces no contribution at all to the detector outputs. However, the

propellant orientation is not random so that the presence or absence of mass in one particular volume increment conveys significant information concerning the presence or absence of mass in nearby increments. In a sense, the volume increment within a particular sampling beam represents those adjacent and nearby volume increments as well as itself; the sum of those volume increments represented by a volume increment within a particular sampling beam is defined to be a sampled volume element. The fundamental sampling axiom is that all sampled volume elements interrogated by a particular sampling beam must be equally weighted; that is, the presence of mass in any of the sampling volume elements interrogated by a particular sampling beam must render a constant contribution to the proper output function of the detectors.

A typical sampling beam which passes through a number of sampled volume elements is pictured in Figure 8. The sampled volume elements are pictured as disks (rectangles in the two-dimensional diagram) centered over the sampling beam. For all of the sampled volume elements, the volume increment within the radiation beam is assumed to represent correctly the status of the sampled volume element. The fundamental sampling axiom states that the presence of matter within an element must have an effect on the detected signal that is independent of the location of the element.

Therefore, it is desirable to arrange the sampling beams in a pattern such that the sampled volume elements are as compact as possible (so that all increments of a sampled volume element are close to the radiation beam),

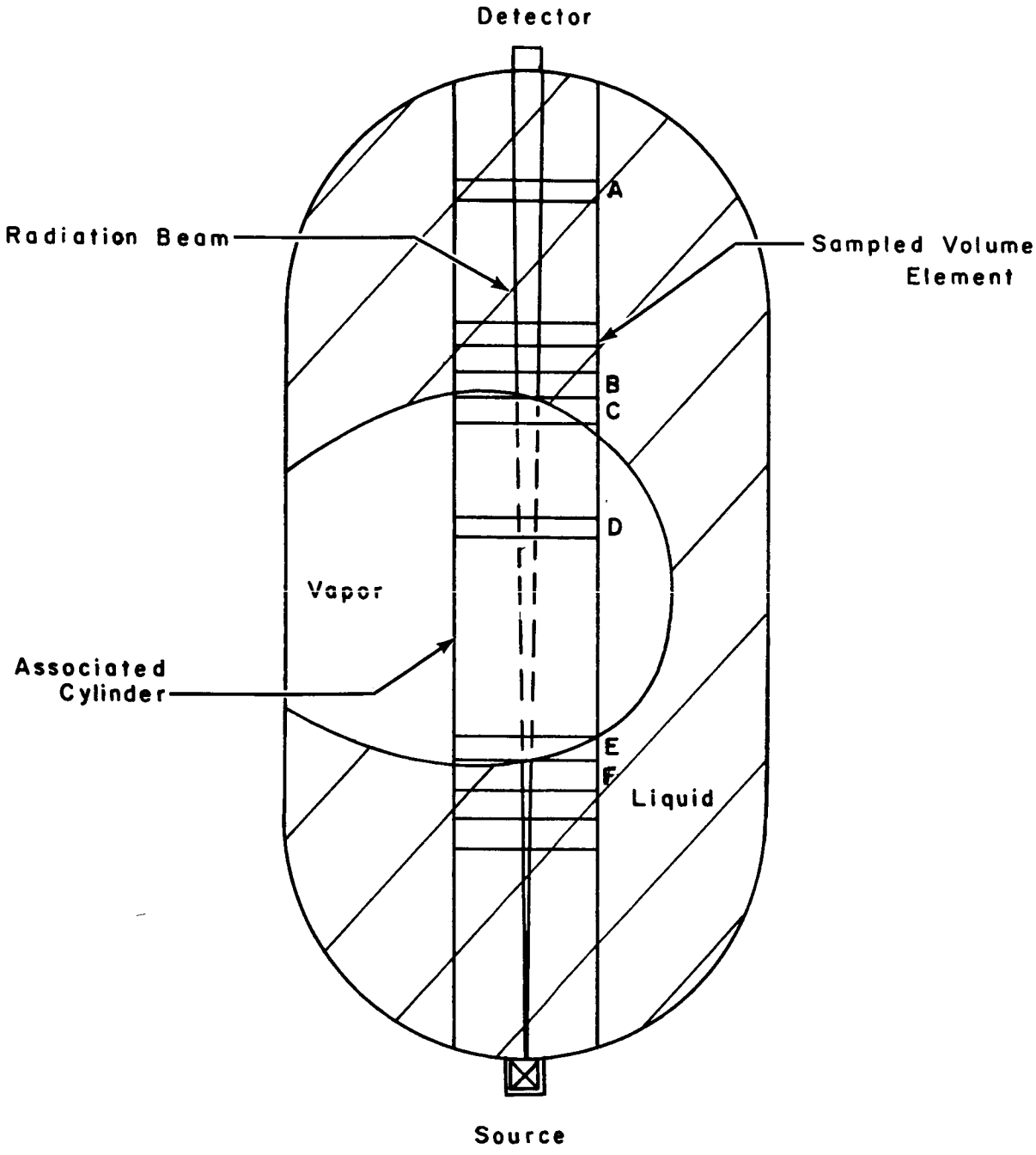

Collimated Radiation Beam and Associated Cylinder

Figure 8

and as uniform in size as possible (so that a given mass of propellant contains a number of sampled volume elements that is independent of its geometrical location). The location of parallel sampling beams at the center of zones similar to the Wigner-Seitz zones established by atoms in crystalline lattices provides a sampling pattern in which all points within a particular zone are nearer to the sampling beam at its center than to any other sampling beam. For optimal application to a cylindrical tank geometry, the zones assume hexagonal shapes modified at the tank perimeter to conform with the circular boundary. Thus, the sampling beams represent the amount of propellant located in associated hexagonal or quasi-hexagonal cylinders whose axes are congruent with the sampling beams. The cross sectional areas of the associated cylinders should be equal (so that all sampled volume elements are uniform in size); hence, $A_i = A_c/n$ as indicated in Equation (3-4). For the equal-sized sampled volume element situation, the weighting factors, W_i of Equation (3-4), should all be unity.

Figure 9 depicts the interpretation of a parallel beam sampling scheme. The dashed lines outline the associated cylinders of the various sampling beams (degenerated to rectangles in the two-dimensional representation); the liquid-vapor interfaces are determined by the sampling beams which lie along the axes of the associated cylinders (only one sampling beam is shown in the diagram). In an actual data processing system, the longitudinal placement of the liquid and vapor portions of the cylinders is indeterminant, a feature which does not influence total mass estimation.

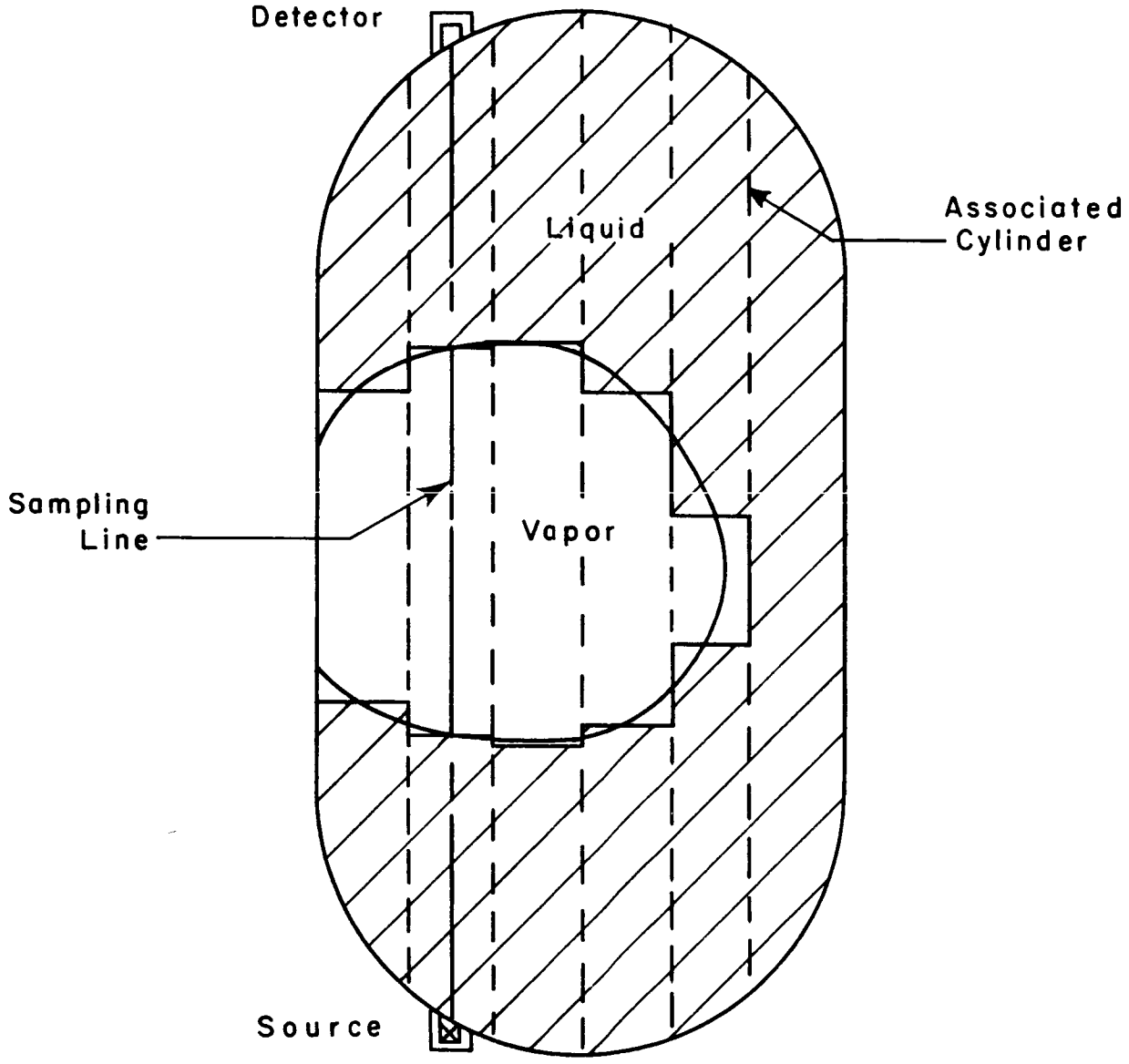

Two Dimensional Model: Rectangular
Approximation of Interface Geometry.

Figure 9

The uniformly-distributed parallel beam sampling systems, compatible with Equations (3-3) and (3-5), can provide a sufficiently accurate estimation of propellant mass in the orientation of Figure 1a through the careful location of a number of beams. Optimization of beam location is achieved for arrays of seven, ten, twelve, and fifteen through computer simulations of the spherical bubble environment. The estimation of mass in the configuration of Figure 1b generally is more accurate than the estimation for the configuration of Figure 1a because deviations across the associated cylinders increasingly compensate as the liquid-vapor surface flattens (if one side of the cylinder holds more fluid than indicated by the sampling beam along the axis, then the other side contains an equal amount less for a flat interface). Some problem is anticipated for the unique case when the liquid-vapor interface is parallel to the radiation beams, but the addition of several cross-tank beams should eliminate the difficulty. In general, the parallel sampling beam transmission system should operate more accurately in high Bond number regimes than in low Bond number regimes; 1% measurement technique accuracy is achievable in both regimes.

3.1.1.3 Computer Optimizations of Sampling Arrays

In order to obtain extensive statistical information regarding measurement technique error (σ_T), the simulation of a single large vapor sphere within a tank containing liquid hydrogen has been accomplished by various computer studies. The position of the spherical vapor bubble is determined either in a systematic fashion or by means of a matrix of

random numbers. Computer simulations have been made for both cylindrical and hemispherically-capped tanks. Features of the various simulations are listed subsequently.

Simulation SPHCC (sphere centered within a cylinder): In this case, a spherical vapor bubble is centered within a cylindrical tank, and the size of the vapor bubble is increased systematically from 2% of tank capacity to about 40% of tank capacity, the 40% of capacity bubble being the largest sphere that can fit into the tank.

Simulation SPHTC (sphere tangent to a cylinder): For this simulation, a spherical vapor bubble is located internally tangent to the wall of a cylindrical tank. The size of the vapor bubble is increased systematically from about 2% to 40% of tank capacity; the position at which the bubble is tangent is rotated about the cylinder so that all relative locations of source, detector, and bubble are examined systematically.

Simulation RNSPV (randomly oriented spheres within the tank volume): For this case, a spherical bubble either of a predetermined size or of a size randomly selected between 2% and 40% of tank capacity is randomly located within a hemispherically-capped tank. The position of the center of the bubble is determined by three computer-generated random numbers which correspond to the three coordinates of the center.

Simulation RNSPT (randomly oriented sphere tangent to the tank): In this simulation, a spherical bubble either of a predetermined size or of a size randomly selected between 2% and 40% of tank capacity is located

internally tangent to the walls of a hemispherically-capped tank, but otherwise at random. Again, the position of the center of the bubble is determined by three computer-generated random numbers which fix the coordinates of the tangent sphere.

The performance of the system in the presence of vapor bubbles ranging from 2% to 40% of the tank capacity is an adequate index of system performance under any conditions of fill. Small bubbles (less than 2% of capacity) on the average provide small measurement technique errors. Bubbles larger than 40% of capacity become elongated, but the measurement technique errors for the elongated bubbles are the same as those for the 40% of capacity bubbles because system error associated with the estimation of the cylindrical midsection of the elongated bubble is zero. Hence, the 2% to 40% bubbles subject the measurement technique to an adequate test.

The computer simulations of the zero gravity mass measurement systems have produced optimal sampling patterns for seven, ten, twelve, and fifteen sampling beams. The sampling beams are parallel to the tank axis (tank shape as specified in Figure 2) and optimization is based on the information processing scheme of Equations (3-3) and (3-5) for associated cylinders with equal weighting factors. In addition to the results given for beams directed parallel to the tank axis, results are presented for an array of fifteen beams directed across the tank.

The optimal configurations were determined by trial and error alteration of parameters and evaluation of results by the four computer-simulated

zero gravity situations. In general, relatively gross errors were detected in the centered sphere simulation (SPHCC), the gross errors occurring for spheres with radii nearly equal to a radius at which several sampling lines were located. Such gross errors were rarely detected in the randomly oriented sphere simulation (RNSPV) due to the low statistical frequency of occurrence of such bad cases. Examination of the various simulations indicated that the largest errors were associated with (1) large spheres centered on a particular sampling line and with a radius nearly equal to the distance from the sphere center to nearby sampling lines, and (2) small spheres intersected by zero or one sampling line.

Figures 10 and 11 indicate the measurement error as a function of spherical vapor bubble radius for a cylindrical tank containing a centered sphere (Simulation SPHCC) and an internally tangent sphere (Simulation SPHTC) for the optimal array of twelve sampling locations. Figures 12 and 13 indicate the error distributions for 440 bubbles randomly located tangent internally to the tank wall (RNSPT) for the optimal array of twelve. Similar data for the arrays of seven, ten, and fifteen sampling locations are contained in the appendices. In addition, the effects of modifying an initial Wigner-Seitz sampling pattern of seven are described in detail in the appendices.

The optimal configurations determined by alteration of parameters and comparison of results are given in Tables 2 - 5. A top view of the

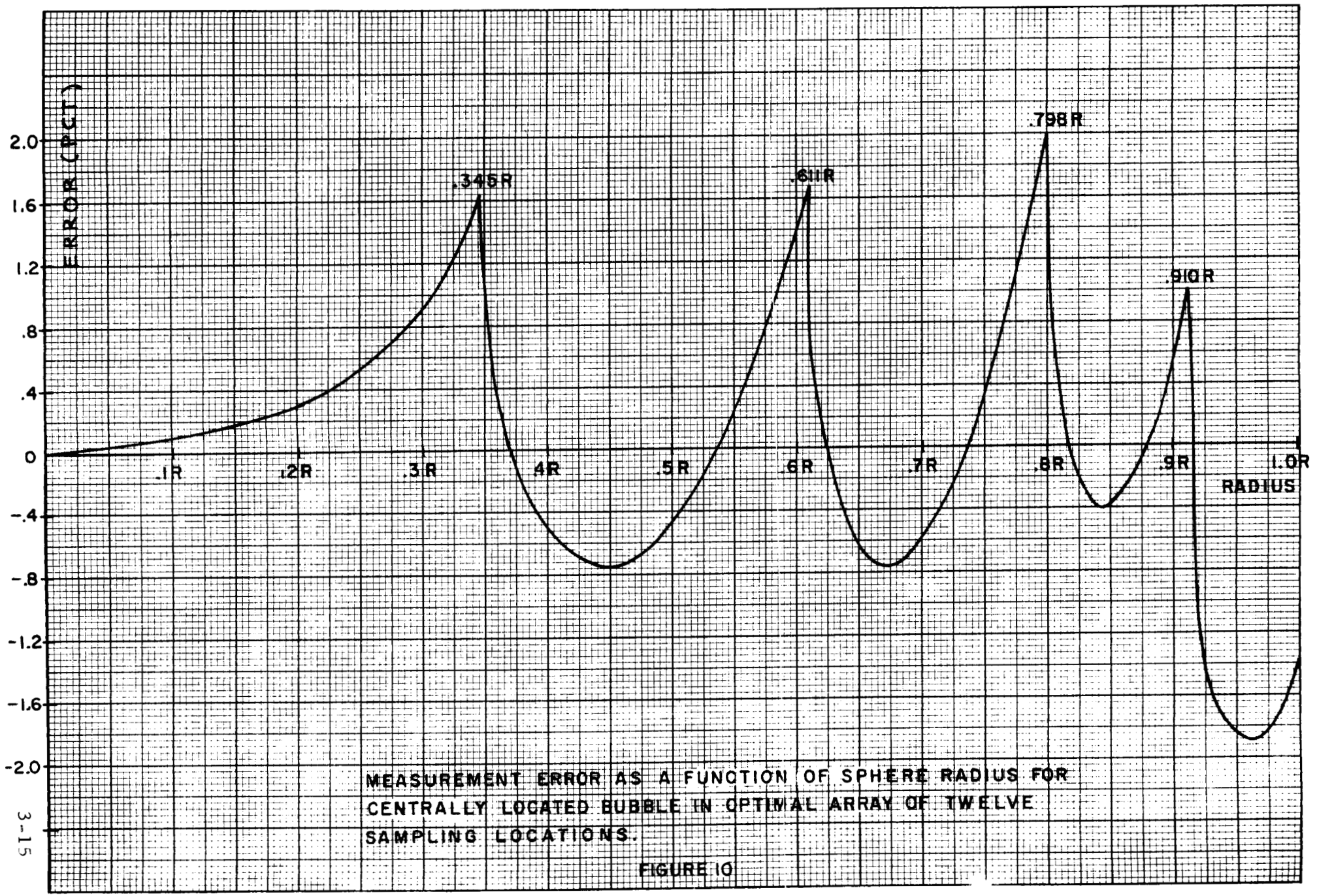

MEASUREMENT ERROR AS A FUNCTION OF SPHERE RADIUS FOR CENTRALLY LOCATED BUBBLE IN OPTIMAL ARRAY OF TWELVE SAMPLING LOCATIONS.

FIGURE 10

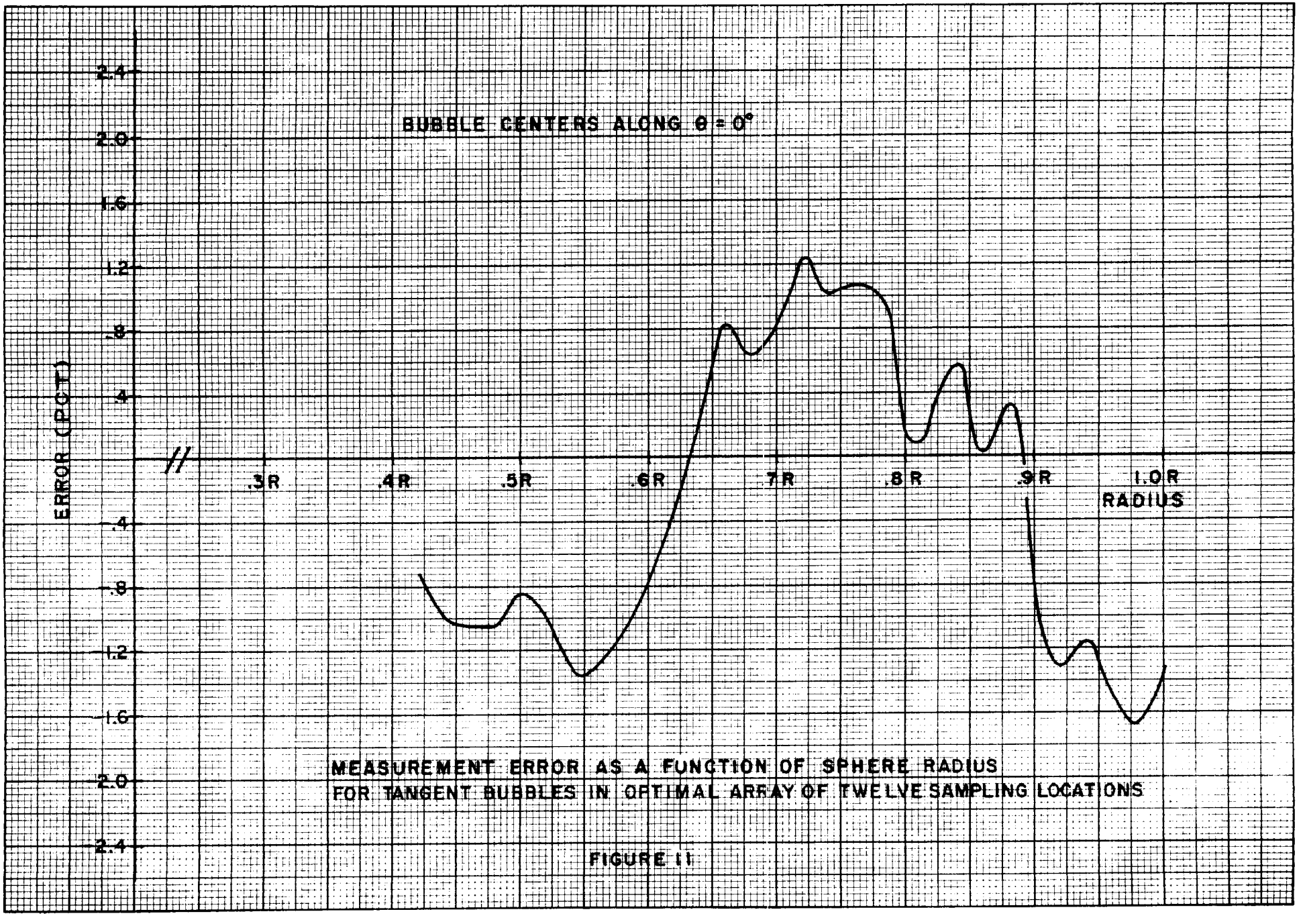

MEASUREMENT ERROR AS A FUNCTION OF SPHERE RADIUS
FOR TANGENT BUBBLES IN OPTIMAL ARRAY OF TWELVE SAMPLING LOCATIONS

FIGURE 11

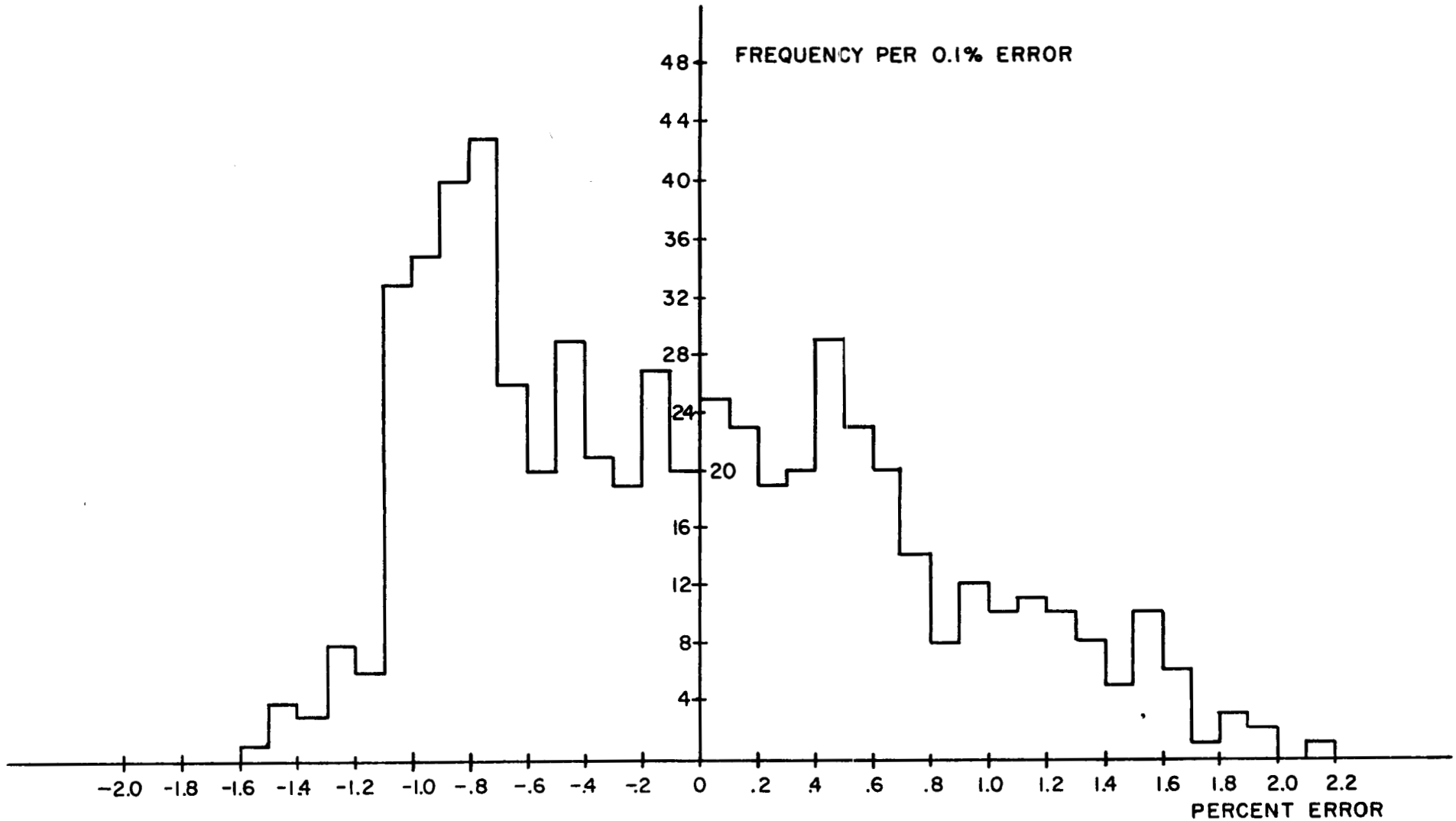

FREQUENCY OF ERROR (PER 0.1% ERROR INCREMENT) FOR OPTIMAL ARRAY OF TWELVE SAMPLING LOCATIONS, DATA FOR 595 RANDOMLY ORIENTED TANGENT SPHERES OF VOLUME 2% TO 40% OF TANK CAPACITY.

FIGURE 12

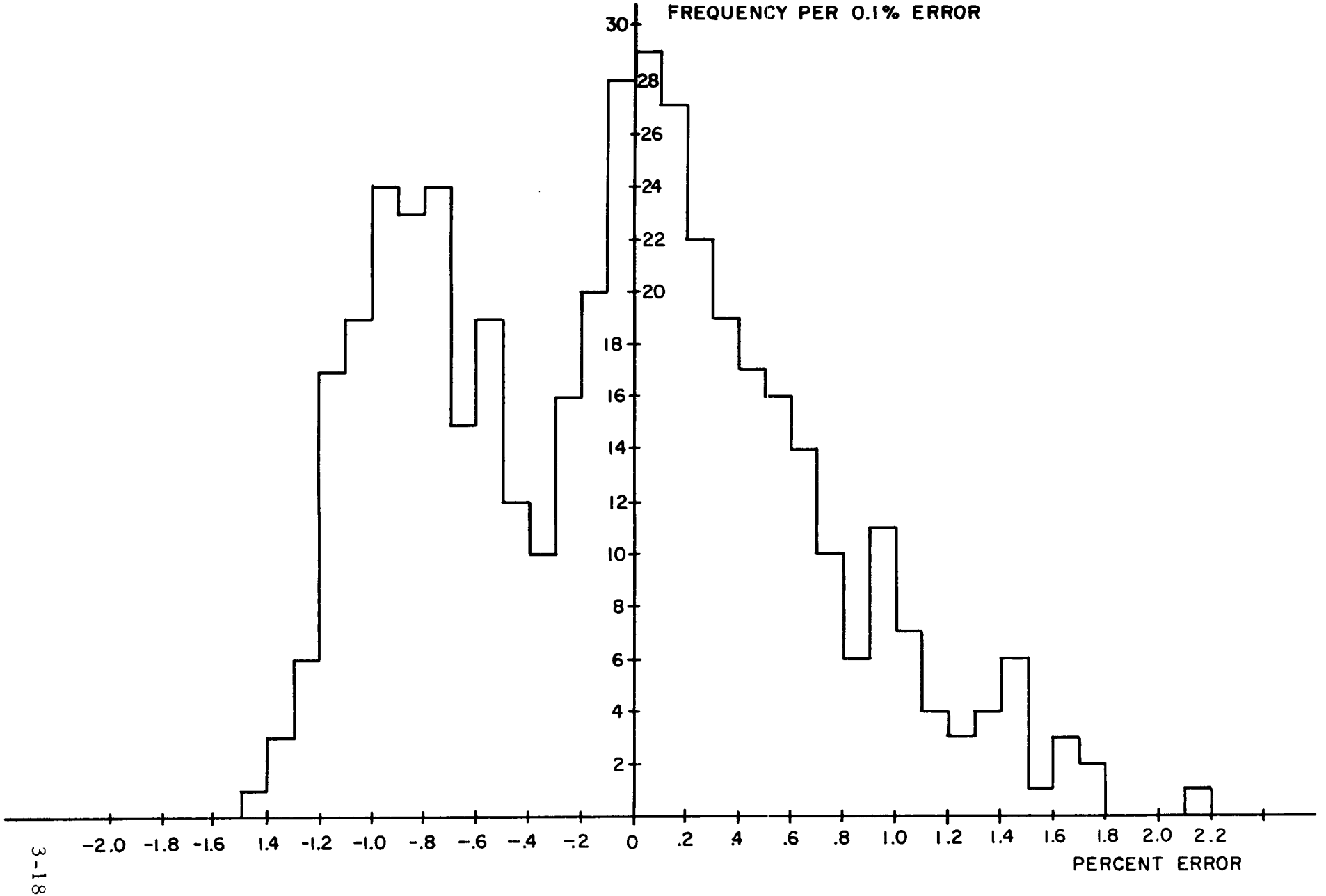

FREQUENCY OF ERROR (PER 0.1% ERROR INCREMENT) FOR OPTIMAL ARRAY OF TWELVE SAMPLING LOCATIONS, DATA FOR 440 RANDOMLY ORIENTED SPHERES OF VOLUME 2% TO 40% OF TANK CAPACITY.

FIGURE 13

Table 2. Optimal Array of Seven Sampling Locations*

Location	Radius	Angle°
1	0.000 x R	0.0
2	.600	0.0
3	.610	120.0
4	.620	-120.0
5	.833	60.0
6	.843	180.0
7	.853	-60.0

*See Figure 14 a).

Table 3. Optimal Array of Ten Sampling Locations*

Location	Radius	Angle°
1	0.275 x R	90.0
2	.275	-90.0
3	.600	0.0
4	.600	180.0
5	.730	45.0
6	.890	90.0
7	.830	135.0
8	.740	-135.0
9	.890	-90.0
10	.830	-45.0

*See Figure 14 b).

Table 4. Optimal Array of Twelve Sampling Locations*

Location	Radius	Angle°
1	0.345 x R	0.0
2	.345	120.0
3	.345	-120.0
4	.611	60.0
5	.611	180.0
6	.611	-60.0
7	.798	25.0
8	.798	145.0
9	.798	-95.0
10	.910	90.0
11	.910	-150.0
12	.910	-30.0

*See Figure 14 c).

Table 5. Optimal Array of Fifteen Sampling Locations*

Location	Radius	Angle°
1	0.300 x R	0.0
2	.300	120.0
3	.300	-120.0
4	.565	60.0
5	.565	180.0
6	.565	-60.0
7	.722	20.0
8	.842	100.0
9	.722	140.0
10	.842	-140.0
11	.722	-100.0
12	.842	-20.0
13	.908	60.0
14	.908	180.0
15	.908	-60.0

*See Figure 14 d).

sampling locations is given in Figure 14. In addition, the various measurement technique errors encountered in the measurement of tank mass while a spherical vapor bubble is present are indicated in Table 6. The standard deviation of the measurement technique errors is approximately equal to the root mean squared errors given in Table 6. As indicated in the table, transmission across the tank for fifteen beams is inferior to transmission through the tank with seven beams; however, the advantages inherent in maintaining the structures external to the tank may warrant the use of the cross-tank transmission techniques in certain instances. The errors must be considered in light of the spherical vapor bubble approximation. For non-spherical bubbles, particularly for elongated sausage-shaped bubbles, the errors encountered can be in excess of 2%; however, energy considerations indicate that such bubbles are not in equilibrium with their surroundings, and hence, they represent rarely occurring configurations.

The possibility exists that errors for spherical bubbles in excess of the maximum errors indicated in Table 6 might be encountered since, in fact, an infinite number of sphere sizes and orientations are possible, and the computer simulations check but a finite, albeit large, number of cases (over 2,000 cases for each optimal configuration, many thousand additional cases for closely-related configurations). However, in view of the large number of cases examined, it is highly unlikely that errors much in excess of the tabulated maximum errors would be encountered for spherical bubbles.

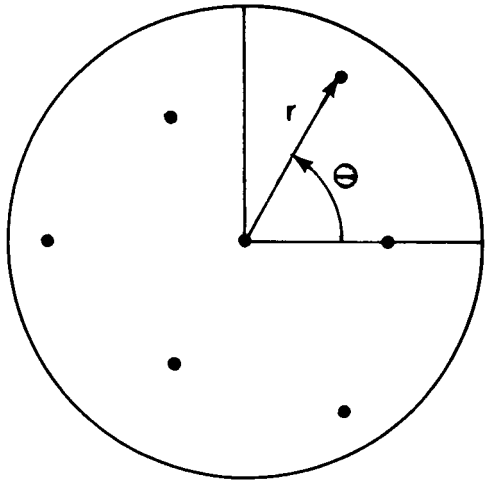

a) ARRAY OF SEVEN

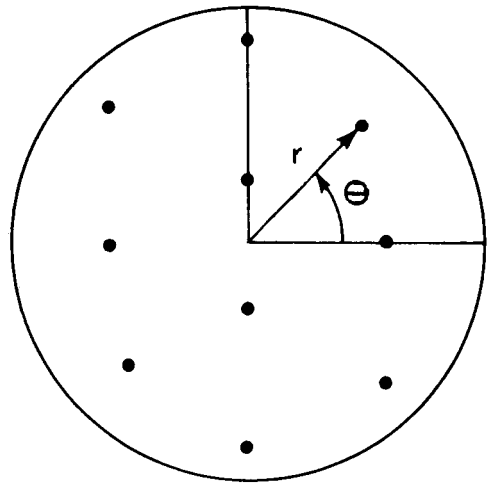

b) ARRAY OF TEN

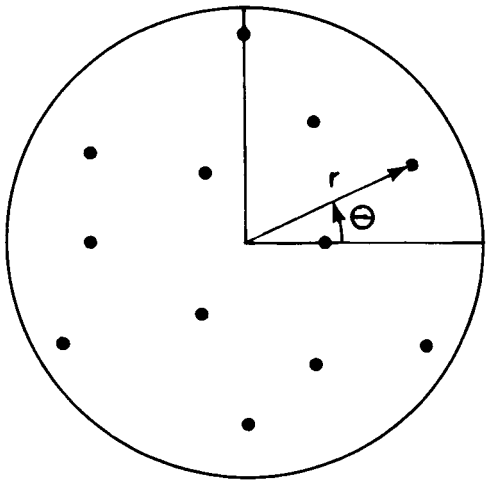

c) ARRAY OF TWELVE

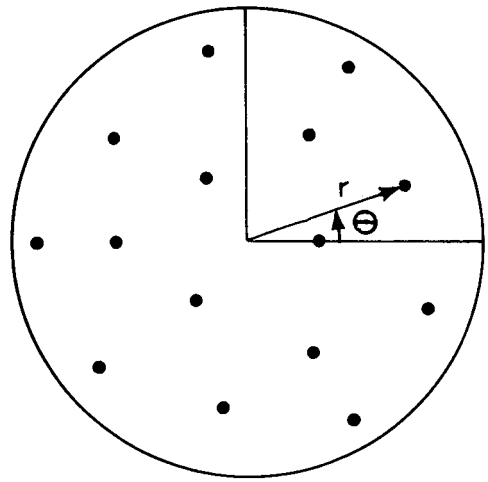

d) ARRAY OF FIFTEEN

TOP VIEW OF OPTIMAL ARRAYS FOR SEVEN, TEN, TWELVE, AND FIFTEEN SAMPLING LOCATIONS.

FIGURE 14

Table 6. Errors in Per Cent of Tank Capacity for Various Optimal Sampling Arrays

Computer Simulation	Average Error	Average Absolute Error	Root Mean Squared Error	Maximum Positive Error	Maximum Negative Error	Maximum Absolute Error
Centered Spheres (SPHCC)						
Array of Seven	-	-	-	3.81	-4.25	4.25
Array of Ten	-	-	-	2.64	-2.40	2.64
Array of Twelve	-	-	-	1.70	-1.90	1.90
Array of Fifteen	-	-	-	1.86	-1.91	1.91
Tangent Spheres (SPHTC)						
Array of Seven	-	-	-	4.56	-3.86	4.56
Array of Ten	-	-	-	2.84	-2.65	2.84
Array of Twelve	-	-	-	2.19	-2.01	2.19
Array of Fifteen	-	-	-	1.97	-1.66	1.97
Random Spheres (RNSPV)						
Array of Seven	-	1.39	1.67	4.70	-3.41	4.70
Array of Ten	-	1.02	1.20	3.33	-1.97	3.33
Array of Twelve	-	0.58	0.71	2.22	-1.47	2.22
Array of Fifteen	0.03	0.62	0.74	1.92	-1.31	1.92
Random Tangent Spheres (RNSPT)						
Array of Seven	-0.94	1.34	1.60	4.65	-3.48	4.65
Array of Ten	-0.05	0.93	1.12	3.36	-2.08	3.36
Array of Twelve	-0.07	0.67	0.78	2.12	-1.55	2.12
Array of Fifteen	-0.08	0.60	0.71	1.86	-1.16	1.86
Random Spheres (RNSPV)						
Array of Fifteen						
Directed Across Tank	0.46	1.57	1.93	4.99	-4.99	4.99

On the order of 2,000 cases have been examined for each of the four optimized source-detector arrays through the computer simulations. Many thousand additional cases have been studied for configurations closely related to the optimized arrays; approximately 200,000 individual cases have been simulated. The magnitude of the number of computer simulations permits effective statistical evaluation of the selected measurement techniques, thus establishing confidence that the varied situations encountered at zero gravity can be adequately handled by the appropriate measurement technique.

3.1.1.4 Experimental Studies

The experimental simulation of the propellant configuration of Figure 1a is made possible by the fact that the interaction of radiation with matter is dependent upon interactions of radiation with the fundamental particles which comprise matter (the nuclei and electrons) rather than with the peculiar chemical properties of the various molecules. With regard to absorption and scattering phenomena, adequate description can be made in terms of the ratio of the path length of radiation through the matter to the characteristic length of radiation in the matter.

Simulation of gamma radiation transmission through liquid-vapor hydrogen systems can be adequately achieved by reduced scale models consisting of water and foam due to the fact that for relatively high radiation energies, the primary interaction between the radiation and either system is Compton scattering. When the binding energies of electrons

are small compared to the impinging photon energies, the Compton scattering phenomenon is dependent on the density of scattering electrons and is essentially independent of the properties of the material. When Compton scattering predominates, the characteristic length scales correctly for all energies and scattering angles transform identically. Compton scattering dominates in hydrogen for energies above 1 keV, in oxygen for energies above 28 keV, and in water (or foam) for energies above about 25 keV. Figure 15 indicates the dependence of the gamma attenuation coefficient on photon energy for oxygen and hydrogen; the curves for water (oxygen and hydrogen) and foam (oxygen, hydrogen, and carbon) are essentially coincident with the oxygen curve. The attenuation coefficient for hydrogen is almost exactly twice that for oxygen (and all other elements) in the Compton domain above about 50 keV because hydrogen has one electron per atomic mass unit while oxygen has one electron per two atomic mass units (due to the presence of neutrons in the oxygen nucleus); thus, in order that the product $\mu \rho$ gives correct weighting to electron density for both hydrogen and oxygen, the attenuation coefficient of hydrogen is twice that of oxygen. The curves of Figure 15 have essentially the same shape for energies greater than 50 keV so that the water-foam system can be employed to simulate the liquid-vapor hydrogen system effectively.

At 662 keV, an energy which corresponds to the cesium-137 gamma-ray, the characteristic length in hydrogen is

$$\lambda_H = (.154 \text{ cm}^2/\text{gm})^{-1} (.071 \text{ gm/cm}^3)^{-1}$$

$$= 93 \text{ cm}$$

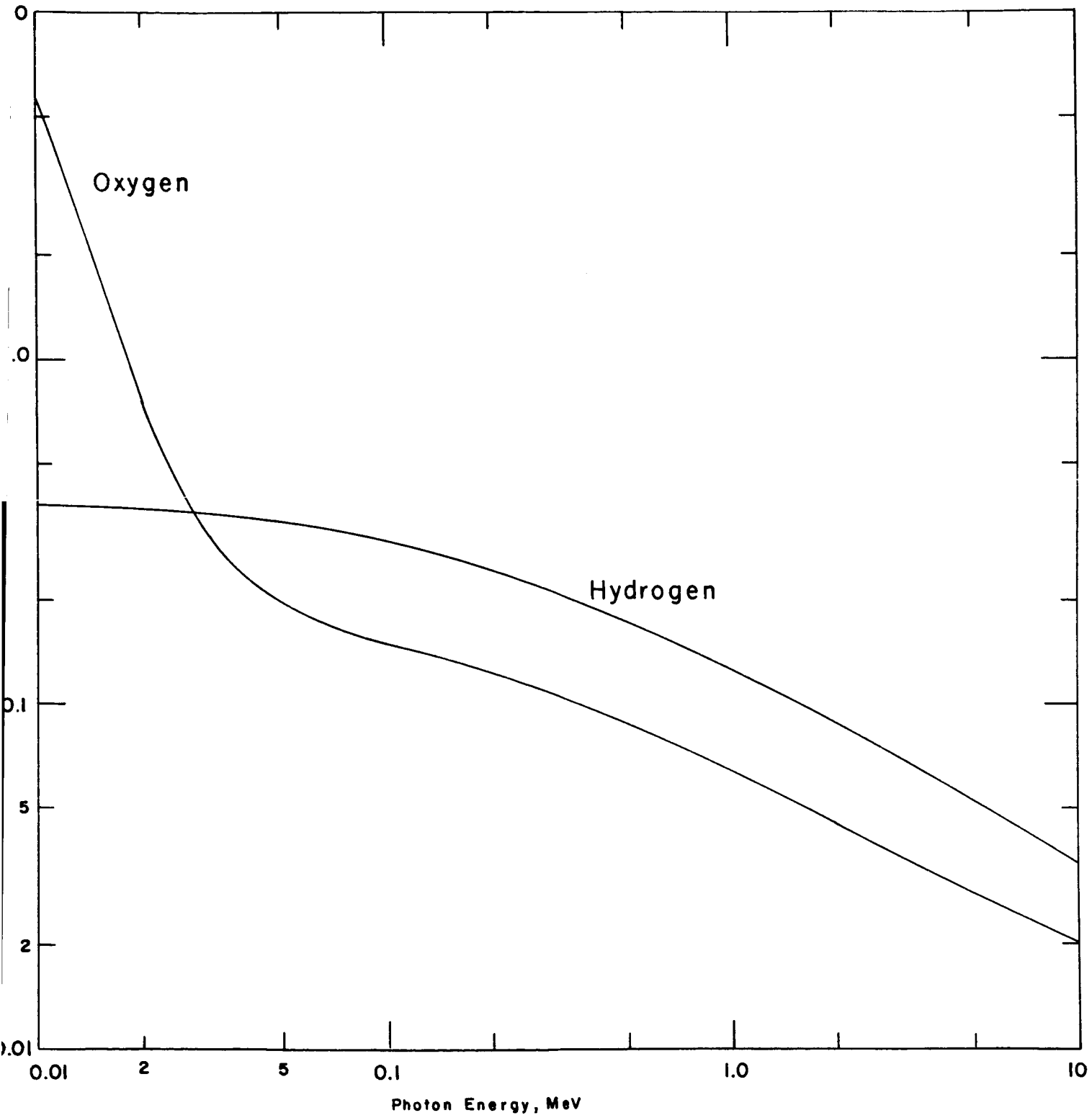

Gamma Attenuation Coefficient, μ, as a Function of Photon Energy for Oxygen and Hydrogen

Figure 15

while the characteristic length in water is

$$H_2O = (.086\ cm^2/gm)^{-1} (1.00\ gm/cm^3)^{-1}$$

$$= 11.7\ cm\ .$$

In view of the scaling of characteristic lengths, a liquid hydrogen system can be correctly simulated by a one-eighth linear scaled water system. The characteristic length correctly scales so that the correct similitude depicted in Figure 16 is accomplished by the water system. Some additional features of similitude scaling are discussed in Appendix D.

Large liquid-vapor hydrogen systems have been simulated by water systems in which large foam voids were inserted. The foam was selected to possess a density of about 0.02 gm/cm^3 so that the ratio of the characteristic length in water to that in foam was about 1/50, the ratio identical with the liquid-vapor hydrogen system. Simulation of the transmission technique in hydrogen tanks up to 25 feet in length was achieved with a cylindrical tank 3' 6" high by 3' in diameter. Additional tests have been performed using a 3' high by 2' in diameter cylindrical tank with a hemispherical bottom. Figure 17 pictures the cylindrical tank on the test stand with a source and detector mounted on a movable "O"-frame for the simulation of zero gravity gamma transmission measurement systems. Foam voids inserted into the water-filled tanks effectively simulated the propellant configuration depicted in Figure 1a.

Centered along the lower beam of the "O"-frame was a Cs^{137} source of either 20 or 50 millicuries. A lead collimator was employed to restrict the radiation to a narrow beam (ratio of half-maximum beam width to

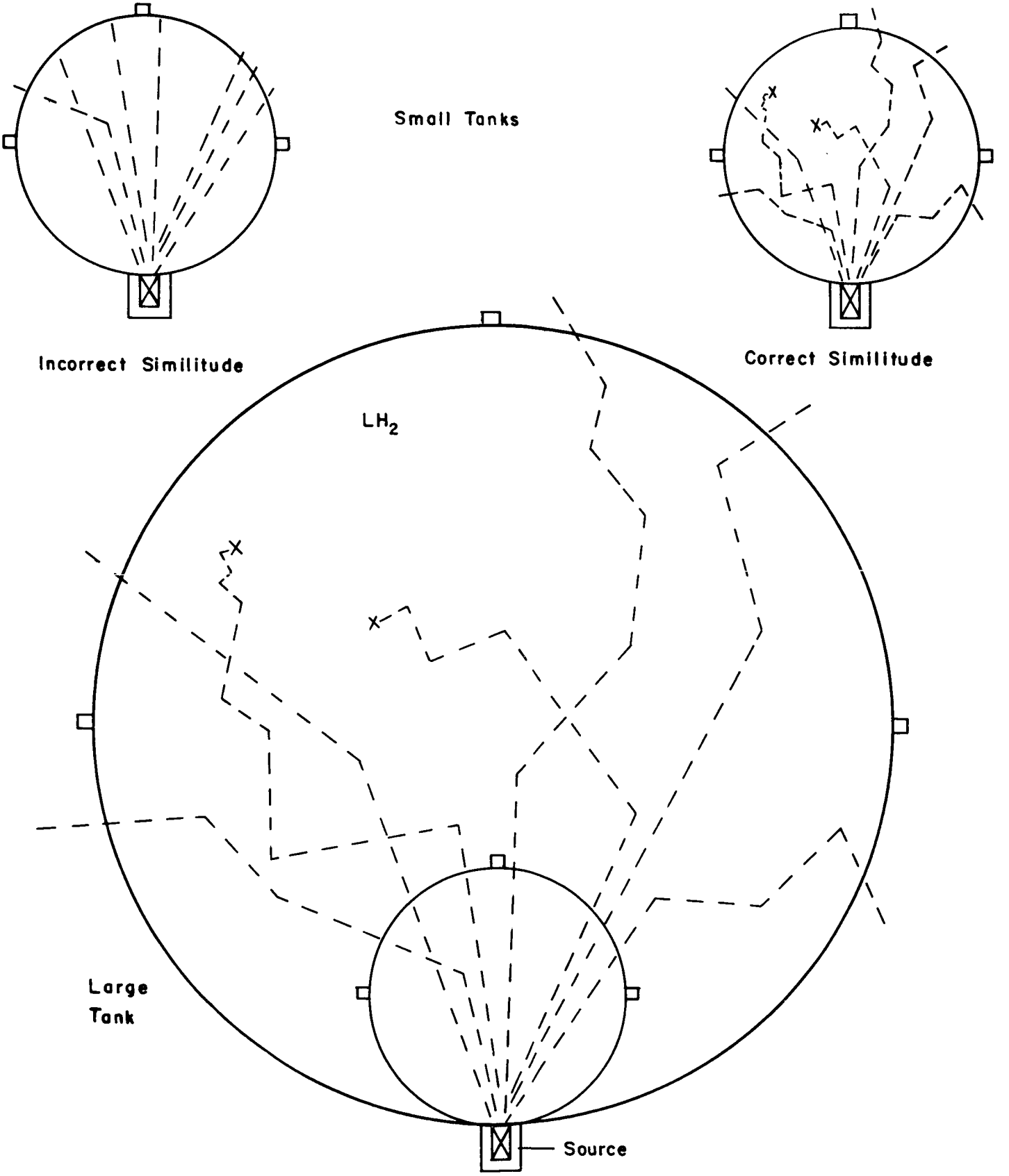

Comparison of Correct and Incorrect Simulation of Photon Paths in Small and Large Tanks

Figure 16

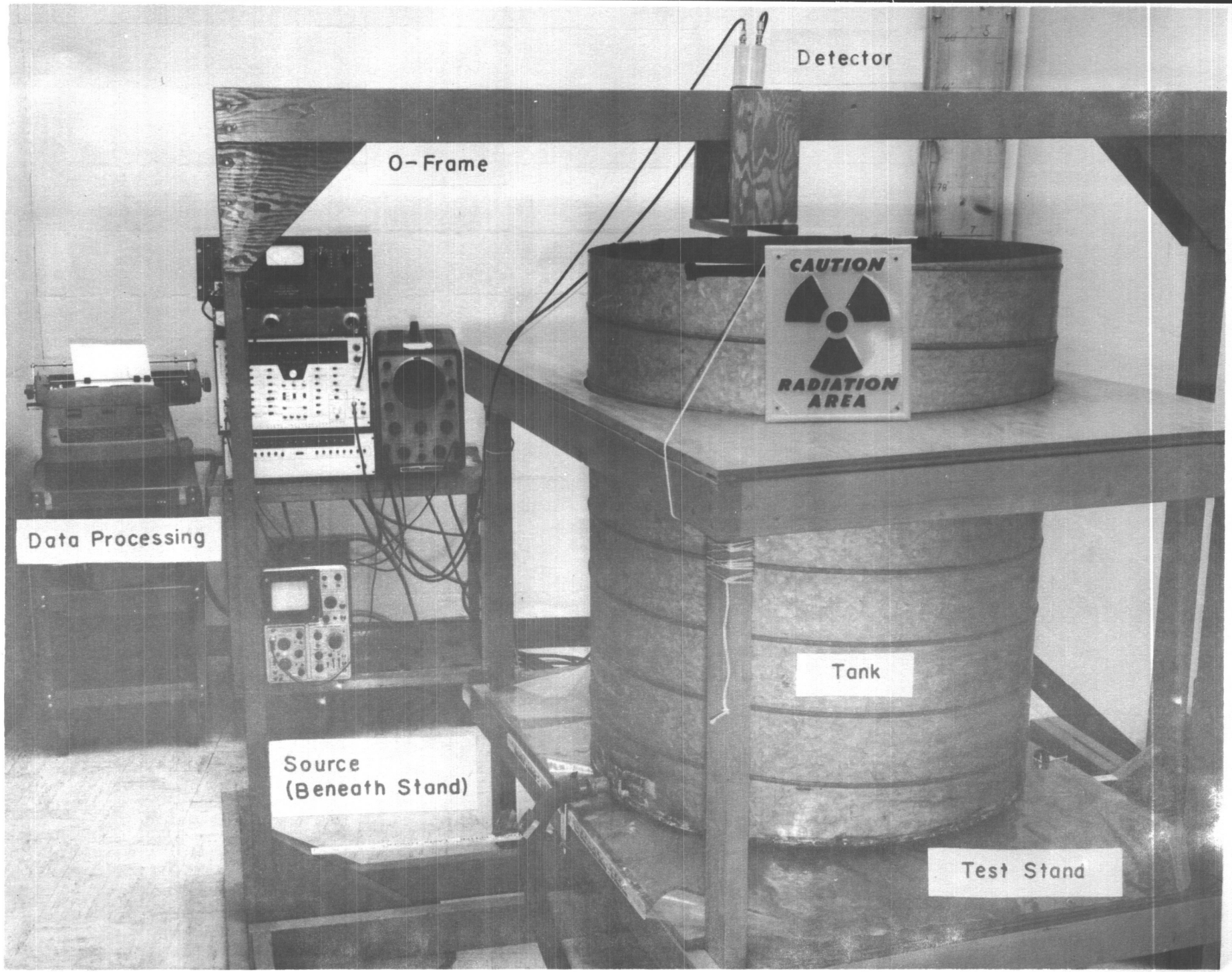

Figure 17 - Experimental Apparatus for Propellant Mass Measurements

distance from the source was approximately 0.1). Positioned collinearly with the radiation beam on the upper beam of the "O"-frame was a 2" x 2" NaI(Tl) crystal detector which possessed an efficiency of about 30% at the 662 keV cesium gamma energy. Electronic energy discrimination was employed to isolate the primary cesium radiation.

Measurements were made for numerous random locations of 20", 17", and 10" diameter foam spheres in the tanks, the large sphere occupying about 16% of the volume of the cylindrical tank and about 35% of the hemispherically-capped tank. The measurements were made by positioning the movable source-detector "O"-frame at the required sampling locations and noting the radiation attenuation for the 662 keV gamma photons; determination of "measured mass" was made by comparison of the individual radiation levels at the various sampling locations with calibration plots of count rate as a function of thickness of absorbing material and summing the appropriately weighted absorbing thicknesses to yield total mass.

Emphasis in the experimental program was directed toward the optimal array of twelve sampling locations since the computer studies indicated that about twelve locations were required to constrain measurement technique error to the 1% level. The source size and counting period were selected so that approximately 1% statistical counting error was expected for the maximum water thicknesses. Therefore, approximately 2% measurement system error was expected with the experimental configuration.

The results of measurements for the array of twelve sampling locations are indicated in Table 7. In several cases, errors in excess of 2% occurred;

Table 7. Experimental Zero G Simulations for Array of Twelve Sampling Locations

Experiment Number And Tank	Sphere Size (10^4 cm^3)	Total Volume (10^5 cm^3)	Per Cent Sphere %	Total Mass (10^5 gm)	Measured Mass (10^5 gm)	Error (10^5 gm)	Per Cent Error %
1. Cyl.	7.60	4.73	16	4.01	3.90	-0.11	-2.7
2. Cyl.	"	"	"	"	3.97	-0.04	-1.0
3. Cyl.	"	"	"	"	4.07	0.06	1.5
4. Cyl.	"	"	"	"	3.94	-0.07	-1.7
5. Cyl.	"	"	"	"	4.01	0.00	0.0
6. Cyl.	"	"	"	"	4.07	0.06	1.5
7. Cyl.	"	"	"	"	4.02	0.01	0.2
8. Cyl.	"	"	"	"	3.95	-0.06	-1.5
9. Cyl.	"	"	"	"	3.92	-0.09	-2.2
10. Hemi.	"	2.15	35	1.41	1.40	-0.01	-0.7
11. Hemi.	"	2.22	34	1.48	1.49	0.01	0.7
12. Hemi.	1.41	1.85	8	1.72	1.73	0.01	0.6
13. Hemi.	7.60	2.26	34	1.52	1.50	-0.02	-1.3
14. Hemi.	4.19	1.99	21	1.58	1.56	-0.02	-1.3
15. Hemi.	4.19	1.99	21	1.58	1.62	0.04	2.5
16. Hemi.	4.19	1.96	21	1.55	1.53	-0.02	-1.3

Cyl. - Cylindrical Tank

Hemi. - Hemispherically-capped Tank

Average Absolute Error 1.3%

the average measurement system error for the sixteen cases was 1.3%. A portion of the error can be attributed to calibration difficulties attendant to the flexibility of the source-detector "O"-frame, difficulties which would be minimized for an actual rigidly mounted system. Further experimental details, including a sample calculation in which the measured mass is computed from the raw data, are given in Appendix E.

Thus, system error was estimated from the experimental simulations. Throughout the course of the program, approximately 30 cases were investigated experimentally, 16 of the cases being for the optimal array of twelve sampling locations (reported in Table 7), the other cases being exploratory in nature for arrays of seven, ten, and fifteen sampling locations (reported in Appendix E). The experimental work indicated that 2% system accuracy could be attained through the monoenergetic transmission technique and verified that the error levels estimated by the 200,000 computer simulations were representative of physical systems.

3.1.1.5 Counting Statistics

Due to the statistical nature of radiation emission, interaction with matter, and detection, statistical fluctuations in the detected count occur, independent of other system variables. Typically, the statistical fluctuations can be described by

$$\sigma_N = \sqrt{N} \quad , \tag{3-6}$$

where σ_N is the standard deviation and N is the number of counts detected. The mathematical description of the statistical fluctuations proceeds from a binomial or Poisson probability model for radiation emission, interaction with matter, and detection, and the mathematical model is validated by experimental evidence. Radiation safety requirements establish an upper limit on the rate of photon emission by the source (Figure 18 indicates gamma flux equivalent to 1 r/hr as a function of gamma energy); as a result, the statistical counting error, $dN/N \simeq \sqrt{N}/N$, is of concern in high energy radiation information transmittal systems. As mentioned with respect to General Specifications, the 2% system accuracy requirement implies that the standard deviation of the statistical counting error should be constrained to the 1% level while flux levels must be constrained to 5 mr/hr at the tank surface.

Statistical counting requirements determine the source size for a particular application. Contingent upon the validity of the attenuation model, the primary count (N) for a fixed source-detector geometry is exponentially dependent on the thickness of interposed matter (x) so that

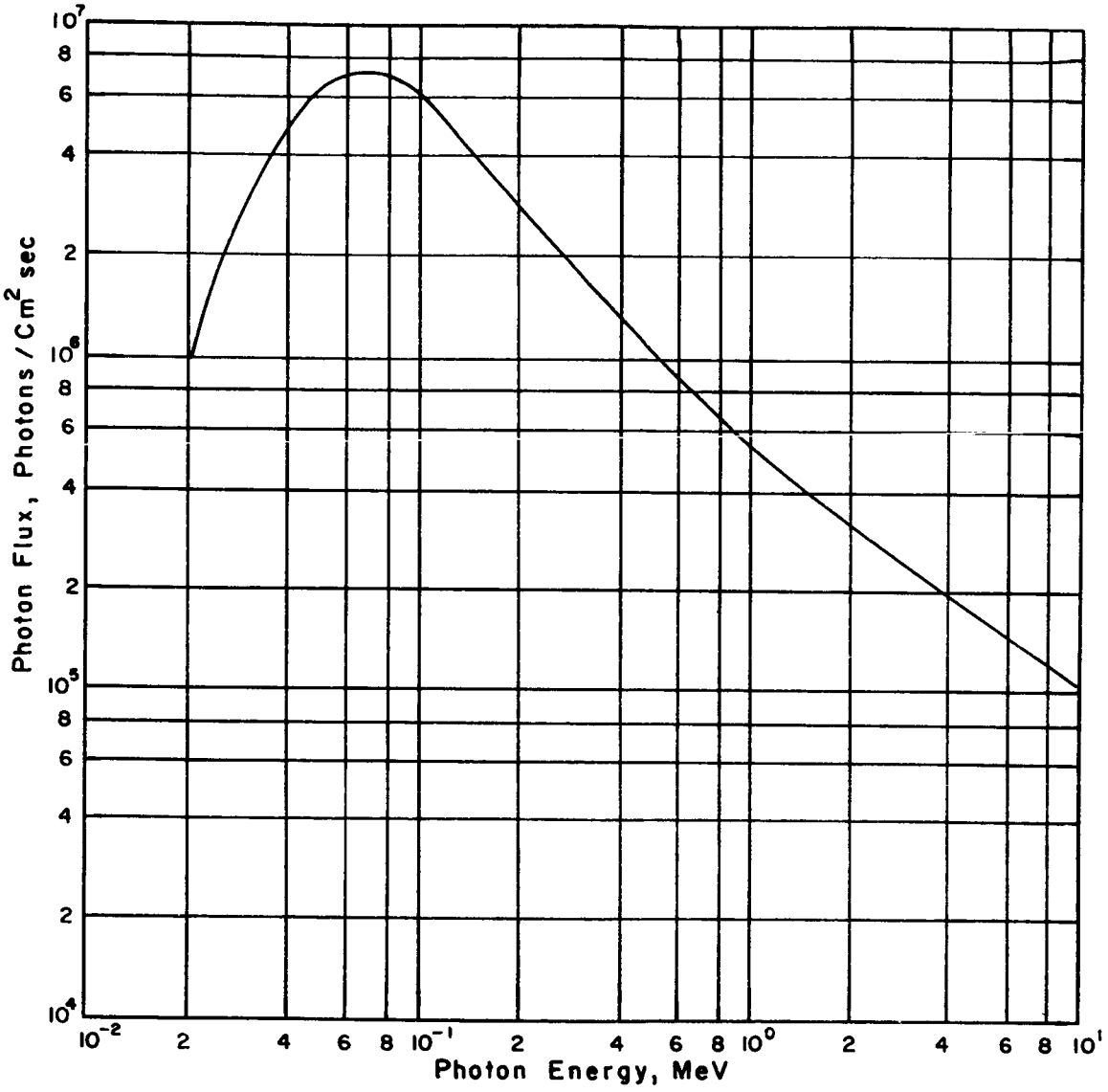

Gamma Flux Equivalent to One Roentgen Per Hour

as a Function of Gamma Photon Energy

Figure 18

$$N = N_o e^{-x/\lambda} \tag{3-7}$$

as described by Equation (3-1). Differentiation of Equation (3-7) indicates that fluctuations in the count obtained are interpreted as fluctuations in the thickness of interposed matter:

$$\left|\frac{dN}{N}\right| = \frac{dx}{\lambda} \quad , \tag{3-8}$$

or

$$\frac{dx}{L} = \frac{\lambda}{L}\left|\frac{dN}{N}\right| \quad , \tag{3-9}$$

where L is the maximum possible thickness of absorbing material, approximately equal to the source-detector distance. The quantity dx/L corresponds to the fractional error level, 0.01 for 1% accuracy. The one standard deviation fractional error is related to the full tank count as a result of Equation (3-9):

$$\left.\frac{dx}{L}\right|_{max} \equiv F = \frac{\lambda}{L}\,\frac{\sqrt{N_f}}{N_f} \quad , \tag{3-10}$$

where N_f represents the full tank count; that is, N_f is required when the maximum thickness of absorber is interposed between source and detector. Hence, the required count to yield a one standard deviation fractional counting error F is

$$N_f = \frac{\lambda^2}{F^2 L^2} = N_o e^{-L/\lambda} \quad . \tag{3-11}$$

The parameter N_o, the number of counts detected when the absorber is removed, is:

$$N_o = \frac{\lambda^2}{F^2 L^2} e^{L/\lambda} \quad . \tag{3-12}$$

Equation (3-7) becomes

$$N = \frac{\lambda^2}{F^2 L^2} e^{(L - x)/\lambda} \quad . \tag{3-13}$$

The fractional statistical counting error is much better than F when some of the absorber is removed ($x < L$):

$$\frac{dx}{L} = \frac{\lambda}{L} \frac{\sqrt{N}}{N} = F e^{-(L - x)/2\lambda} \tag{3-14}$$

so that

$$\frac{dx}{L} < F \text{ for } 0 \leq x < L . \tag{3-15}$$

The source strength in curies required to yield a maximum fractional counting error F is

$$S = \frac{4 \pi R^2 N_o}{\eta A_d T} (3.7 \times 10^{10} \text{ counts sec}^{-1} \text{ curie}^{-1})^{-1} \tag{3-16}$$

where A_d is the detector area, η the detector efficiency, T the counting time interval, and R the source-detector distance ($R \simeq L$).

Unfortunately, the existence of background noise requires the use of a source greater than that determined by Equation (3-16). Under full tank conditions, the detected count N_f consists of signal counts (N_s) and background counts (N_b):

$$N_T = N_s + N_b \quad . \tag{3-17}$$

The signal count can be extracted from the total count by various subtractive techniques, but the standard deviation of the total count is subject to fluctuations in both the signal count and the background count. As a result, Equation (3-10) indicates that

$$\left.\frac{dx}{L}\right|_{max} \equiv F = \frac{\lambda}{L}\left(\frac{N_s + N_b}{N_s}\right)^{1/2} \quad . \tag{3-18}$$

To achieve a fractional statistical counting error equal to or less than F at full tank,

$$N_s \geq \frac{\lambda^2}{2F^2L^2} + \left(\frac{\lambda^4}{4F^4L^4} + \frac{\lambda^2 N_b}{F^2L^2}\right)^{1/2} \tag{3-19}$$

Division of the right hand member of Equation (3-19) by λ^2/F^2L^2 yields the factor by which source strength in a noisy environment (S_b) must be increased over the source strength in a noiseless environment (S) in order to maintain the same statistical counting accuracy:

$$\frac{S_b}{S} = \frac{1}{2} + \left(\frac{1}{4} + \frac{F^2 L^2 N_b}{\lambda^2} \right)^{1/2} \qquad (3\text{-}20)$$

The full tank signal count required to give fractional statistical counting errors of one or two per cent as a function of background noise count is indicated in Figure 19 for various values of the ratio L/λ .

Statistical counting errors can be maintained at the 1% level without causing undue radiation hazard. For example, a cesium-137 transmission system of ten radiation beams can reach 650 cm of LH_2 (7λ) with 1% statistical counting accuracy and a flux level of less than 5 mr/hr at the detector under empty tank conditions when the radiation level is a maximum. The required count under full tank conditions is determined by noise limitations. In outer space, the background noise is not known with a great deal of certainty, but a reasonable estimate for a pair of 3" diameter by 3" thick crystal detectors in the 662 keV energy window is about 40 counts/second of background noise. For ten such detection units, a total noise count of 400 counts/second or 200 counts per 0.5 second response time can be expected. From Figure 19, the total detected count required to yield 1% accuracy is about 300 counts/0.5 second response time or 60 counts/second per detector pair. Since the detectors are about 30% efficient at 662 keV, a total of about 200 counts/second per detector pair is required.

From Equation (3-11), the empty tank count rate per detector pair would be

$$N_o = N_f e^{L/\lambda} = e^7 (60 \text{ cps}) = 6.6 \times 10^4 \text{ cps.}$$

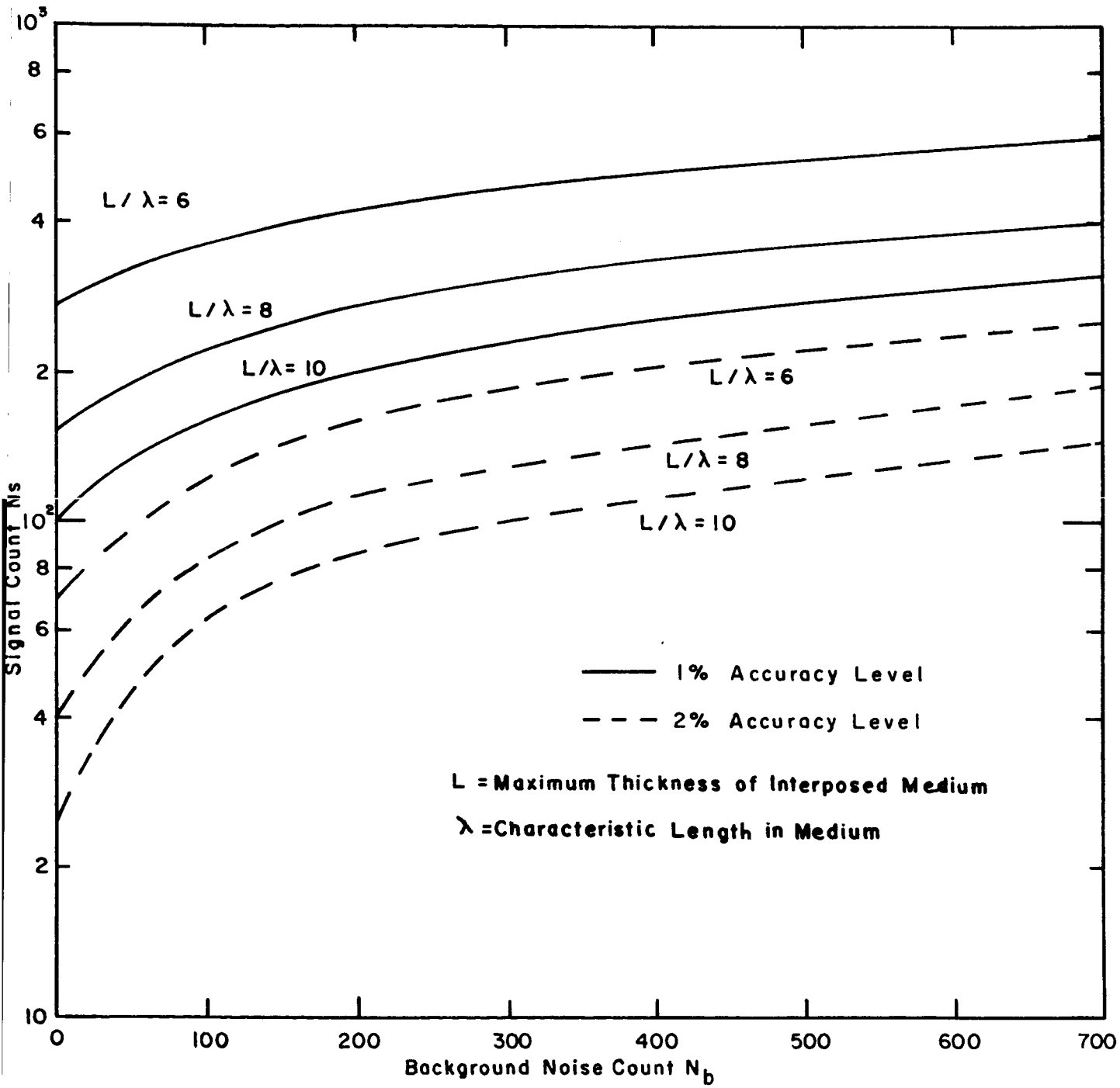

Signal Required for Certain Statistical Counting Accuracy as a Function of Noise.

Figure 19

The corresponding flux level at the detector would be

$$\phi_o = \frac{N_o}{\eta A_d} = \frac{6.6 \times 10^4}{0.3 \times 2 \times \frac{\pi}{4} (3 \text{ in} \times 2.54 \text{ cm/in})^2} = 2.4 \times 10^3 \frac{\text{counts}}{\text{sec cm}^2}$$

Figure 18 indicates that such a flux level corresponds to about 3 mr/hr.

Thus, a single transmission beam is capable of penetrating about 650 cm of LH_2, or about 21 feet. A system in which the sources are located in the center of the tank and the detectors are located at opposite ends of the tank is capable of providing a 2% zero gravity mass measurement for a 42-foot tank. Use of higher energy radiation increases the tank length for which the transmission technique is applicable, but the upper limit is about 30 feet for a single plane of detectors. Alternatively, the direction of radiation beams across the tank provides the required mass measurement for liquid hydrogen tanks of any length, as long as the tank diameter is less than 30 feet.

3.1.1.6 Tank Size, Shape, and Internal Structure Considerations

The number of sampling beams required to achieve measurement technique accuracy of 1% of tank capacity is independent of tank size (for the specified length-to-radius ratio of 4) as long as the radiation beams penetrate through the tank volume, but it is dependent on tank shape as long as only a small volume of the tank is sampled. Quantitative studies of the number of sampling lines required as a function of the tank length-to-radius ratio have not been pursued, but qualitatively, the required number of

sampling lines is inversely dependent on the length-to-radius ratio.

The restrictions imposed by the conflict between counting statistics and radiation safety requirements indicate that the gamma transmission technique is applicable with a single plane of detectors to liquid hydrogen tanks up to 30 feet long. With sources positioned within the tank and planes of detectors located at the tank extremities, the mass measurement can be provided for hydrogen in tanks up to 60 feet in length. However, due to the extremely short characteristic length of even high energy gamma radiation in liquid oxygen, the transmission technique is inapplicable for all but the smallest of oxygen tanks. The practical limit on transmission for a single plane of detectors is less than three feet of oxygen. Hence, the monoenergetic gamma transmission technique is applicable in general to the measurement of hydrogen mass in large tanks, but it is inadequate for the measurement of oxygen mass.

Fixed internal structures are of negligible concern for the radiation mass measurement systems since their sole influence is to cause a constant absorption and/or scatter of radiation, effects that can be eliminated through calibration. Similarly, lightweight movable internal structures (nylon baffles and the like) are essentially negligible due to their slight interaction with the radiation. Dense moving structures, however, are of serious concern as they cause a changing absorption of radiation that can be interpreted as mass changes. Detailed knowledge of the position of such structures is required to permit proper calibration to compensate for their

dynamic absorption properties. For low Bond number situations, the internal structures modify the tendency of surface forces to form spherical vapor bubbles, particularly for nearly empty tank situations, but the extent to which the structures affect the propellant location is not known at the present.

The most typical internal structures are expected to be static if heavy or light if movable; hence, it is expected that compensation for their presence either is not required or can be accomplished readily through proper calibration techniques.

3.1.1.7 Recommendations

The monoenergetic gamma transmission technique is applicable without internal structures to liquid hydrogen tanks of any length with diameters of thirty feet or less for sources and detectors located along the tank sides or for tanks up to thirty feet in length for sources and detectors located at the tank ends. With internal structures, the technique is applicable to any size of hydrogen tank. In general, the technique is inadequate for the measurement of liquid oxygen.

As indicated in Table 6, arrays of twelve or fifteen radiation beams parallel to the tank axis are capable of a measurement technique error of less than one per cent in the measurement of spherical vapor bubbles. The arrays of seven and ten beams are marginally satisfactory.

The prime disadvantages of the transmission technique are radiation hazard in accident situations (which must be minimized by source

encapsulation techniques) and interference with nuclear experiments. The latter disadvantage can be minimized by tightly-collimating the radiation beams (particularly for the system in which the sources are placed along the tank sides and directed across the tank into space), and by providing shutters for the sources. Other disadvantages include shielding weight (on the order of several hundred pounds) and inapplicability to certain propellant configurations (notably sausage-shaped bubbles).

The monoenergetic gamma transmission technique is recommended for zero gravity liquid hydrogen mass measurement; system details are given in Section 4.

3.1.2 X-Ray Transmission Techniques

Continuous radiation techniques can employ either nuclear bremsstrahlung or X-ray radiation. Since X-ray techniques offer certain advantages over nuclear bremsstrahlung techniques, attention is devoted to X-ray systems.

3.1.2.1 General Description and Applicability

X-ray sources, which emit a spectrum typified by Figure 5, find wide use in industry and medical practice. In these applications, there is no requirement for high stability of the source or monochromaticity of photon energies.

The total X-ray energy under the curve of Figure 5 is proportional to the square of the X-ray tube anode voltage for a fixed anode current.

Thus any X-ray tube which is to have output fluctuations less than 1 per cent must control the anode voltage to better than 1/2 per cent. Since other factors also affect the output, the anode voltage must be controlled to about 1/4%. Techniques used to circumvent the stability problem by monitoring the output and compensating with electronically variable gains in the detectors become quite complex.

Additionally, for compact X-ray tubes and power supplies, the anode voltage rarely exceeds 100 kilovolts. An examination of Figure 5 shows that the number of photons emitted with energy in electron volts equal to the anode voltage in volts approaches zero; in no case are photons emitted with energies in excess of the anode voltage. Figure 15 shows that the mass attenuation coefficient for hydrogen is 0.154 cm^2/gm at 662 keV for Cs^{137} and 0.295 cm^2/gm at 100 keV. Thus the mass absorption coefficient in hydrogen at 662 keV is 0.52 of that at 100 keV, so one could expect a 100 keV source to provide a penetration depth of approximately half that attainable with a 662 keV source. One might argue that a 100 keV X-ray source could be used through hydrogen for distances of 13 feet, if a 662 keV Cs^{137} source could be used for penetration depths of 25 feet. In many applications, this would be true if the X-ray source voltage were increased above 100 kV so that the number of photons with energies near 100 keV equaled the number of photons emitted by the 662 keV Cs^{137} source.

Weight considerations for an X-ray transmission measurement system depend largely on recent developments in the production of the small,

compact power supplies which have been reported. The use of a single high voltage supply and heavy high voltage cables connected to the individual units might prove to be less advantageous than the use of individual power supplies actually constructed around the X-ray tubes. High voltage insulation requirements in or near the propellants might be decisive.

Questions arise concerning the ability to develop a one-to-one correspondence between a function of detector outputs and the propellant mass within the tank. Since the X-ray spectrum is essentially continuous (relatively little energy is radiated in the characteristic X-ray peaks), it is difficult to isolate primary radiation (that radiation which has not interacted with the interposed matter) by the use of energy discrimination, a technique which permits the use of the unique relationship between count and thickness of interposed absorber given by Equation (3-2). It is difficult to establish a unique relationship between the detector signal received from diffused or scattered nuclear or X-ray radiation and the mass of fuel present for a practical number of detectors and sources if one is to require 2% accuracy for all cases. The problems of obtaining uniqueness with high accuracy with point detectors has been too superficially treated in many proposed approaches.

To assure uniqueness of the sampling system of twelve or fifteen sampling cylinders as recommended by this study, it is essential that each detector sense only interactions within its own associated cylinder. Since Compton scattering from other cylinders occurs with energy

degradation, one cannot select a band of energy within the X-ray energy spectrum but instead, one must utilize a band of the highest energies and exclude all lower energies. Figure 5 shows that this requirement is not compatible with conventional X-ray spectra unless exceedingly high requirements are placed on the stability of the source and detector electronics. In contrast, the monochromatic nuclear source is ideally suited to energy discrimination since the major fraction of the energy emitted is at a high discrete energy with a low energy plateau immediately below the discrete emission so that high stability in the electronics for discrimination is not required.

Collimation of the X-rays and/or the individual pulsing of source-detector pairs in time sequence does not solve the problem of uniqueness although it eliminates crosstalk. The difficulty regarding uniqueness arises from the fact that the measurement involves fuel thicknesses of many characteristic lengths which axiomatically implies complex, geometry dependent multiple scattering. Uniqueness requires that the detection technique be restricted to non-scattered photons or to photons scattered through a small angle. Energy discrimination with the selected energy band at the top of the energy spectrum must be used to assure that these requirements are met.

X-rays can be produced which approximately meet the monochromatic requirement if the low energy photons are usable and the low efficiency associated with the method of photon production can be tolerated. The

technique involves using the continuous radiation (bremsstrahlung) produced from a heavy target such as uranium which is bombarded with an electron beam of the order of 125 keV. The bremsstrahlung produced is allowed to strike a material of lower atomic number such as lead. The lead, which has an absorption edge at 88.0 keV and a $K_{\alpha 1}$ emission line of 74.9 keV, then isotropically emits a $K_{\alpha 1}$ line. Platinum or iridium or a PtIr alloy can be used as a filter since their absorption edges are at 78.4 keV and 76.1 keV, respectively. This procedure provides a "line" spectrum at 74.9 keV whose energy bandwidth is probably narrow enough to be used with energy discrimination and collimation, especially if the pulsed time sequential mode of operation is used to eliminate cross-talk and scatter from adjacent beams.

The energy discrimination technique of assuring uniqueness of interaction volume and output signal becomes more difficult as the energy is lowered. This can be understood from the energy formula for Compton scattering, which is

$$T = \frac{0.196\, E_o^2\, (1 - \cos\phi)}{1 + 0.196\, E_o (1 - \cos\phi)} \quad , \qquad (3\text{-}21)$$

where T is the energy loss of the incident photon in the collision (equal to the energy gain of the ejected electron), E_o is the energy of the incident photon, and ϕ is the angle between the direction of the incident photon and that of the scattered photon. T and E_o are measured in MeV. It is readily obvious from Equation (3-21) that the fractional energy loss

$\left(\frac{T}{E_o}\right)$ for E_o less than 1 MeV is approximately proportional to E_o; therefore, it is of the order of $\frac{662}{75} \approx$ 8 times more difficult to use energy discrimination in Compton scattering at 75 keV than it is at 662 keV.

Experimental tests would have to be run with all of the elements in place to determine how well the low energy X-ray technique would work in actual measurements.

An alternative approach in which the total radiation count is considered ignores the primary radiation and depends on a non-exponential relationship between count and interposed mass. Such an approach takes advantage of build-up, whereby the majority of the photons reaching the detector has been scattered. However, inclusion of build-up in the data processing destroys the uniqueness of the relationship between count and interposed mass.

The adverse effect of build-up on the unique interpretation of detected count for a transmission measurement scheme in which the thickness of the absorber is interpreted from an inverse function of the count rate is indicated in Figure 20. Typical photon paths are indicated by the solid lines; the dashed lines in the upper illustration correspond to the photon paths in the lower diagram. In the lower diagram, more photons reach the detector than in the upper diagram, despite the fact that more absorbing material is present. In contrast, the number of non-interacting photons (exemplified by beam 2) is the same in both cases. Thus, if build-up is included in order to increase the count rate, the one-to-one correspondence

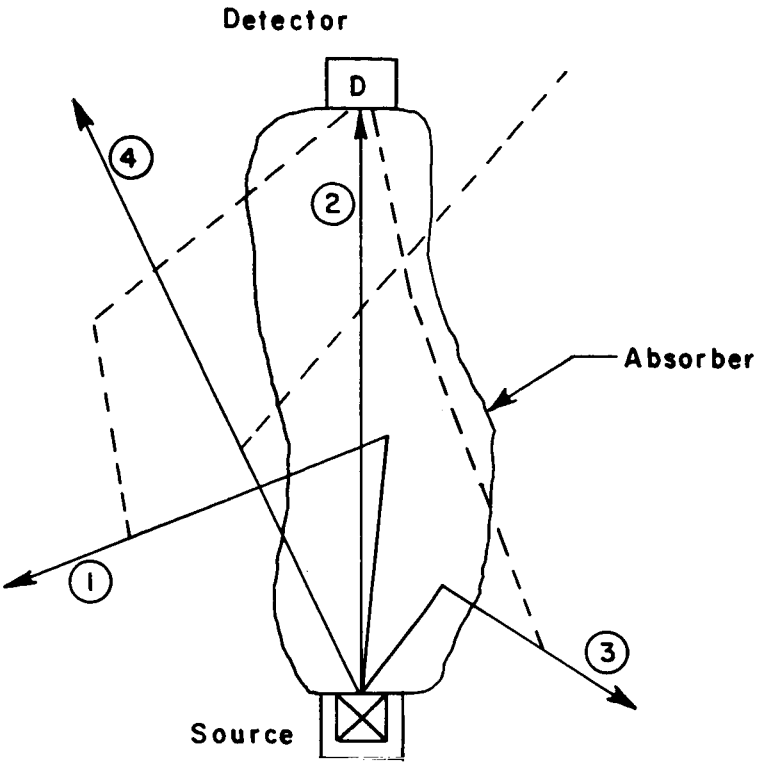

Figure 20a

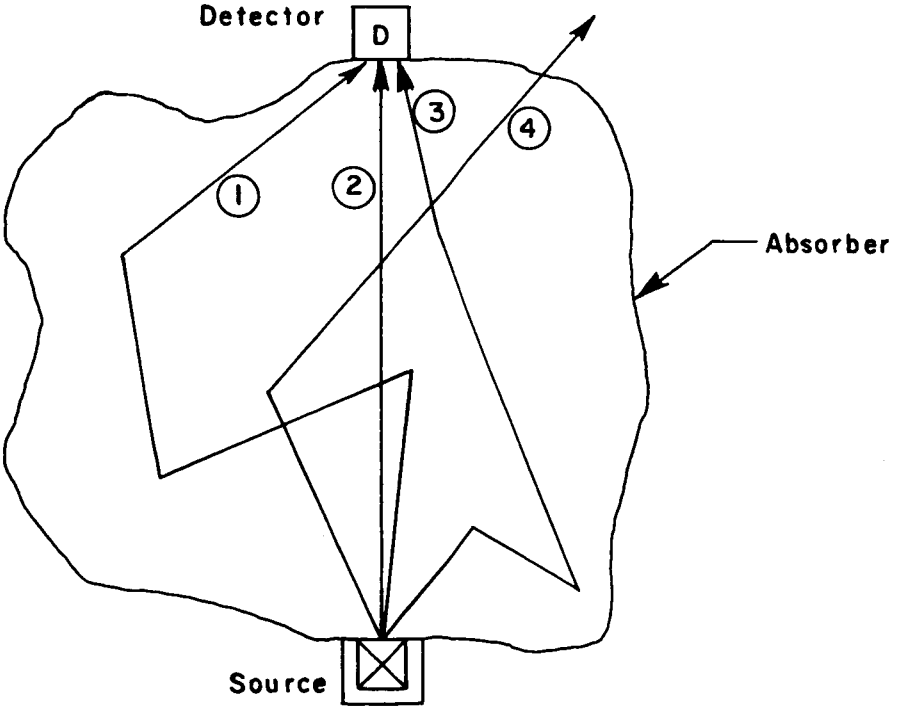

Figure 20b

Geometry Dependent Effects of Buildup on Photon Count.

Figure 20

between count rate and absorber thickness is destroyed. Figures 20a and 20b depict an extreme example; nonetheless, they illustrate the unintelligibility of build-up information in the unique determination of propellant mass between source and detector.

The effects of build-up on count rate are indicated in Figure 21, experimental data relating one minute counts to the thickness of a water absorbing medium for a 20 mCi cesium-137 source. At 662 keV, the energy characteristic of the cesium-137 photons, the characteristic length is 11.7 cm in water, 11.2 cm in liquid oxygen, 93 cm in liquid hydrogen. The lower curve indicates the count rate in the 662 keV energy window; the upper curve indicates the total count rate. The contribution of build-up to the total count rate is evidenced by the non-logarithmic behavior of the total count rate.

As the figure indicates, deviation in the logarithm of the count rate exceeds 2% at about 90 to 95 centimeters, a distance corresponding to about 8 characteristic lengths. For this particular experiment, the spurious nature of the count rate for extreme water thicknesses is due to a background of about 10 counts/second, as described by Figure 19 and Equation (3-19).

Even under ideal conditions in which the uniqueness between the propellant mass and the count at the detector can be optimized so that 2% measurement technique accuracy can be obtained, consideration of the total count fails to produce any significant range extension due to a

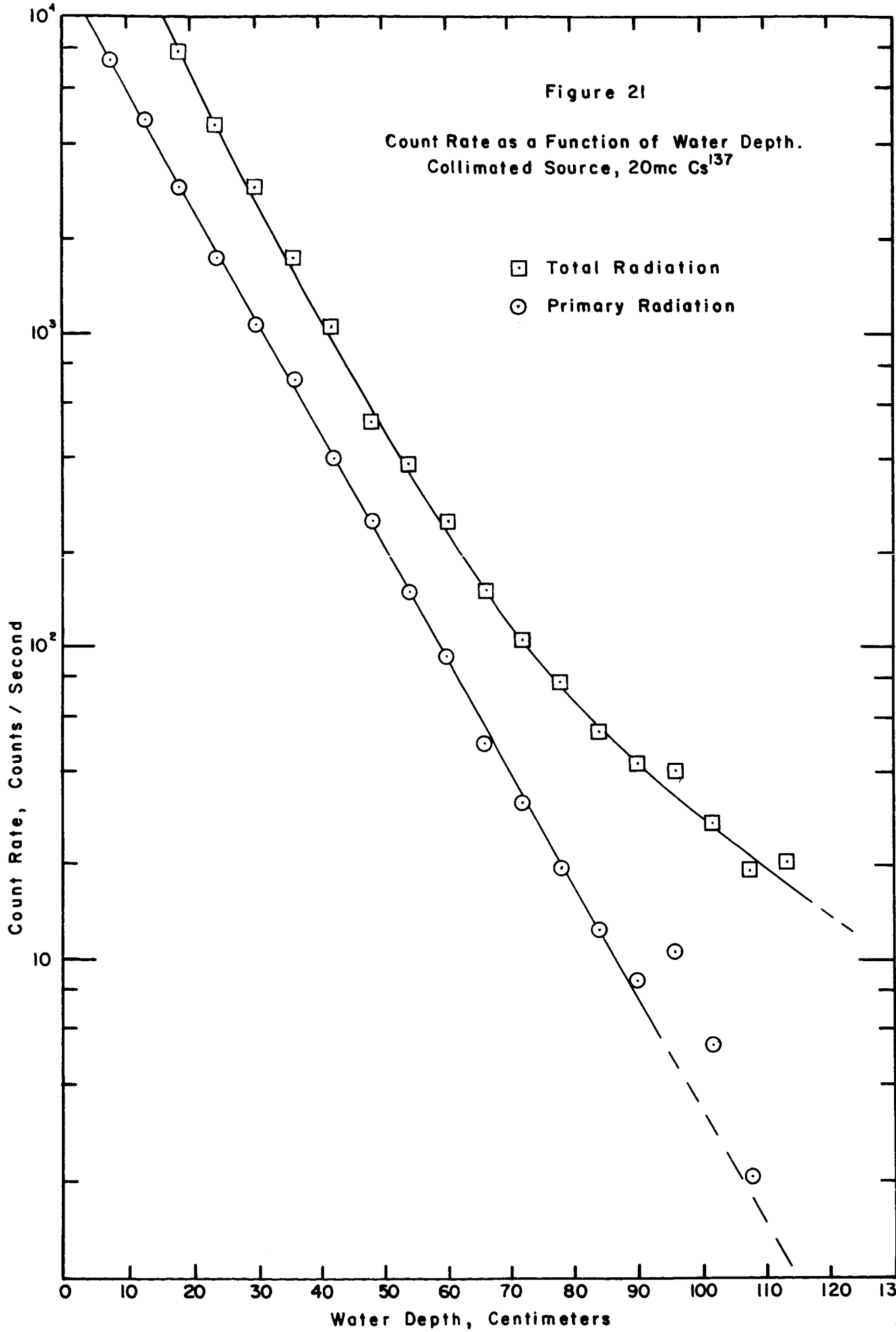
Figure 21
Count Rate as a Function of Water Depth.
Collimated Source, 20mc Cs137
Total Radiation
Primary Radiation
Count Rate, Counts / Second
Water Depth, Centimeters
10⁴
10³
10²
10
0
10
20
30
40
50
60
70
80
90
100
110
120
130

flattening of the curve relating count rate to penetration distance through the absorber.

The build-up factor can be modeled as a geometry-dependent multiplier of the primary count:

$$N_t = B N_p \quad , \tag{3-22}$$

where N_t is the total count, N_p the primary count, and B the build-up factor. The build-up factor exhibits complex geometrical dependences and can be determined for given geometries only by sophisticated numerical techniques and experimentation. An approximate function, appropriate in some geometries, exhibits an exponential dependence on thickness of absorber[5]

$$B \approx e^{b x/\lambda} \quad , \tag{3-23}$$

where b is a positive coefficient ($0 \leq b < 1$). As a result of Equations (3-1), (3-22), and (3-23), the total count may be written

$$N_t \approx N_o e^{-x/\lambda (1 - b)} \quad . \tag{3-24}$$

Differentiation of (3-24) yields

$$\left| \frac{dN_t}{N_t} \right| = \frac{(1 - b)}{\lambda} dx \quad . \tag{3-25}$$

Therefore,

$$\left. \frac{dx}{L} \right|_{max} \equiv F = \frac{\lambda}{L(1 - b)} \frac{\sqrt{N_{t_f}}}{N_{t_f}} , \tag{3-26}$$

where N_{t_f} is the full tank total count.

Since the factor (1 - b) is less than unity, the fractional counting error F is more sensitive to count fluctuations in N_{t_f} than in N_{p_f} (full tank primary count), as comparison of (3-26) with (3-10) indicates. Compensation for the increased sensitivity is provided by the increased count since $N_t > N_p$. The extent of the compensation can be determined by numerical evaluation of (3-26) and (3-10). In general, the increased sensitivity of fractional counting error to fluctuations in the count due to the flattening of the total count curve implies that 1% counting accuracy requirements cannot be achieved beyond about ten characteristic lengths (of the primary or highest energy radiation) consistent with the 5 mr/hr safety requirements.

3.1.2.2 Recommendations

The most promising X-ray transmission system is one in which the "on" cycle of various source-detector pairs is commutated to eliminate crosstalk, and energy discrimination in a high energy band of filtered characteristic radiation is employed to permit detection of primary photons so that a geometry-independent exponential relationship between count at the detector and interposed mass such as Equation (3-2) illustrates can be employed. For such a system, the characteristic length for the high energy X-rays is about one-half that for cesium or cobalt monoenergetic gamma emitters so that the technique would be effective for

hydrogen tanks up to about 25 feet in length. The required commutation scheme would influence system response time and count loss; by pulsing groups of three or four widely separated radiation beams at a time, counting times on the order of 200 milliseconds per detector could be achieved so that the 0.5 second response time requirement could be met without encountering severe count loss problems. However, since only a small fraction of the X-ray energy would be of concern, high flux levels might be required at the detectors, even under full tank conditions so that feedback control of the X-ray generation might be required if filtering of the undesirable radiation does not prove effective. Hence, the discriminated high energy X-radiation transmission system might be subject to electronic complexity in order to attain 2% system accuracy.

With respect to X-ray transmission techniques, it is recommended that an experimental study be initiated to determine the ability to produce and use monochromatic high energy X-rays. The technique of employing a 125 kV X-ray tube and a uranium target to generate considerable high energy bremsstrahlung, and directing this bremsstrahlung onto a lead target appears feasible. If the energy spectrum obtained can be made sufficiently intense in a relatively narrow energy band, the need for commutation of X-ray tubes along with its attendant electronic complexity might be eliminated. Range studies and zero gravity simulations could be achieved with water and water-foam systems as they were achieved in this study for cesium-137 radiation. Industrial Nucleonics Corporation is

constructing a 125 kV X-radiation source and would be capable of implementing the X-ray generation and range studies with existing test fixtures and apparatus. The recommended study should lead to conclusions regarding the necessity of feedback control and commutation of the X-ray tubes as well as the experimentally determined ranges of penetration and measurement system accuracy.

3.1.3 Diffusion Techniques

Diffusion measurement systems are those in which the detection of radiation is accomplished with little regard to the direction from which the radiation strikes the detector. In general, the total radiation count is considered and the development of a unique correspondence between some function of the detectors and the mass in the tank is dependent on a clever location of sources and detectors.

3.1.3.1 General Description and Applicability

Serious question arises concerning the ability to determine a one-to-one correspondence between propellant mass and a function of the outputs of the detectors. The geometrical effects of build-up considered for X-ray systems are exaggerated if no directional information is extracted from the radiation. Consideration of total radiation count is incapable of 1% statistical counting accuracy beyond about ten characteristic lengths, even independent of the geometrical effects. In addition to the dependence of the count rate on the geometrical location of the propellant due to build-up,

diffusion techniques are subject to the unintelligibility of crosstalk between sources and detectors. An example which indicates the magnitude of crosstalk errors for a sistuation in which a flat liquid surface assumes various orientations in the tank is given in Appendix C.

It is not possible to prove that no location of numerous sources and detectors can be found such that measurement technique error is less than one or two per cent for the arbitrary fuel configurations given in Figure 1 while permitting the existence of and taking advantage of crosstalk and build-up. Every prospective configuration must be examined individually; very few guiding principles are available with which to reduce an infinite number of possible configurations to a tractable number. Even the use of high speed computers fails to compensate for a lack of guiding principles. As a result, it can only be stated that, on the basis of errors typically associated with measurements in which crosstalk and build-up predominate, it is highly unlikely that a source-detector configuration exists capable of 1% measurement technique error.

3.1.3.2 Recommendations

Diffusion techniques are not recommended because they fail to provide a one-to-one correspondence between propellant mass and some function of the detector outputs. The two phenomena most significantly responsible for the lack of a unique correspondence are count rate dependences on geometrical location of propellant due to build-up, and unintelligible crosstalk. It is improbable that any source-detector configuration exists in

which measurement technique error of 1% or less is attainable.

3.1.4 Scattering Techniques

Scattering measurement systems are based on appropriate measurements of scattered radiation only so that the detectors are placed such that the primary radiation detected is minimized. In general, the primary radiation beam is collimated and measurement is made of the scattered radiation at certain angles to the collimated beam. Backscatter devices measure the radiation that has been scattered through 180^{o}.

3.1.4.1 General Description and Applicability

As mass sensitive techniques, scattering methods are subject to the same difficulties that beset diffusion techniques, namely, count rate dependence on geometrical location and unintelligible crosstalk. Precise evaluation of scattering systems is dependent on sophisticated numerical analysis.

Probably the most relevant data concerning the use of scattering or diffusion techniques for fuel tank measurements have been calculated by M. O. Burrell of George C. Marshall Space Flight Center (N62 14720 NASA TN D-1115). The results of a part of his Monte Carlo calculations concerning an 18.4 foot high by 30 foot diameter liquid hydrogen cylinder (right circular) are shown in Figure 22. A 1 MeV gamma source was located on the axis of the cylinder 11.25 feet from an end of the cylinder. The curves (A), (B), and (C) represent the relative number of photons

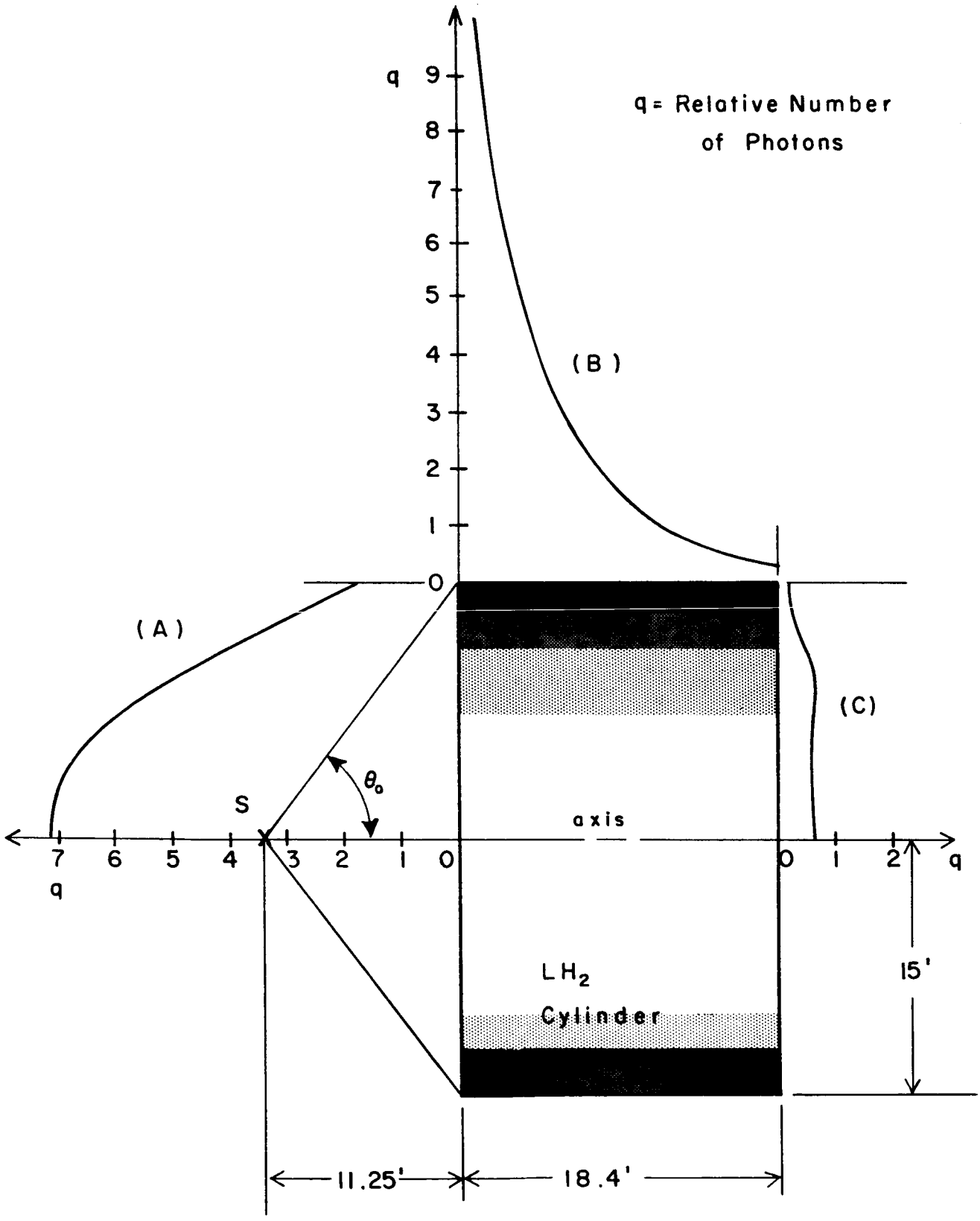

Relative Number of Photons per Unit Area Escaping Through LH Cylinder Wall for External Source Collimated Through Half Angle θ_o

Figure 22

escaping per unit area of cylinder wall at various positions around the cylinder. The cut-off energy was taken at 25 keV in the Monte Carlo calculation, an appropriate energy for fuel tank applications since photons with energies of less than 25 keV would not penetrate through the aluminum walls of an actual fuel tank.

Even though the photon flux distribution within the tank is not explicitly calculated, it is apparent that the change in flux within and around the cylinder is quite significant. No simple solution of fuel quantity measurement is apparent and it is highly doubtful that any optimized solution can be obtained even with a sophisticated computer analysis.

Again, it is difficult to establish a unique correspondence between the mass within the tank and a function of the detector outputs.

3.1.4.2 Recommendations

Scattering techniques are not recommended as mass sensitive measurement schemes because it is improbable that any one-to-one correspondence between propellant mass and a function of detector outputs can be found accurate to one per cent. For scattering techniques, gross count rate dependences on the geometrical location of the propellant due to build-up and unintelligible crosstalk are chiefly responsible for the lack of unique correspondence.

3.2 Volume Sensitive Measurement Schemes

Three fundamental radiation techniques are volume sensitive in nature. These techniques are shadow methods, logic methods, and tracer techniques. Pressure and/or temperature measurements must accompany the sensing of volume so that propellant mass can be inferred.

3.2.1 Shadow Techniques

Shadow measurement systems comprise those systems in which a "shadow", or low radiation flux region, is cast by interposed matter on a large detector. A fundamental feature of the shadow system is the extent of sources and/or detectors over one or more dimensions. An example of a typical shadow system is given in Figure 23a, in which a line source and line detector extend along the entire tank. The mass interposed between source and detector prevents low energy radiation emanating from the source from reaching the detector; essentially, a radiation "shadow" is cast on the detector. In certain variations, either the source or detector may be degenerated to point size, but the mated unit must extend significantly over one or more geometrical dimensions, as depicted in Figure 23b.

Since the detector outputs are functions of the geometrical extent of the shadows cast by the mass in the tank, the shadow measurement methods are volume sensitive in nature despite the fact that the interaction between the radiation and matter is mass sensitive.

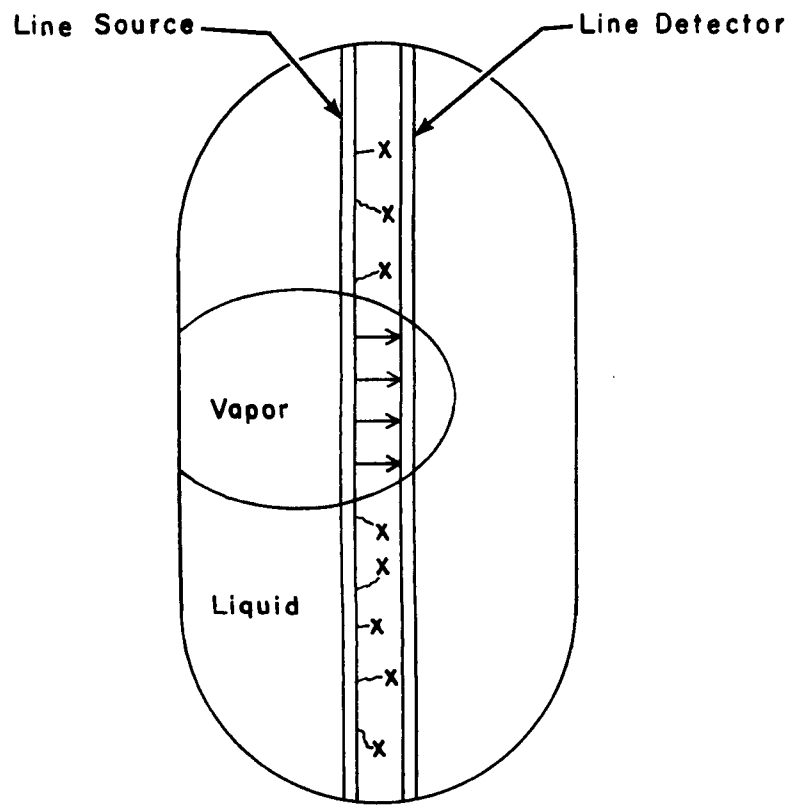

(a) High&Low Bond Number Applications

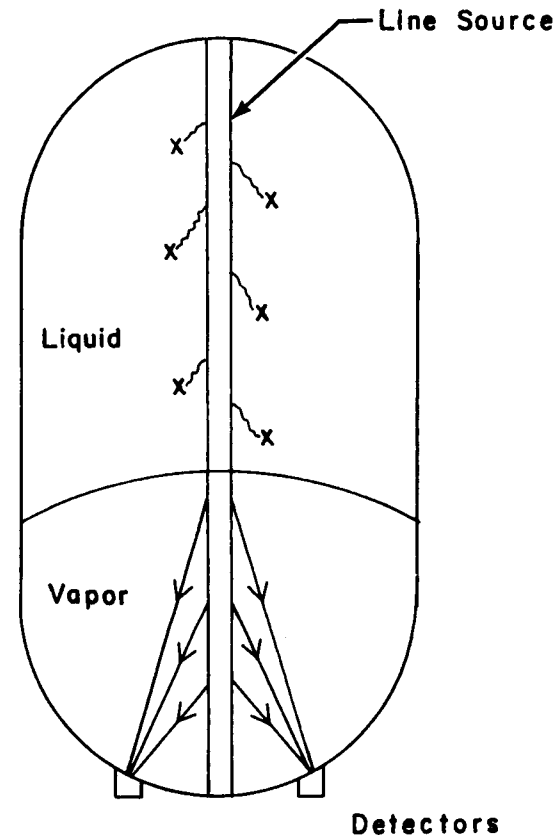

(b) High Bond Number Application

Shadow Measurement Systems

Figure 23

3.2.1.1 General Description and Applicability

Shadow measurement systems may take on a variety of appearances dependent upon the geometrical extent of the sources and detectors. A representative system consists of pairs of line sources and detectors positioned parallel to the tank axis as shown in Figure 23a. The sampling techniques considered for the monoenergetic gamma transmission system are readily applicable to the shadow system; the collimated monoenergetic gamma radiation beams can be replaced by pairs of line sources and line detectors, the source and detector of a particular pair being spaced only a few centimeters apart.

A one-to-one correspondence between the detector outputs and the mass interposed between the line sources and the line detectors can be established. Individual line sources must be collimated so that the direct radiation beams are incident upon and stopped by detectors, thus minimizing crosstalk between source-detector pairs. The back of the detectors can be covered with material of high atomic number in order to prevent radiation from passing through them and interfering with other detectors.

If such a collimated source-detector pair is immersed partially in propellant liquid and propellant vapor as shown in Figure 23a. The detector signal is

$$S = \text{const}\,(\ell_v + a\ell_\ell), \qquad (3\text{-}27)$$

where ℓ_v is the length exposed to vapor, ℓ_ℓ the length exposed to liquid,

and a the ratio of signal attenuation in liquid to that in vapor for the source-detector distance. The signal can be conditioned to yield an output dependent on the mass in the tank. Since the total length is

$$\ell = \ell_v + \ell_\ell \quad , \tag{3-28}$$

the signal can be interpreted

$$S = \text{const} \left[a\ell + (1 - a)\ell_v \right] = S_0 + S_1 (1 - a)\ell_v \quad . \tag{3-29}$$

Therefore,

$$\ell_v = \frac{S - S_0}{S_1 (1 - a)} \quad , \tag{3-30}$$

and the mass surrounding the source-detector pair can be approximated by

$$M_i = A_i W_i (\rho_g \ell_{v_i} + \rho_\ell \ell_{\ell_i}) , \tag{3-31}$$

analogously to Equation (3-3) for gamma transmission. Low energy radiation is preferred to high energy radiation so that S_0, the constant component of the signal, is small in comparison with the variable component of the signal. Thus the shadow technique is capable of providing a unique correspondence between a function of the detector outputs and the mass in the tank.

Precisely the same weighting and sampling considerations hold for the shadow technique as for the gamma transmission technique. Statistical

considerations indicate that, due to the proximity between sources and detectors, a relatively weak low energy source is required for the shadow techniques as compared to a strong high energy source for the gamma transmission technique. X-rays may be employed as the gamma source. For an X-ray system, a collimated X-ray beam would have to be directed through an empty tube and scattered into the tank from various sites along the tube.

3.2.1.2 Recommendations

The shadow techniques are capable of providing a one-to-one correspondence between propellant mass and a function of the outputs of the detectors. Shadow techniques perform adequately in either liquid hydrogen or liquid oxygen tanks since the distances between the line sources and detectors are no more than a few characteristic lengths. The primary disadvantage of the shadow techniques is that they require internal tank structures. The primary advantages are that the techniques are applicable to both liquid hydrogen and liquid oxygen tanks of any size, and that required radiation levels are low.

Thus, shadow systems are recommended for both liquid hydrogen and liquid oxygen applications in which internal structures are allowed. Details of a backscatter shadow technique are presented in Section 4.

3.2.2 Logic Methods

Logic measurement systems are defined as those systems in which

numerous source-detector pairs are positioned according to certain patterns throughout the tank in order to interrogate isolated volume increments concerning the existence of propellant liquid within them. (In the truest sense of the word "logic", all systems employ logic methods.)

3.2.2.1 General Description and Applicability

In general, a large number of spot detectors distributed throughout the tank volume provides a sufficient number of sampled volume increments with which an estimation of total mass can be made. Typically, the spot detectors make a logical decision, the decision whether or not mass is located between the source and detector, although operation in an analog mode is feasible (even in analog operation, most of the source-detector pairs would be immersed in liquid or vapor entirely). The no-fuel count rate is not determined statistically for this on-off gauge. It is only necessary that the count rate clearly exceeds background.

The per cent of the detectors which are in the fuel on the average equals the per cent of the tank which is filled with fuel. The electronic analyses need determine only the total number of detectors which are in the fuel, but not which ones. A series or parallel circuit in which the total impedance or some other single parameter is sensed should suffice. The readout is discrete with a number of values equal to the number of logic elements immersed in the propellant.

The standard deviation of the gauge varies with the amount of fuel in the tank. At full or empty tank, the gauge necessarily reads correctly.

Under the assumption of a random distribution of fuel, the a priori probability that a particular spot unit is immersed in liquid is p, the fractional volume of liquid when the tank is partially filled. The probability that any number m of spot units is immersed in liquid is binomial:

$$P(m) = \frac{K!}{m!\,(K - m)!}\, p^{m}\, (1 - p)^{K - m} , \qquad (3\text{-}32)$$

where K is the total number of spot units within the tank. The expected or average value of m is

$$E(m) = Kp , \qquad (3\text{-}33)$$

and the standard deviation is

$$\sigma = \sqrt{Kp(1 - p)} , \qquad (3\text{-}34)$$

which is a maximum for $p = 0.5$. For 100 spot units in a half-filled tank of randomly oriented propellant, the average value of m is 50 with a standard deviation of 5. The number of units required to constrain $\sigma \leq 1\%$ for the half-filled case is 2.5×10^{3}. In actuality, the location of the fuel is not random so that the possibility of reducing the number of spot units by proper patterning exists, but it is doubtful whether the required number of units can be reduced by an order of magnitude.

Thus it is possible to establish a one-to-one correspondence between propellant mass and the output of a logic system, but such a large number of separated units is required that the logic system appears somewhat

impractical. It is applicable to any size of hydrogen or oxygen tank in which internal structures are permitted.

3.2.2.2 Recommendations

A unique relationship between propellant mass and a function of the outputs of the detectors can be established for a logic system. Implementation of such a system is closely related to the implementation of the shadow system mentioned previously; that is, rather than being distributed at random throughout the tank, the spot units would be located along sampling lines so that a recommended logic system would closely resemble the shadow system described previously and in Section 4.

3.2.3 Tracer Methods

Tracer methods comprise those methods in which a radioactive element is dispersed throughout either the liquid or vapor phase of the propellant and detected at various geometric locations. Detection of the radiation emanating from the vapor phase can be accomplished at a single point, while detection of tracer in the liquid phase generally requires an array of detectors.

3.2.3.1 General Description and Applicability

Tracer injected into the vapor phase of a propellant rarifies as the vapor phase occupies an increased fraction of the tank volume. Detection of this rarification can be accomplished by measuring the radiation emanating from a constant shielded volume of vapor. Several difficulties

are inherent in such a measurement.

First, it is difficult to maintain the tracer in the vapor phase. Effectively, the tracer in the vapor rarifies if there is any propensity for it to dissolve in the liquid phase. For typical situations in which the tank is vented, tracer must be continually injected into the vapor phase, a process which requires constant recalibration of the measurement technique. Second, for some random configurations of propellant, the proper locations of both injection apparatus and detection apparatus are difficult to determine. Third, the existence of foam and numerous vapor bubbles within the tank does not permit the tracer to uniformly diffuse throughout the vapor phase.

Internal structures are required for the detection of tracer injected into the liquid phase. Since the tracer does not rarify or concentrate as liquid is expended, a measurement of the total radiation emanating from the liquid is required. Hence, detection of tracer in the liquid must be accomplished as described for the shadow and logic systems.

The physical means of tagging either hydrogen or oxygen poses significant problems. Tritium might be employed for hydrogen, but it is expensive and its emitted decay radiation, 18 keV beta particles, is difficult to detect. All of the radioactive isotopes of oxygen have short half-lives. Contaminants might be employed as tracers and neutron activation methods might be used, but in general, such methods appear too complex in view of the other available methods.

3.2.3.2 Recommendations

Tracer techniques are not recommended due to the complexity of tracer injection and detection for hydrogen and oxygen. Typically, the detection apparatus required is similar to that already described for shadow and logic techniques so that no advantage over these other volume sensitive techniques can be derived. Tracer techniques have a natural application to systems in which bladders are employed for propellant management, but otherwise they are less satisfactory than other volume sensitive techniques.

4.0 RECOMMENDED NUCLEONIC MASS MEASUREMENT SYSTEMS

Two nucleonic systems are recommended for the measurement of mass in low Bond number regimes. Evaluation of accuracy capabilities is made in Section 3; detailed description of the recommended systems is given in this section. A system which makes use of the monoenergetic gamma transmission technique as evaluated in Section 3.1.1 is capable of providing 2% system accuracy for hydrogen tanks up to about 30 feet in length without internal structures and up to about 60 feet in length with a single plane of sources located within the tank. A system which makes use of the shadow technique as evaluated in Section 3.2.1 is capable of providing 2% system accuracy for hydrogen or oxygen tanks of any size, though internal structures must be employed. Both systems are capable of better than 2% accuracy in high Bond number regimes.

4.1 Monoenergetic Gamma Transmission System

Emphasis is devoted to transmission systems in which the radiation beam is directed through the tank parallel to the axis of the tank. As indicated in Table 6, Section 3.1.1.3, the number of source-detector pairs required to achieve a given accuracy level is approximately doubled for transmission across the tank perpendicular to the tank axis; therefore, such systems are not emphasized.

Some features of high Bond number applications are considered in detail. In addition, basic system features such as the detection and data processing system and the source, shield, and detector requirements for various tank sizes are considered.

4. 1. 1 High Bond Number Application

In general, the monoenergetic gamma transmission system is capable of 1% measurement technique error in low Bond number situations for arrays of 12 or more sampling beams, as described in Section 3. 1. 1. 3. Under high Bond number conditions, the measurement technique accuracy is improved in general. However, when the flattened surface is situated parallel to the tank axis and radiation beams, gross measurement technique errors can occur. A high Bond number situation in which the liquid-vapor interface is parallel to the tank axis is indicated in Figure 24. As the top view of the array of fifteen beams indicates, as many as three or four radiation beams can experience a change from maximum to minimum attenuation with an incremental change in volume. Errors on the order of 25% of tank capacity are possible.

The gross measurement technique errors occur only when the liquid-vapor surface is parallel to the radiation beams. If the surface partially intersects a number of beams, the parallel array of beams produces an adequate estimation. It may be the case that the orientation of the liquid surface parallel to the tank axis is such a rarely occurring situation that it need not be considered. However, provision can be made for such an adverse orientation by locating two source-detector pairs symmetrically about the center of the tank, as indicated in Figure 24. The two pairs are capable of providing a measurement technique accuracy of 1% as long as the liquid surface is nearly planar; the parallel radiation beams provide

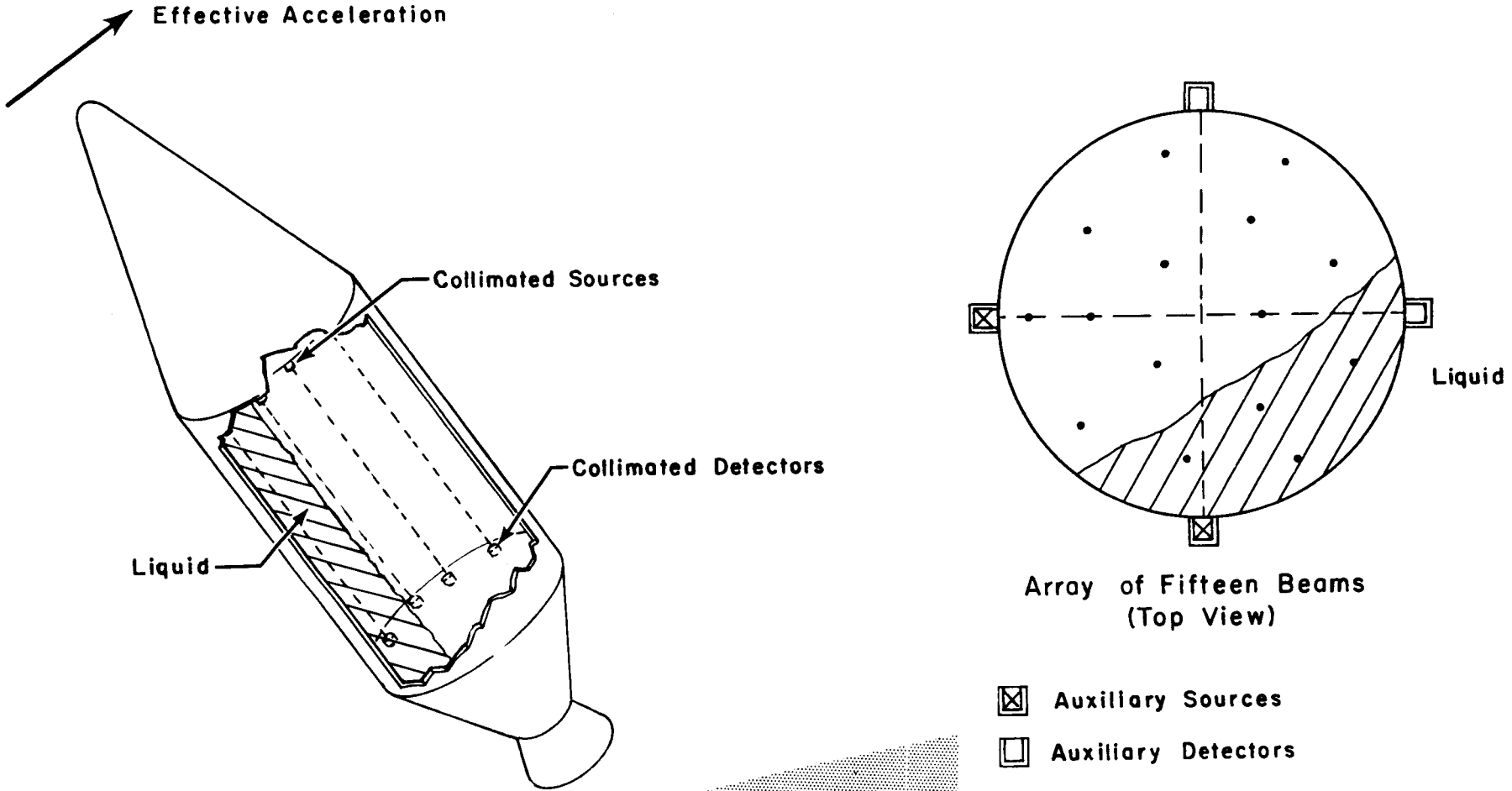

High Bond Number Orientation of Propellant Parallel to Tank Axis

Figure 24

1% accuracy when the surface deviates from its parallel attitude. Thus, compensation can be provided for even the worst high Bond number situations. Again, propellant configurations can be found in which the measurement system performs badly, but such configurations either occur extremely rarely or they fail to represent static situations.

Data processing for the adverse high Bond number situation must be accomplished logically. Data from the parallel beam array can be analyzed in conjunction with accelerometer data to determine whether any of the beams experiences maximum attenuation while an adjacent beam experiences minimum attenuation--an indication that the liquid-vapor interface is parallel to the tank axis. If the adverse high Bond number orientation is deemed to exist, the mass measurement is determined by the two auxiliary cross tank beams. Mass measurement by the cross tank beams must be effected by analog computations on the basis of logical decisions concerning whether or not the auxiliary beams are directed through liquid, vapor, or a liquid-vapor combination. The result of the logical decisions is to establish the location of the liquid-vapor plane; analog computations determine the mass in the tank from the location of the plane.

Therefore, the auxiliary radiation beams directed across the tank permit the estimation of propellant mass to within several per cent even under rarely occurring adverse high Bond number conditions. As a result, an average measurement technique error (absolute value) of better than 1% can be achieved for high Bond number environments.

4.1.2 Detection and Data Processing System

Photon detection is best achieved digitally so that energy discrimination of the individual pulses can be accomplished. Three types of detectors are applicable to the digital counting operation: proportional counters, scintillation-photomultiplier combinations, and solid-state devices. Of these detectors, the scintillation-photomultiplier combination offers the best efficiency in the detection of high energy gamma radiation.

Gamma sensitive scintillators exist in several forms: crystals, plastic solids, gases, and liquids. Two basic classes exist: detectors employing organic phosphors and those using inorganic phosphors. For both classes, the scintillator emits light pulses when a charged particle passes through. The light is subsequently collected at a photomultiplier cathode and ejected electrons are accelerated and multiplied in the dynode structure of the tube.

Limitations on response time and resolution are generally dependent on the phosphor type. Inorganic scintillators are on the order of 20% - 50% efficient; however, due to the delicate nature of the crystals, they are susceptible to cracking under thermally-induced stresses. Organic scintillators of the plastic type offer extreme ruggedness, but are less efficient than inorganic crystal scintillators. Typically, the plastic scintillators are about 5 - 10% efficient. Scintillator decay time (time required for light output to fall to e^{-1} of its initial value after the occurrence of a scintillation event) is of the order of tens of nanoseconds for plastic scintillators and 0.1 - 0.5 μ sec for crystal scintillators at cryogenic temperatures.

In general, photomultipliers require about 100 volts per dynode so that the required voltage for typical eleven-stage multipliers may be well over 1000 volts; electron transit time is on the order of 50 nanoseconds. Since the gain of the photomultiplier is roughly proportional to the eighth power of the voltage for an eleven-stage tube, a highly stabilized power supply is imperative. Photomultipliers are sensitive to magnetic fields and must be shielded by mu-metal for optimum performance to be realized. The multiplier phototubes are capable of operating at reduced temperatures, and, in fact, their noise is decreased in cold environments. Power supply stability and physical bulk comprise the major drawbacks of the scintillator-photomultiplier combination.

For some applications, cryogenically-cooled solid-state detectors may be superior to the scintillator-photomultiplier combination. The desirable features of solid-state detectors include good energy resolution, extreme compactness, and very high count rate capabilities. The undesirable features include a potential for radiation damage, noise sensitivity to the thermal environment, and low efficiency in the detection of gamma radiation.

The finite response time of scintillator-photomultiplier combinations is responsible for counting error at high count rates. Since arriving photons do not impinge on the detector at regular intervals but rather as described by a Poisson probability distribution, an appreciable number of counts is lost if the resolving time τ is comparable with the average period between

counts. If $\dot{m}$ is the observed counting rate, then the fraction of the time which the counter system is insensitive is $\dot{m}\tau$. Consequently, the number of counts lost per unit time is $\dot{n}\dot{m}\tau$, where $\dot{n}$ is the counting rate which would be observed if the resolving time were negligibly small. Therefore,

$$\dot{n} - \dot{m} = \dot{n}\dot{m}\tau , \qquad (4-1)$$

$$\dot{n} = \frac{\dot{m}}{1 - \dot{m}\tau} . \qquad (4-2)$$

Equation (4-2) may be rewritten

$$\dot{n} = \frac{(1 - y)}{\tau y} , \qquad (4-3)$$

where $y = \frac{\dot{m}}{\dot{n}}$, the fraction of detected photons that are counted. For one per cent accuracy in counting, electronic correction for the lost count can be made for situations in which the count loss is as high as 20% of the total count. Hence, the detector must have a resolving time τ sufficiently short that Equation (4-4) is satisfied:

$$\frac{\lambda^2}{T F^2 L^2} e^{L/\lambda} \leq \dot{n} \leq \frac{0.25}{\tau} , \qquad (4-4)$$

where T is the required response time.

The lower limit is established by the requirement of Equation (3-12) and the upper limit is established by Equation (4-3) for $y = 0.80$. The resolving time for the plastic scintillator-photomultipliers is about 50 - 100 n sec so that $\dot{n}_{max} \simeq 3 \times 10^6$ counts sec^{-1}/detector; resolving time for

the crystal scintillator-photomultiplier is about 0.2 - 1.0 μsec so that $\dot{n}_{max} \simeq 4 \times 10^5$ counts sec^{-1}/ detector. These maximum rates are not exceeded in the systems described in Section 4.1.3.

Figure 25 shows a simplified diagram of a data processing system which might be developed. The output of the system is the function $\Sigma_i \ln N_i$, which is a measure of the total fuel mass. A digital system (as opposed to an analog system) is suggested because "high" accuracy is required. The exact number of sources and detectors to be used must be determined from accuracy, cost, and system complexity considerations. The diagram shows data processing for twelve sources located in a plane within the tank and twenty-four detectors located at the tank extremities.

The output pulses from each detector are amplified and threshold detected by the window discriminators. If the pulse amplitude is too low (noise) or if it is too high (high energy), it does not pass through the window discriminators and is not counted. If the pulse amplitude lies within the "window", it passes through to the binary counters. The counters thus measure N_i, the signal count rate (counts/seconds) from each detector.

The pulse amplifiers can be integrated circuit video amplifiers or wide band operational amplifiers such as the Fairchild UA 709. The Fairchild UA 711 Dual Comparator is an integrated circuit window discriminator which could be used. Most other circuits in Figure 25 would use digital integrated circuits. Several versions of decade counters, or four flip-flops in one package, are available as a single integrated circuit. If the

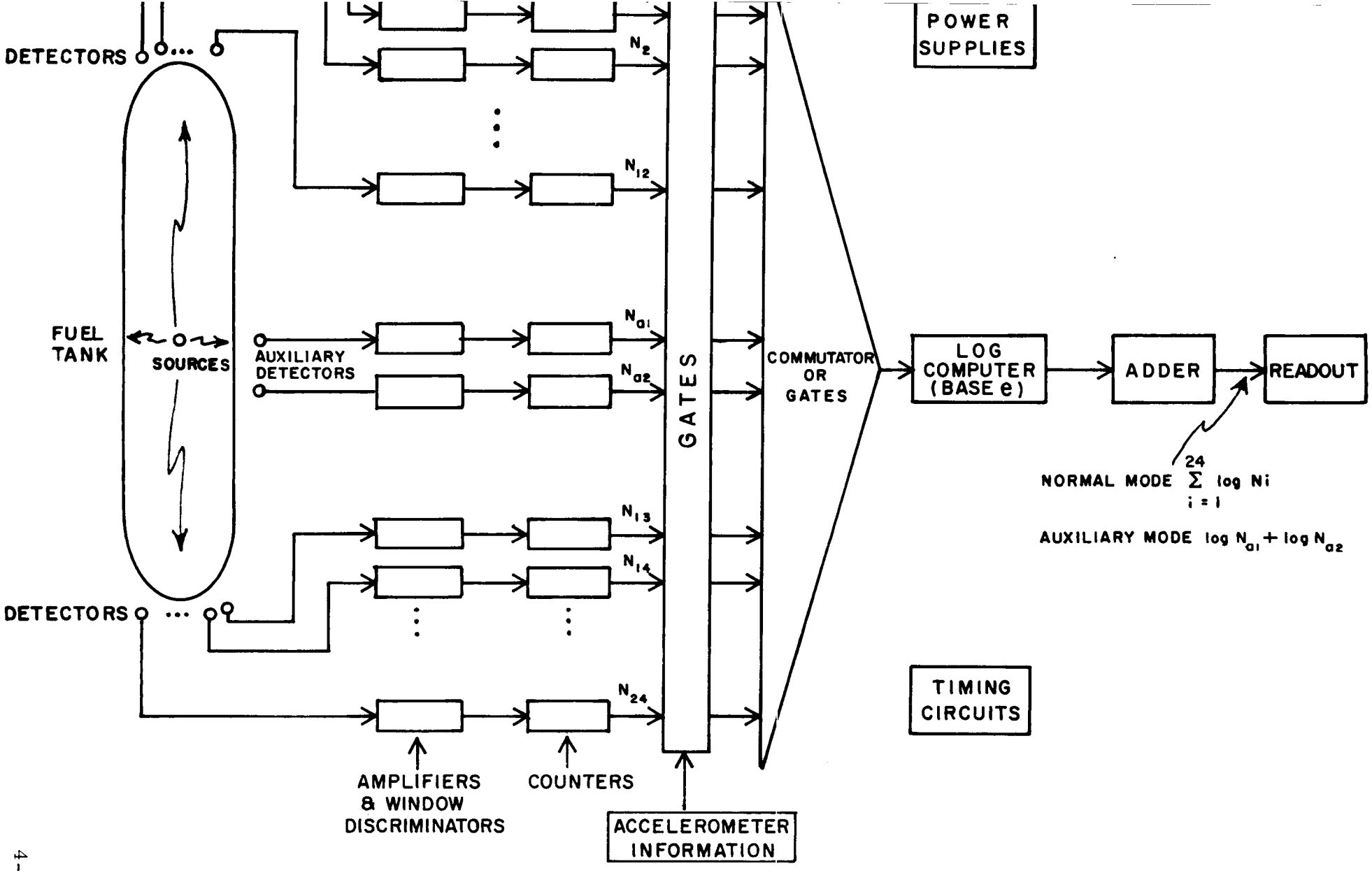

EXAMPLE SHOWN FOR 24 NORMAL MODE AND 2 AUXILIARY MODE DETECTORS

SIMPLIFIED SYSTEM DIAGRAM

FIGURE 25

relatively slow speed of serial arithmetic operations (as opposed to parallel operations) can be used, the multibit MOS shift registers by General Instrument would be useful. The MEM 3021, for example, has 21 bits in a single integrated circuit.

A separate counter is used for each detector instead of the sequential switching of a single common counter from one detector to the next. This is done so that no counts are "thrown away"; that is, the effective counting time for each detector channel is maximum. By counting "all" the signal counts, statistical fluctuations in the readout are minimized. The diagram thus assumes that the combination of desired system response time (effective counting time), maximum practical count rates, and desired system accuracy requires that no counts be "thrown away" in order to reduce the statistical fluctuations to an acceptable value.

The counter outputs are switched one at a time through the gates and commutator to the log computer. The accelerometer information tells whether to sum the 24 normal mode detector channels or the two auxiliary mode detector channels.

The log computer computes the natural logarithm (base e) of the output of each counter one at a time. Thus, when the input to the log computer is N_1 from counter number 1, the output of the log computer is $\ln N_1$. The adder calculates a running total sum of the logs, $\Sigma_i \ln N_i$. This total is a measure of the total fuel mass in the tank and is the output of the system. An alternative technique in computing the output $\Sigma_i \ln N_i$

is to form the product of all the N_i, $\pi_i N_i$, and then take the log of the product since the log of a product is equal to the sum of the logs: $\ln \pi_i N_i = \Sigma_i \ln N_i$. The readout box in Figure 25 is the interface between the system and the device (or person) using the fuel mass indication. It translates the system language (binary numbers) into the language or type of readout desired. Appropriate scaling and count loss corrections for each detector count rate must be performed in the counters preceding the log computer.

The use of a single common log computer assumes its computation time is fast enough to be time-shared by all detector channels. Such a log computer is the Radiometrics series TFC-80 non-linear digital function generator. A 10-bit version (1,024 increments) operates in 5 microseconds while a 12-bit version (4,096 increments) operates in 6 microseconds. An alternative, but probably more expensive, method would be to use a separate log computer in each detector channel. Serial type (continuous) digital log computers which might be used in this case are described in:

1. NASA Technical Note NASA TN D-3042,"Design of Real Time Computers Utilizing Counting Techniques", by George J. Moshos, Lewis Research Center, Cleveland, Ohio,
2. General Instrument Corporation Microelectronic Application Note, "MOS Integrated Digital Differential Analyzer", by J. D. Callan. This note describes use of the integrated circuit MEM 5021 Digital Differential Analyzer.

The timing circuits box in Figure 25 provides all the timing for the system. It comprises a multi-phase clock with various reset pulses for the counters, gating pulses, shift pulses, etc.

The power supplies box provides "high" voltage dc for the detectors and low voltage dc for the electronics. If the readout employs a digital visual readout, such as Nixie tubes, the power supplies must also provide a "medium" voltage for the tubes.

Note that if an X-ray system is used instead of the radioisotope system, a high voltage of between 100 kV dc and 150 kV dc would be required. Development and use of such a high voltage supply imposes weight limitations (the power supply must be oil-filled or gas-filled) and design problems to prevent high voltage breakdown, especially at the critical altitude.

4.1.3 System Parameters

Calculations are made concerning a number of system parameters for the gamma radiation transmission technique in liquid hydrogen. Five parameters--source size, shielding weight, detector size, dynamic count range, and the maximum radiation flux at the detector--are computed for various photon energies at different ranges for the arrays of seven, ten, twelve, and fifteen radiation beams. The photon energies considered are: 70 keV, 100 keV, 662 keV, and 1.2 MeV; the high energy sources correspond to monoenergetic gamma emission (Cs^{137} at 662 keV, Co^{60} at about 1.2 MeV) while the low energy sources correspond to X-ray and nuclear bremsstrahlung sources.

The structures associated with the sources consist of the source material, encapsulation, shield, and collimator for nuclear sources, and the source tube, power supplies, shield, and collimator for machine sources. For nuclear sources, the source material comprises a radioisotope highly concentrated for shielding and collimation economies. The source may be made quite small; for example, a two-curie source of cesium-137 (specific activity of 25 curies/gm, density of 3 gm/cm^3) can be concentrated into less than 0.03 cm^3, about the volume of a matchhead. In order that dispersion in accident situations is controlled, the source material is encapsulated in an integral unit with walls of a structurally strong material such as stainless steel. A bremsstrahlung target for nuclear β emitters may also be incorporated within the encapsulation structure, or high atomic number bremsstrahlung target material can be blended homogeneously with the source material. The source capsule is clad with shielding; physically, the capsule is usually mechanically fixed within the shield. Generally spherical in shape to maximize shielding thickness and minimize shielding weight, the radiation shield assures further source integrity in accident situations. According to NASA specifications, shielding must be provided so that the flux level at the tank surface is 5 mr/hr or less. The shielding weights are computed to meet a more stringent requirement of 5 mr/hr one meter from the source so that source handling hazards are minimized. Source collimators consist of additional shielding affixed in order to restrict the geometrical radiation pattern. Collimation of ten

per cent (ratio of half-width of radiation pattern to distance from the source) is readily achieved. A representative source structure is presented in Figure 26.

Compact X-ray tubes are currently available, most notably those commercially available from Machlett, but these tubes are generally of relatively low voltage (less than 150 kV) and hence, emit soft gamma-rays with little penetrating power (Figure 5 indicates that few photons are emitted with energies approaching the maximum electron energy; the mean radiation emission is at an energy of approximately one-third the maximum energy). X-ray tubes possess the advantage of requiring no moving parts for on-off control; power supply stability requirements represent a disadvantage. The photon flux level from an X-ray source is orders of magnitude greater than that available from nuclear sources, a feature of dubious value in this application since X-ray systems (as nucleonic systems) are subject to maximum radiation level requirements outside the tank, and hence, at the detector, so that upper limits on source strength are established. Commercially available X-ray power supplies are heavy (on the order of 75 pounds for a 200-kilovolt supply), but relatively lightweight supplies have been reported. Undoubtedly, the ultimate X-ray power supply development will incorporate the power supply around the tube as an integral part, thus eliminating the necessity for high voltage cables in proximity with the propellant and reducing the weight significantly; alternatively, a single power supply can be used for a number of sources.

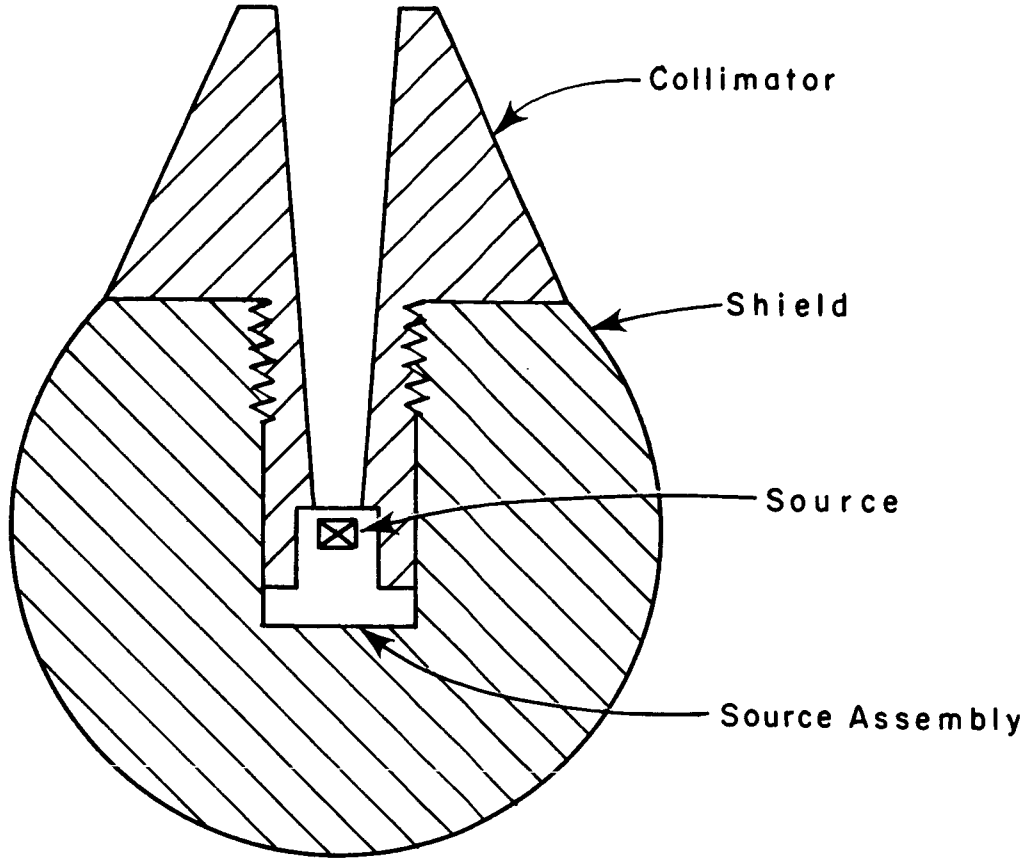

Source, Shield, and Collimator

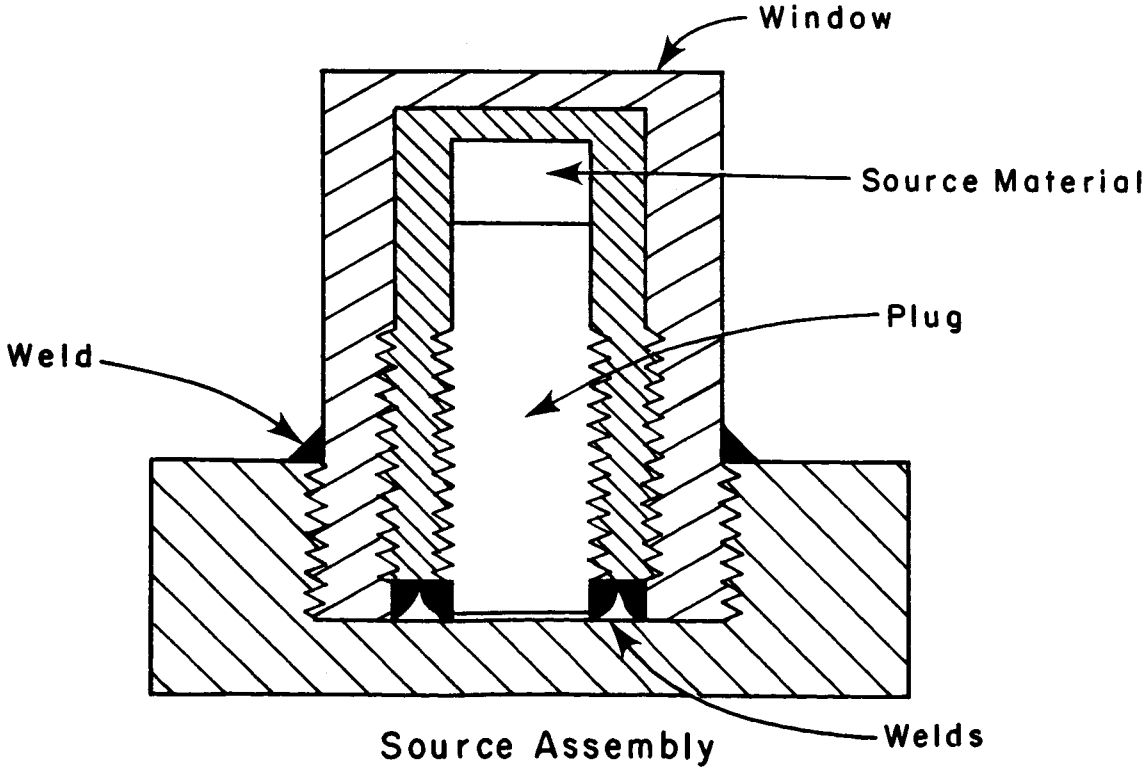

Source Assembly

Source and Associated Structures

Figure 26

Studies must be made to determine which approach is best. Collimation and shielding are achieved for X-ray sources as they are for nuclear sources.

The crystal detectors discussed in Section 4. 1. 2 are employed for all cases, although the low energy radiation may be detected adequately by cooled solid-state devices. Count loss for crystal detectors becomes excessive for count rates around 4×10^5 cps/detector. As shown in Figure 27, the efficiency of the 3" x 3" crystal detectors is about 25% for the high energy radiation (the efficiency of Tl-doped NaI crystals at room temperature is similar to that of pure NaI crystals at cryogenic temperatures).[6] The dynamic count range encountered in a particular situation expresses the change in count level as the tank changes from the full condition to the empty conditions. When the tank is empty, the flux level at the detector is at its maximum, a value restricted to 5 mr/hr.

Tables 8 - 11 indicate the system parameters as a function of range through the liquid hydrogen for the various source sizes. The standard deviation of the statistical noise is less than 1% and the radiation flux at the detector is less than 5 mr/hr except where otherwise noted. The tables are given for various ranges rather than for various tank sizes since the ranges for transmission through a hemispherically-capped tank are dependent on the distance of the sampling beam from the tank axis.

The tables indicate that the following factors limit the range of transmission through hydrogen:

(1) Flux at the detector exceeds 5 mr/hr for empty sampling cylinder,

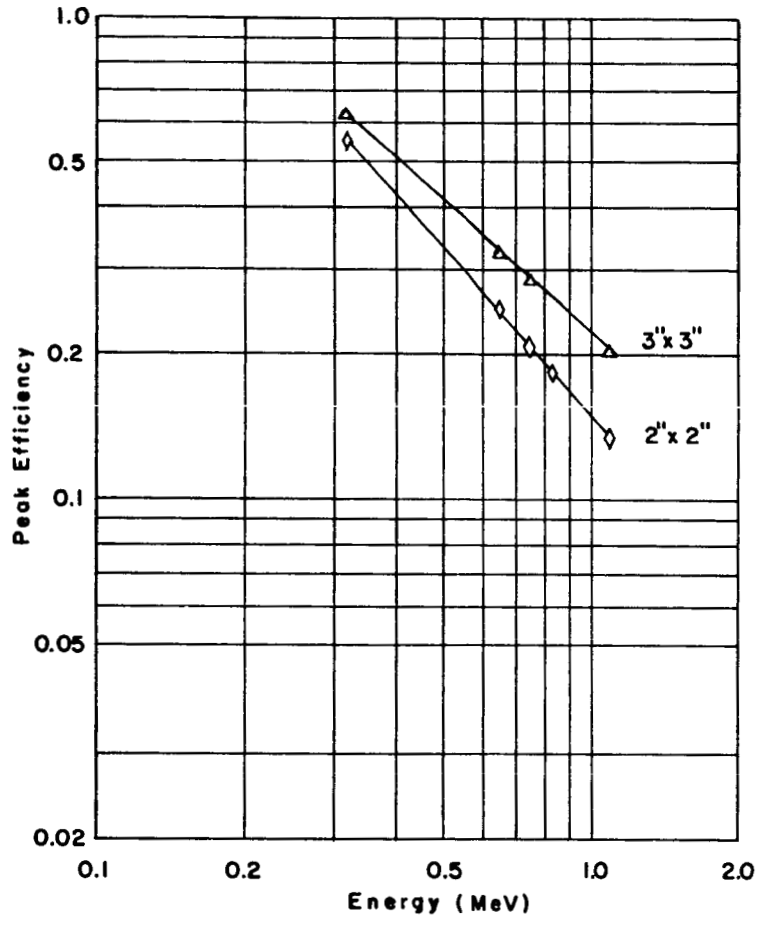

Peak Detection Efficiency as a Function of Peak Energy for Thallium Activated NaI Crystal Scintillators.

Figure 27

Table 8. LH_2 Transmission Gauge for 70 keV Radiation

Range (cm)	Detector (Each Site)	Count Range (Total, cps)	Source (Each Site) (7)	(10)	(12)	(15)	Max. Flux at Detector (cps/cm^2)
100	$10\ cm^2 \times 1$ cm	$4 \times 10^3 - 4 \times 10^4$	1.8 mc	1.3 mc	1.1 mc	.9 mc	5.5×10^2
200	"	$10^3 - 10^5$	19 mc	14 mc	12 mc	10 mc	1.4×10^3
300	"	$5 \times 10^2 - 5 \times 10^5$	460 mc	320 mc	270 mc	220 mc	7.2×10^3
400	"	$2 \times 10^2 - 2 \times 10^6$	1.8 c	1.3 c	1.1 c	810 mc	3.3×10^4

70 keV typical of X-ray, nuclear bremsstrahlung.

Characteristic length 45 cm of liquid hydrogen.

Background noise approximately 5 cps per detector in the 70 keV energy window.

Detector ~ 98% efficient.

Allowed flux (5 mr/hr) 3.5×10^4 cps/cm^2.

Shielding weight required for 5 mr/hr at one foot from the(point)source less than 1 pound of tungsten per site (more for large X-ray tubes).

Table 9. LH_2 Transmission Gauge for 100 keV Radiation

Range (cm)	Detector (Each Site)	Count Range (Total, cps)	Source (Each Site) (7)	(10)	(12)	(15)	Max. Flux at Detector (cps/cm^2)
100	$10\ cm^2$ x 1 cm	4×10^3 - 4×10^4	1.8 mc	1.3 mc	1.1 mc	.9 mc	5.5×10^2
200	"	10^3 - 10^5	13 mc	8.8 mc	7.3 mc	5.9 mc	9.7×10^2
300	"	5×10^2 - 3×10^5	120 mc	79 mc	67 mc	53 mc	3.7×10^3
400	"	3×10^2 - 10^6	890 mc	630 mc	520 mc	420 mc	1.7×10^4
450	"	2×10^2 - 3×10^6	2.7 c	1.9 c	1.5 c	1.3 c	3.7×10^4

100 keV typical of X-rays, nuclear bremsstrahlung.

Characteristic length 48 cm of liquid hydrogen.

Background noise approximately 5 cps per detector in the 100 keV energy window.

Detector 95% efficient.

Allowed flux (5 mr/hr) 3.0×10^4 cps/cm^2.

Shielding Weight required for 5 mr/hr at one foot from the (point) source less than 1 pound of tungsten per site (more for large X-ray tubes).

Table 10. LH_2 Transmission Gauge Parameters for Cesium-137

Range (cm)	Detector (Each Site)	Count Range (Total, cps)	Source (Each Site) (7)	(10)	(12)	(15)	Shielding Weight (Each Site - lbs.) (7)	(10)	(12)	(15)	Max. Flux at Detector (cps/cm^2)
100	3" x 3"	$2 \times 10^4 - 5 \times 10^4$	2.6 mc	1.8 mc	1.4 mc	1.2 mc	less than 2 lbs.				7×10^2
300	"	$2 \times 10^3 - 5 \times 10^4$	22 mc	16 mc	14 mc	10 mc	less than 2 lbs.				7×10^2
500	"	$8 \times 10^2 - 2 \times 10^5$	180 mc	130 mc	110 mc	90 mc	less than 5 lbs.				2×10^3
700	Two 3"x3"	$4 \times 10^2 - 8 \times 10^5$	880 mc	620 mc	520 mc	410 mc	9	8	7	6	5×10^3 (d)
800	"	$10^2 - 6 \times 10^5$ (a)	880 mc (b)	880 mc (b)	880 mc (c)	880 mc (c)		9			4×10^3
850	"	$10^2 - 10^6$ (a)	2 c (b)	2 c (b)	2 c (c)	2 c (c)		13			8×10^3 (e)

Energy 662 keV.

Characteristic length 93 cm of liquid hydrogen.

Background noise approximately 20 cps per 3" x 3" detector in the 662 keV energy window.

Detector ~ 32% efficient.

Allowed flux (5 mr/hr) 4×10^3 cps/cm^2.

Shielding weight based on a requirement of 2.5 mr/hr or less at one meter from center of (point) source.

(a) For array of seven.

(b) 2.0% - 3.0% statistical accuracy for low count rates.

(c) 1.0% - 2.0% statistical accuracy for low count rates.

(d) Flux greater than 5 mr/hr for array of seven only.

(e) Flux less than 5 mr/hr for array of fifteen.

Table. 11. LH_2 Transmission Gauge for Co^{60}

Range (cm)	Detector (Each Site)	Count Range (Total, cps)	Source (Each Site)				Shielding Weight (Each Site - lbs.)				Max. Flux at Detector (cps/cm^2)
			(7)	(10)	(12)	(15)	(7)	(10)	(12)	(15)	
200	3" x 3"	$8 \times 10^3 - 4 \times 10^4$	12 mc	9 mc	7 mc	6 mc	less than 5 lbs.				9×10^2
500	"	$10^3 - 6 \times 10^4$	125 mc	88 mc	73 mc	59 mc	10	9	9	8	1.5×10^3
700	Two 3"x3"	$6 \times 10^2 - 10^5$	270 mc	190 mc	160 mc	130 mc	13	12	11	10	1.7×10^3
900	"	$2 \times 10^2 - 2 \times 10^5$ (a)	640 mc (b)	640 mc (b)	640 mc (c)	640 mc (c)		25			2.3×10^3
1000	"	$2 \times 10^2 - 4 \times 10^6$ (a)	1.5 c (b)	1.5 c (b)	1.5 c (c)	1.5 c (c)		35			4.6×10^3 (d)

Energy 1.25 MeV.

Characteristic length 125 cm liquid hydrogen.

Background noise approximately 20 cps per 3" x 3" detector in the 1.2 MeV energy window.

Detector 20% efficient.

Allowed flux (5 mr/hr) 2.3×10^3 cps/cm^2.

Shielding weight based on a requirement of 5 mr/hr or less at one meter from center of (point) source.

(a) For array of seven.

(b) 1.5% - 2.0% statistical accuracy for low count rates.

(c) 1.0% - 1.5% statistical accuracy for low count rates.

(d) Flux less than 5 mr/hr for array of fifteen.

(2) Dynamic range becomes excessive,

(3) Background becomes excessive so that statistical accuracy (σ_N) is worse than 1% for full sampling cylinder.

These three factors all become important for about the same range. The maximum flux at the detector could be reduced by a feedback control system for the X-ray system, but the practical range is limited to about ten characteristic lengths or about 500 cm for the low photon energy system. The range for high energy photons is limited to about 700 cm for Cs^{137} 662 keV emission and about 900 cm for Co^{60} 1.25 MeV emission.

The attaching of sources and detectors external to the tank should pose no problem. For positioning within the tank, the sources should be attached to the spokes of a spiderweb structure and supported with guy wires.

4.2 Shadow Systems

Some details are presented concerning several shadow systems which are capable of providing the mass measurement for both oxygen and hydrogen tanks of any size. Emphasis is devoted to a backscatter system for the measurement of oxygen.

4.2.1 Backscatter Shadow System

The backscatter of low energy gamma radiation provides the basis for a variation of the shadow measurement technique in which both sources and detectors are located along the same line. Since the system is comprised of numerous point sources located along an extended detector (or numerous point detectors located along an extended source), the system is characterized by some of the features of the logic systems discussed in Section 3.2.2.

Emphasis is devoted to an oxygen system in which numerous collimated low energy gamma sources are located along a line detector and so shielded so that no radiation emitted from the source can strike the detector without being scattered from the adjacent medium; the source-detector lines are positioned parallel to the tank axis in an array similar to one of the arrays mentioned in conjunction with the gamma transmission system for hydrogen. Each line backscatter detector consists of a long ion chamber reaching from the bottom to the top of the tank with a number of point sources of beta or gamma radiation attached to the ion chamber. The ion chamber must be shielded from the direct beam of radiation so that only the scattered particles or photons are detected.

The mean path lengths (or continuous-slow-down-approximation range) of 700 keV electrons in liquid oxygen and oxygen vapor (at 90° K and 0.981 atmospheres pressure) are 0.3 cm and 80 cm. Since the electron path is not straight, the mean ranges (or penetration depths) are considerably shorter than these values. In view of the short path lengths of the electrons in liquid oxygen, it is doubtful whether a beta backscatter system can be implemented in practice.

Attention is directed toward the gamma or X-ray backscatter techniques. The attenuation of gamma radiation in oxygen is caused mainly by Compton scattering. The characteristic lengths of 60 keV gamma-rays in liquid and saturated vapor for oxygen at 90° K are approximately 1.8" and 470", respectively. Thus, as many photons are scattered in 1.8" of liquid

as in 470" of vapor. The probability of detection of these scattered photons is higher when the source-detector is immersed in liquid than when it is exposed to vapor by a factor approximately proportional to the density ratio (260:1). If the backscatter system is partially immersed in liquid and partially exposed to vapor, the detected signal is proportional to the length of the portion of the system which is immersed in the liquid, similar to the description of Equation (3-29).

Crosstalk between adjacent backscatter detectors must be minimized by proper collimation of the sources so that interference between adjacent units immersed in vapor is minimized. Interference between adjacent units immersed in liquid is small because, even though the characteristic length for absorption in liquid oxygen is 23" (about 13 times the characteristic length for scattering), the photon energies are sufficiently degraded by multiple scatters that they can be absorbed by a thin window which covers the detector.

For the collimated, widely separated source-detector lines, the number of photons backscattered from a point source immersed in a scattering medium can be computed for simple geometries. For example, for a circular disk detector of area A, the number of backscattered photons incident on the detector can be approximated by

$$N = \int_a^\infty \int_\Omega \frac{AKC\, e^{-2\mu\rho r}\, \mu'\rho}{(4\pi r^2)^2} r^2 \, d\Omega \, dr \,, \qquad (4\text{-}5)$$

where

K = 3.7×10^{10} photons/curie,

C = effective source strength in curies,

r = distance from the source to an elemental volume dV,

μ = mass attenuation coefficient,

μ' = Compton scattering coefficient $\simeq \mu$,

ρ = density of liquid or vapor oxygen,

Ω = solid angle subtended by source collimation,

a = minimum distance at which the fields of view of source and detector overlap.

The factor $\frac{KCe^{-\mu\rho r}}{4\pi r^2}$ represents the number of photons per second per unit area reaching the elemental volume $dV = r^2\Omega\, dV$ at distance r from the source. The factor $\mu\rho\, dV$ represents the ratio of scattered to incident photons within the elemental volume dV. The remaining factor $\frac{Ae^{-\mu\rho r}}{4\pi r^2}$ represents the number of photons originating from the elemental volume dV that reaches the detector. The distance r from the source to dV is taken to be the same as the distance from dV back to the detector; the Compton scattering of photons is assumed to be spherically symmetric (a good approximation for low energy photons).

Under the additional assumption that $\mu \simeq \mu'$, Equation (4-5) can be transformed into

$$N = \frac{\Omega A K C \mu \rho}{16 \pi^2 a} \int \frac{e^{-2 \mu \rho a Z}}{Z^2} dZ \qquad (4\text{-}6)$$

$$= \frac{\Omega A K C \mu \rho}{16 \pi^2 a} E_2 (2 \mu \rho a) ,$$

where $Z = r/a$ and $E_2(2 \mu \rho a)$ is an E_2 function of the exponential integrals $E_n(x)$ commonly used in shielding calculations. The integral $E_2 \simeq 1$ for vapor and $E_2 \simeq 0.5$ for liquid. Thus the number of photons incident on a detector from the backscattered radiation is approximately proportional to the density of material immediately surrounding the backscatter source-detector. Precise experimental investigation is required to accurately determine the backscattered count for a particular source-detector geometry.

Since the count rate is nearly proportional to the length of the source-detector line which is immersed in liquid, the maximum statistical fluctuation occurs when the tank is full and the count rate is a maximum. If the statistical fluctuations are to be constrained to 1% with a time constant of 0.5 seconds, a total count rate of 2×10^4 counts per second must be detected. The design and implementation of long detectors that operate successfully at the liquid oxygen temperature may require some significant efforts. Lithium-drifted silicon detectors operate satisfactorily at this temperature, but their cost would be high since a large number of small units must be used in parallel to extend across the tank. Gas-filled detectors are not expensive, but their efficiency is low. Probably the only

gases that can be used for this application are helium, neon, and nitrogen. Plastic scintillators may be considered, but the light collection efficiency may become a problem. Even though detailed investigation is required, 1% detector efficiency is feasible. The number of incident photons on the detector required to achieve the 1% statistical counting accuracy is then 2×10^6 cps.

The required source strength can be calculated from Equation (4-6). Under the assumption that $E_2 = 0.5$ for liquid, $a = 0.5$ cm, $\Omega = 1$, $A = 10$ cm^2, the required number of incident photons (2×10^6 cps) can be obtained by

$$C = \frac{16 \pi^2 \times 0.5 \times 2 \times 10^6}{10 \times 3.7 \times 10^{10} \times 0.189 \times 1.14} = 2 \times 10^{-3} \text{ curies}.$$

Thus, source strength can be implemented by using a Pm^{147} bremsstrahlung source of a few curies. The radiation shielding required is negligible for such a small, low energy source.

4.2.2 Gamma Transmission Shadow System

The conventional shadow system employs arrays of line source and line detector pairs. For such a configuration, pairs of line sources and line detectors are mechanically assembled together a few inches apart. The source is collimated such that the direct beam covers only the window of the detector. The detector wall, extending the window,

should be covered with a thin layer of high Z number material to reduce crosstalk.

If this source-detector pair is immersed partially into the liquid and partially into the vapor, the signal is proportional to the length exposed to vapor, as dictated by Equation (3-29).

The maximum statistical fluctuation occurs when the tank is completely empty. To keep this maximum fluctuation less than the change in signal due to 1% change in the length immersed in vapor, the minimum required count rate within the response time (0.5 sec) becomes

$$\frac{\sqrt{N}}{N} = (1 - a) \times 0.01$$

or

$$N = \left(\frac{100}{1 - a}\right)^2 = 2.25 \times 10^4$$

if $a = 0.33$.

Assuming again 1% detection efficiency, a total incident count rate of 4.5×10^6 photons per second is required. If a line detector of one-inch diameter is used, the fractional solid angle subtended by the detector is approximately 0.03. Thus, the required source strength is

$$\frac{4.5 \times 10^6}{0.03 \times 3.7 \times 10^{10}} \cong 4 \times 10^{-3} \text{ curies .}$$

This is again a reasonable value of source strength, and radiation shielding problems are trivial.

APPENDIX A

Modification of Wigner-Seitz Zones for an Array of Seven Sampling Locations

A first-order approximation to the most efficient position of parallel radiation beams for the measurement of mass in a cylindrical or hemispherically-capped cylindrical tank is given by hexagonal (Wigner-Seitz) zones in which the various sampling beams are the loci for the zone centers. However, such zones fail to conform sufficiently to circular tank boundaries for 2% accuracy and, in addition, produce gross errors for certain spherical bubble locations.

Figures A-1 and A-2 indicate how a gross measurement error present with a Wigner-Seitz array of seven is reduced in the modified configuration of seven in which the symmetry of the configuration is slightly reduced. For the Wigner-Setiz array, six sampling locations are taken at a radius of .72R for the modified array, three locations are taken at a radius of .61R and three other locations at a radius of .84R.

As Figure A-1 indicates, the sphere lies within but a single radiation beam for the Wigner-Seitz location, while it lies within four beams for the modified configuration. Figure A-2 indicates various pertinent lengths associated with the tank and bubble, A cylindrical tank with the same volume as the hemispherically-capped tank is indicated by the dashed lines; for the sake of simplicity, the ensuing calculations are made for the cylindrical tank.

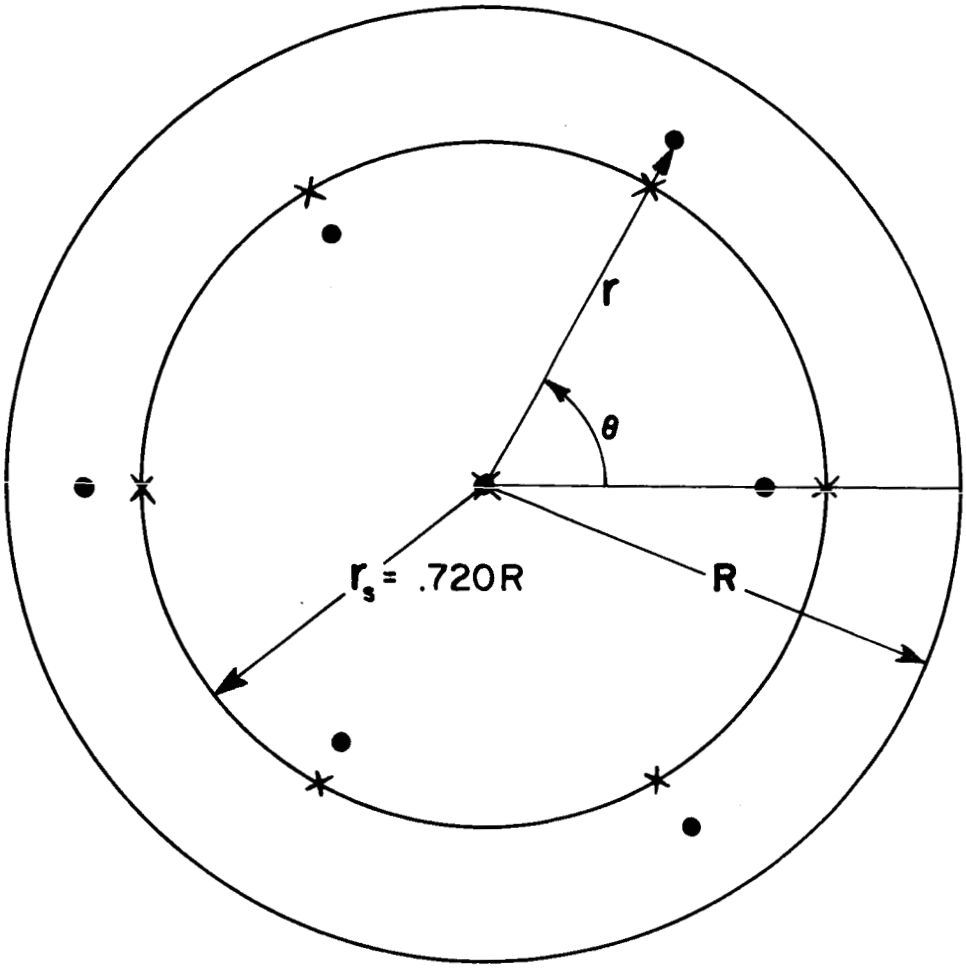

WIGNER – SEITZ LOCATIONS X

MODIFIED WIGNER-SEITZ LOCATIONS ●

SPHERICAL VAPOR BUBBLE CENTERED IN A CYLINDRICAL TANK

FIGURE A-1

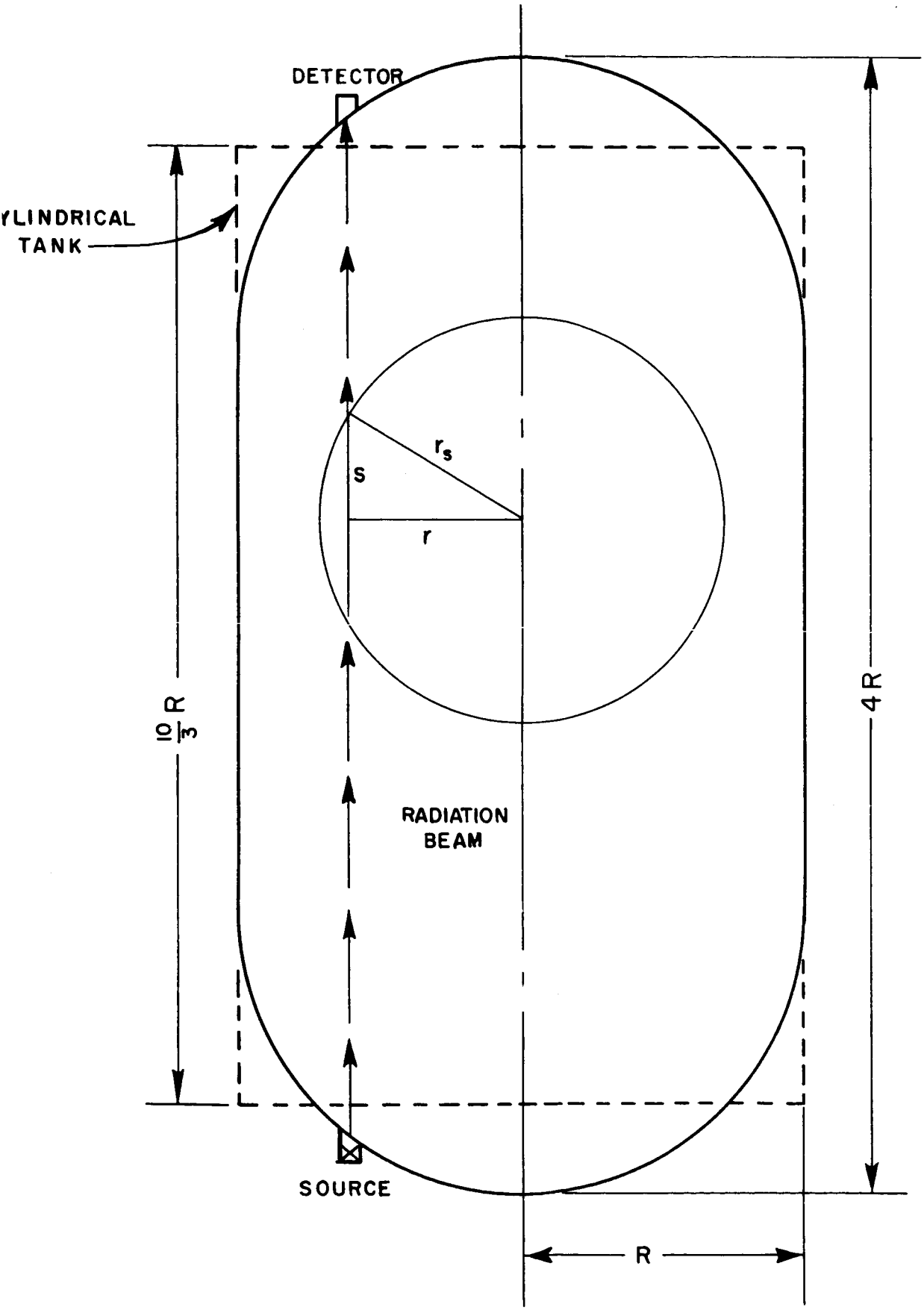

SPHERICAL VAPOR BUBBLE LOCATED IN A TANK WITH VOLUME $10/3\pi R^3$

FIGURE A-2

The volume of the bubble is estimated from the attenuation of the various beams in conjunction with simple data processing. The following general data processing equation is appropriate for collimated radiation beams:

$$M = \rho_L \frac{A_c}{N} \sum_{i=1}^{N} \ell_i + \rho_g \frac{A_c}{N} \sum_{i=1}^{N} t_i \quad , \qquad \text{(A-1)}$$

where M is the total mass in the tank, ρ_L the liquid density, ρ_g the gaseous density, A_c the cross sectional area of the cylindrical portion of the tank, N the number of source-detector pairs, ℓ_i the liquid thickness in the i^{th} radiation beam, and t_i the gaseous thickness in the i^{th} radiation beam. The equation may be rewritten

$$M = \frac{A_c}{N} \sum_{i=1}^{N} (\rho_L \ell_i + \rho_g t_i) \quad . \qquad \text{(A-2)}$$

The quantity in parentheses is exponentially related to the count rate at the detector for a particular radiation beam:

$$N_i = N_{o_i} e^{-\mu(\rho_L \ell_i + \rho_g t_i)} \quad , \qquad \text{(A-3)}$$

where μ is the attenuation cross section and N_{o_i} is the evacuated tank count rate. Therefore,

$$(\rho_L \ell_i + \rho_g t_i) = \frac{1}{\mu} \log \frac{N_{o_i}}{N_i} \quad . \qquad \text{(A-4)}$$

Hence, the mass in the tank can be computed from the sums of the logarithms of the count rates at the various detectors.

For the Wigner-Seitz array of Figure A-1 and a centered spherical vapor bubble of radius $r_s = .720R$, the measured mass in the cylindrical tank is

$$M = \rho_L \frac{\pi R^2}{7} \left[6 \times \frac{10}{3} R + 1 \times \left(\frac{10}{3} R - 2 r_s \right) \right]$$

under the assumption that the gaseous density is negligible (actually, $\rho_g \sim .02\ \rho_L$ at 1 atmosphere and 20° K). Therefore,

$$M = \rho_L \frac{\pi R^3}{7} (20.000 + 2.893)$$

$$= 3.270\ \rho_L \pi R^3 .$$

The actual mass is

$$M_{act} = \rho_L \left(\frac{10}{3} \pi R^3 - \frac{4}{3} \pi r_s^3 \right) = \rho_L \pi R^3 (3.333 - .497)$$

$$= 2.836\ \rho_L \pi R^3 .$$

The error as a per cent of capacity is

$$E = \frac{M - M_{act}}{\rho_L \frac{10}{3} \pi R^3} \times 100 = 13.0\% .$$

For the modified array of Figure 6, the measured mass is

$$M = \rho_L \frac{\pi R^2}{7} \left[3 \times \frac{10}{3} R + 3 \times \left(\frac{10}{3} R - 2s \right) + 1 \times \left(\frac{10}{3} R - 2r_s \right) \right],$$

where s is indicated in Figure A-2 as half the gaseous thickness in the radiation beam. For simplicity of calculation, the three beams which pass through the bubble near the edge (r = .61R) are taken to have the same radius, though their radii differ slightly in the optimal configurations. The gaseous thickness is calculated to be:

$$2s = 2(r_s^2 - r^2)^{1/2} = 2R(.720^2 - .610^2)^{1/2}$$

$$2s = .768R .$$

Hence,

$$M = \rho_L \frac{\pi R^3}{7} (10.000 + 3 \times 2.565 + 2.8933)$$

$$= 2.943 \rho_L \pi R^3 .$$

As before, the actual mass is

$$M_{act} = 2.836 \rho_L \pi R^3 .$$

Hence, the error as a per cent of capacity is

$$E = \frac{M - M_{act}}{\rho_L \frac{10}{3} \pi R^3} \times 100 = 3.2\% .$$

The error in the largest centered sphere through which only the central radiation beam passes ($r_s = .61R$) can be calculated by

$$M = \rho_L \frac{\pi R^2}{7} \left[6 \times \frac{10}{3}R + 1 \times \left(\frac{10}{3}R - 2r_s\right)\right]$$

$$= \rho_L \frac{\pi R^3}{7} \left[20.000 + 2.113\right]$$

$$= 3.159\, \rho_L \pi R^3 ,$$

$$M_{act} = \rho_L \left(\frac{10}{3}\pi R^3 - \frac{4}{3}\pi r_s^3\right)$$

$$= 3.030\, \rho_L \pi R^3$$

$$E = \frac{M - M_{act}}{\rho_L \frac{10}{3}\pi R^3} \times 100 = 3.9\% .$$

Thus, the modified array of seven reduces certain gross measurement errors.

Figure A-3 indicates the distribution of errors for 440 spheres randomly oriented within the volume of the hemispherically-capped tank (RNSPV) for both the Wigner-Seitz locations and the modified Wigner-Seitz locations; the volume of the spheres is uniformly distributed from 2% to 40% of tank capacity, the spheres of 40% tank capacity being the largest that can fit into the tank.

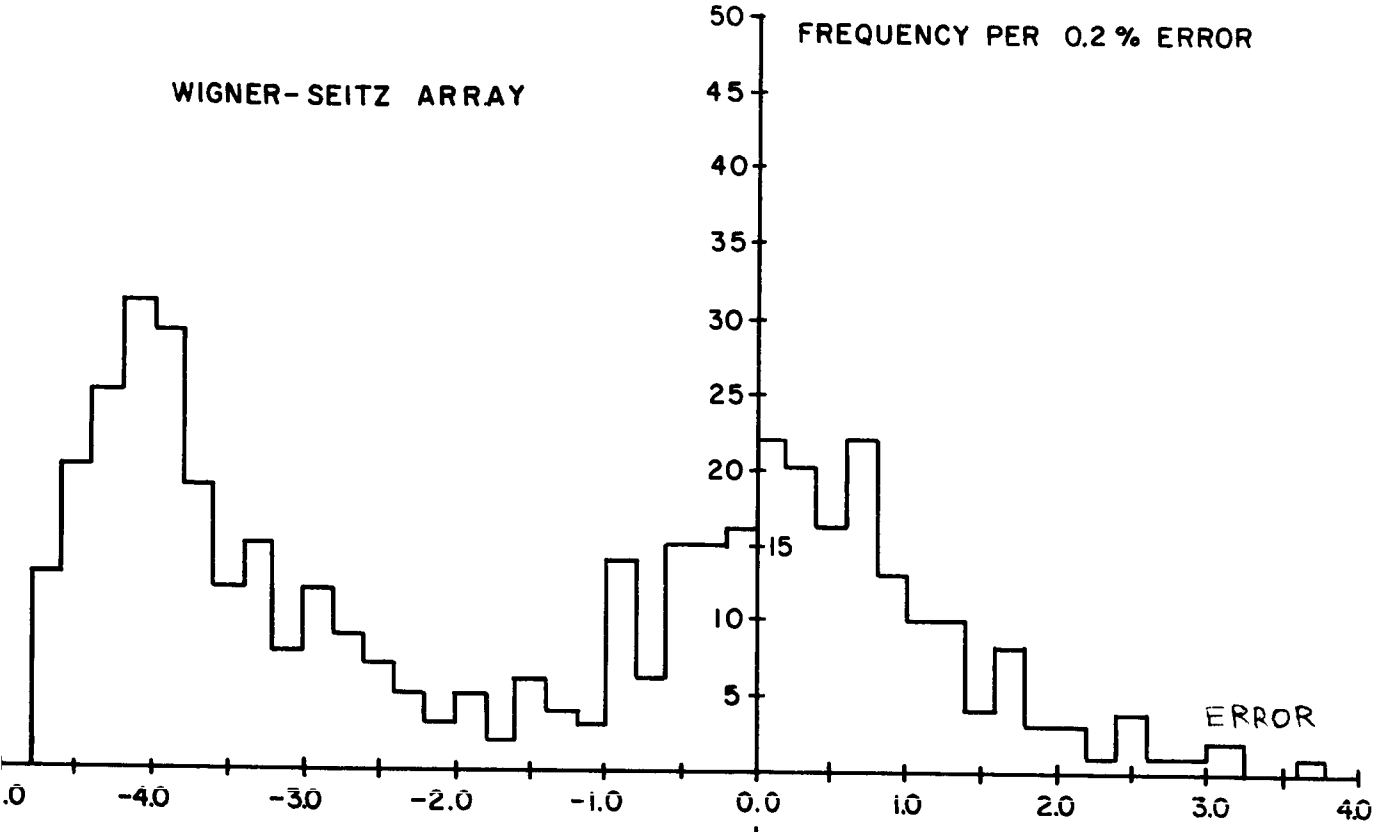

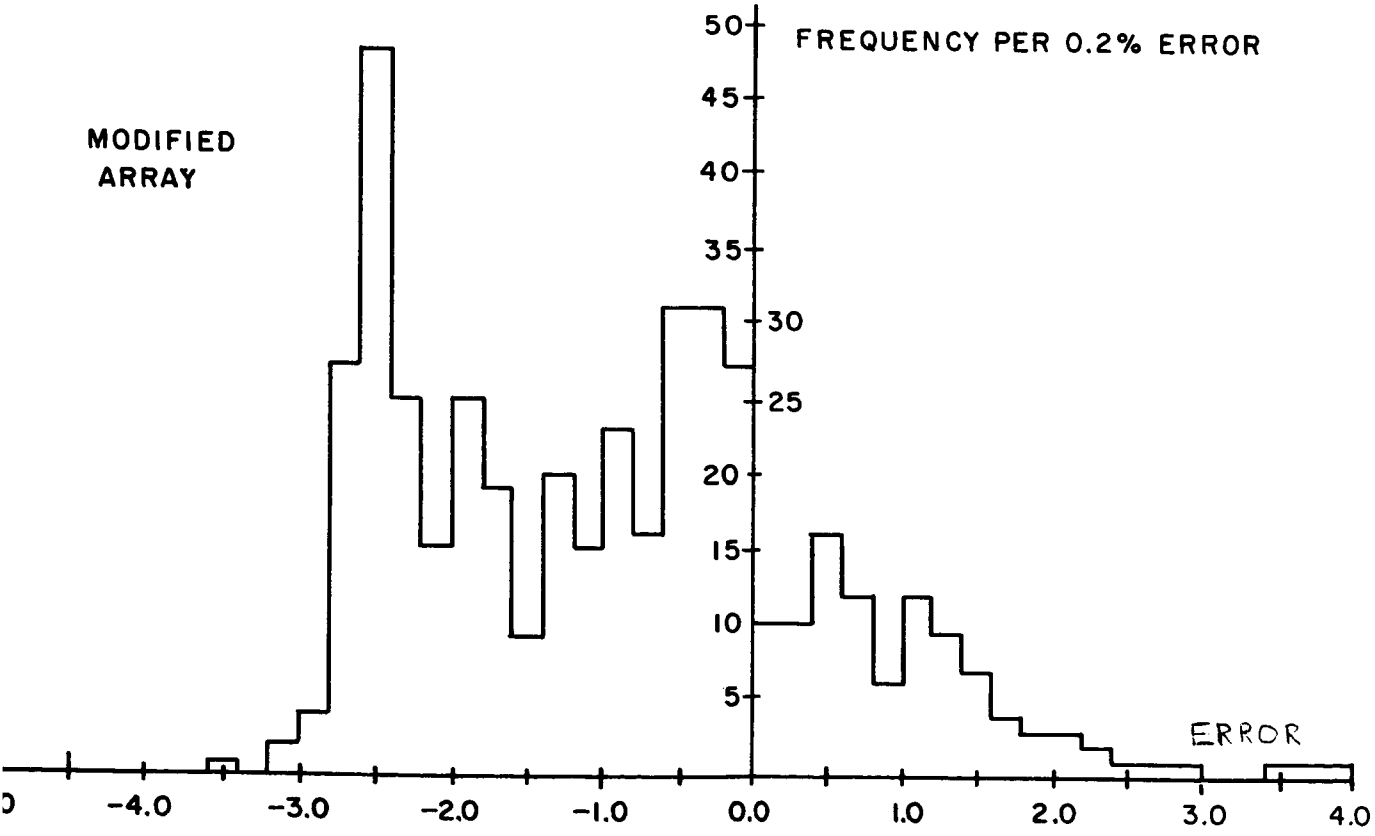

FREQUENCY OF ERROR (PER 0.2% ERROR INCREMENT) FOR WIGNER SEITZ ARRAY AND MODIFIED ARRAY OF SEVEN SAMPLING LOCATIONS, DATA FOR 440 RANDOMLY ORIENTED SPHERES AT VOLUME 2% TO 40% OF TANK CAPACITY.

FIGURE A-3

APPENDIX B

Some Computational Results for Optimal Arrays of Seven, Ten, and Fifteen Sampling Locations

The results of computer simulations of the propellant orientation indicated in Figure 1a are presented for the optimal arrays of seven, ten, and fifteen sampling locations. The four types of simulations discussed in Section 3.1.1.4 for arrays of beams parallel to the tank axis, were employed for tanks with a length-to-radius ratio of four.

Errors typical of the optimal array of seven are given in Figures B-1, 2, and 3. Figure B-1 displays the error distribution for 595 spherical bubbles tangent internally to a hemispherically-capped tank, but otherwise random. Figures B-2 and B-3 give errors for a centrally located bubble and for a tangent bubble as a function bubble radius. The error distribution for 440 bubbles randomly located within the volume of a hemispherically-capped tank is presented in Figure A-3.

Errors typical of the optimal array of ten are given in Figures B-4, 5, 6, and 7. Figures B-4 and B-5 display the error distributions for 595 randomly located tangent bubbles and 440 randomly located bubbles within a hemispherically-capped cylindrical tank. Figures B-6 and B-7 present errors for a centrally located, and for a tangent bubble, as a function of bubble radius.

Errors typical of the optimal array of fifteen parallel sampling beams

are given in Figures B-8, 9, 10, and 11. Figures B-8 and B-9 present the error distributions for 595 randomly oriented tangent bubbles and 440 randomly located bubbles within a hemispherically-capped cylindrical tank. Figures B-10 and B-11 depict errors for a centrally located bubble and a tangent bubble as a function of bubble radius.

Figure B-12 presents the error distribution for 440 randomly located bubbles within a hemispherically-capped cylindrical tank for which fifteen sampling beams are directed across the tank. These beams are arranged in groups of three, located in planes at Z coordinates of 1.30, 0.67, 0.00, -0.67, and -1.30, where the Z = 0 plane bisects the tank and is perpendicular to the tank axis.

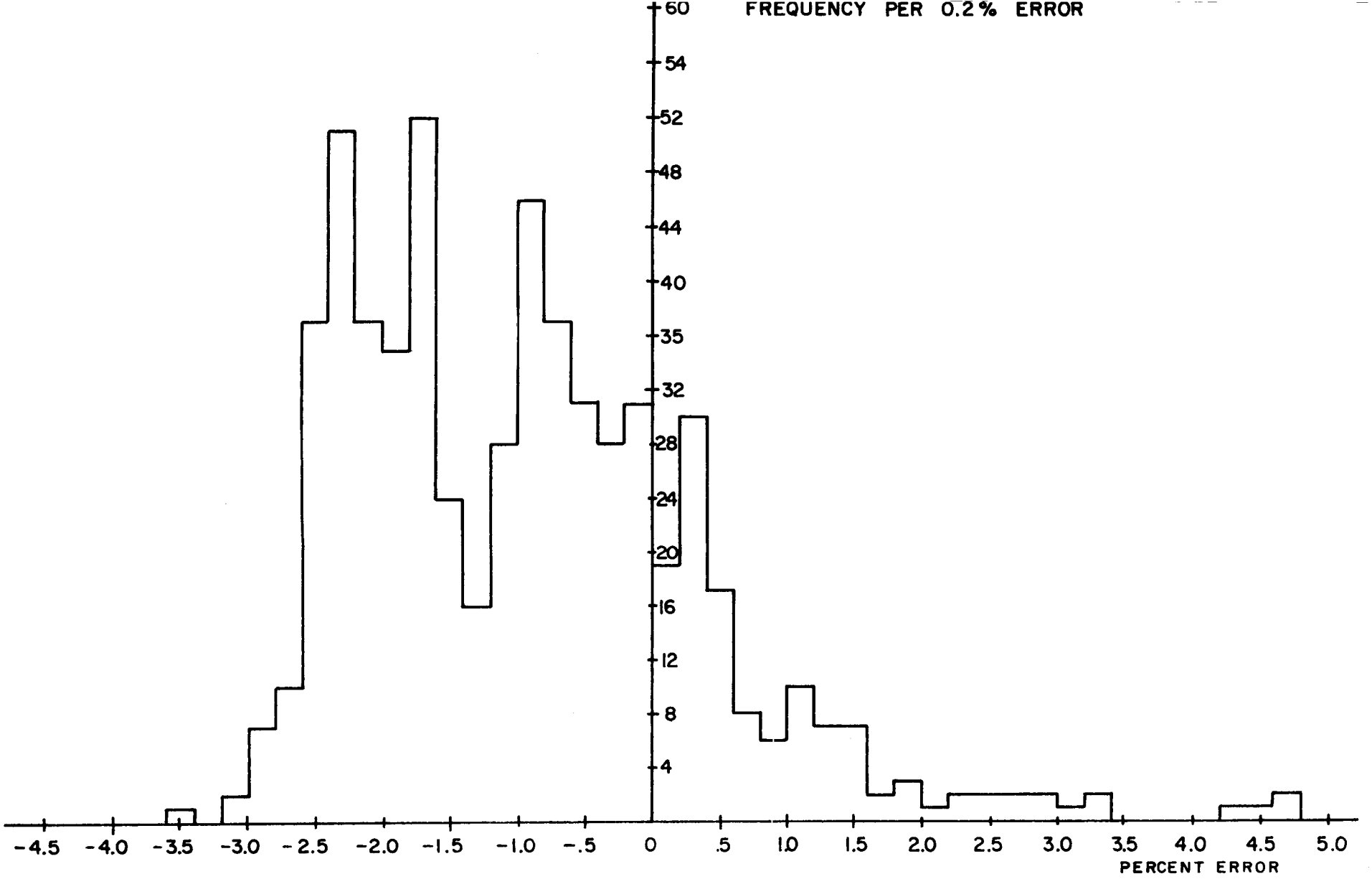

FREQUENCY OF ERROR (PER 0.2% ERROR INCREMENT) FOR OPTIMAL ARRAY OF SEVEN SAMPLING LOCATIONS, DATA FOR 595 RANDOMLY ORIENTED TANGENT SPHERES OF VOLUME 2% TO 40% OF TANK CAPACITY

FIGURE B-1

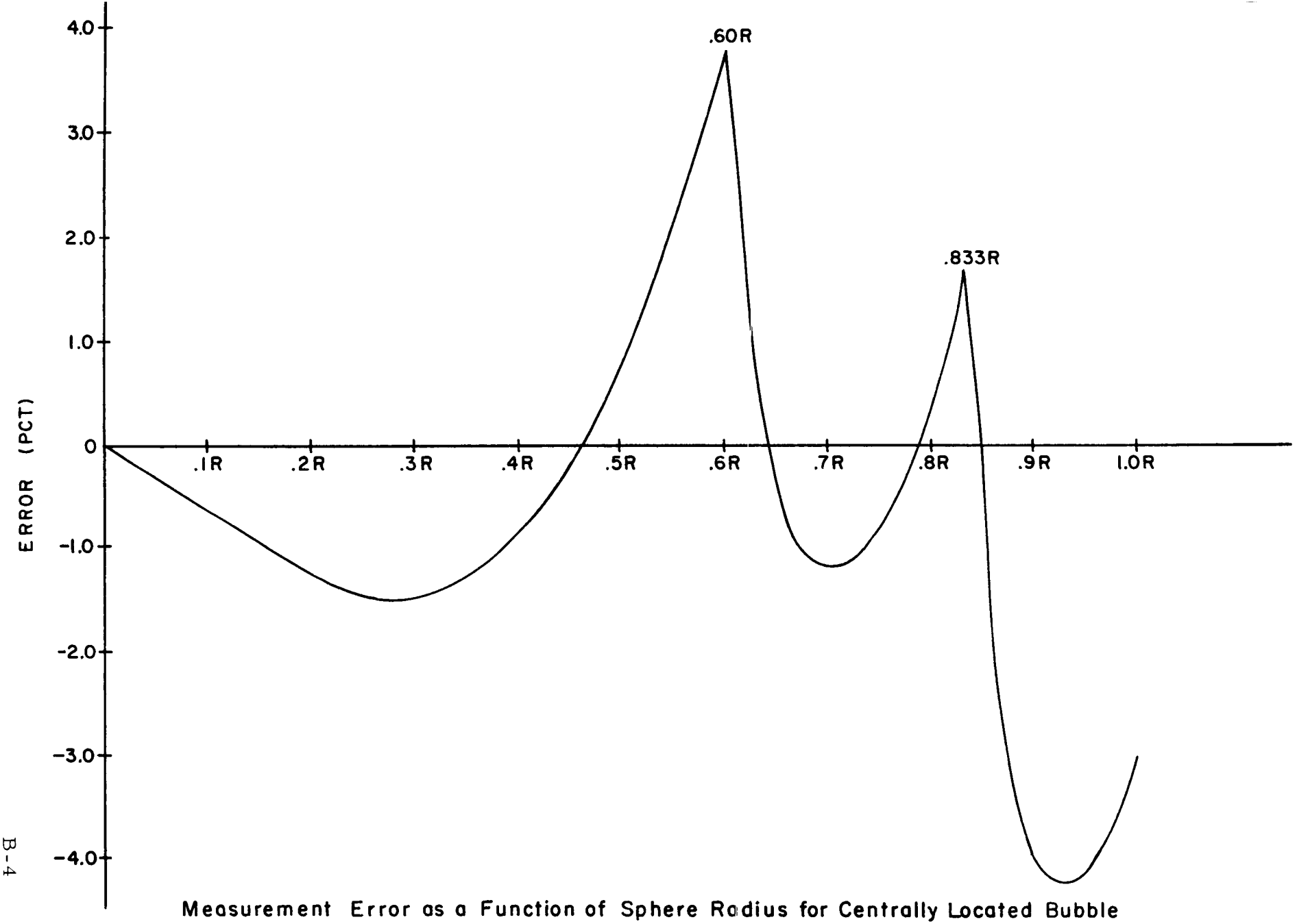

Measurement Error as a Function of Sphere Radius for Centrally Located Bubble in Optimal Array of Seven Sampling Locations.

Figure B-2

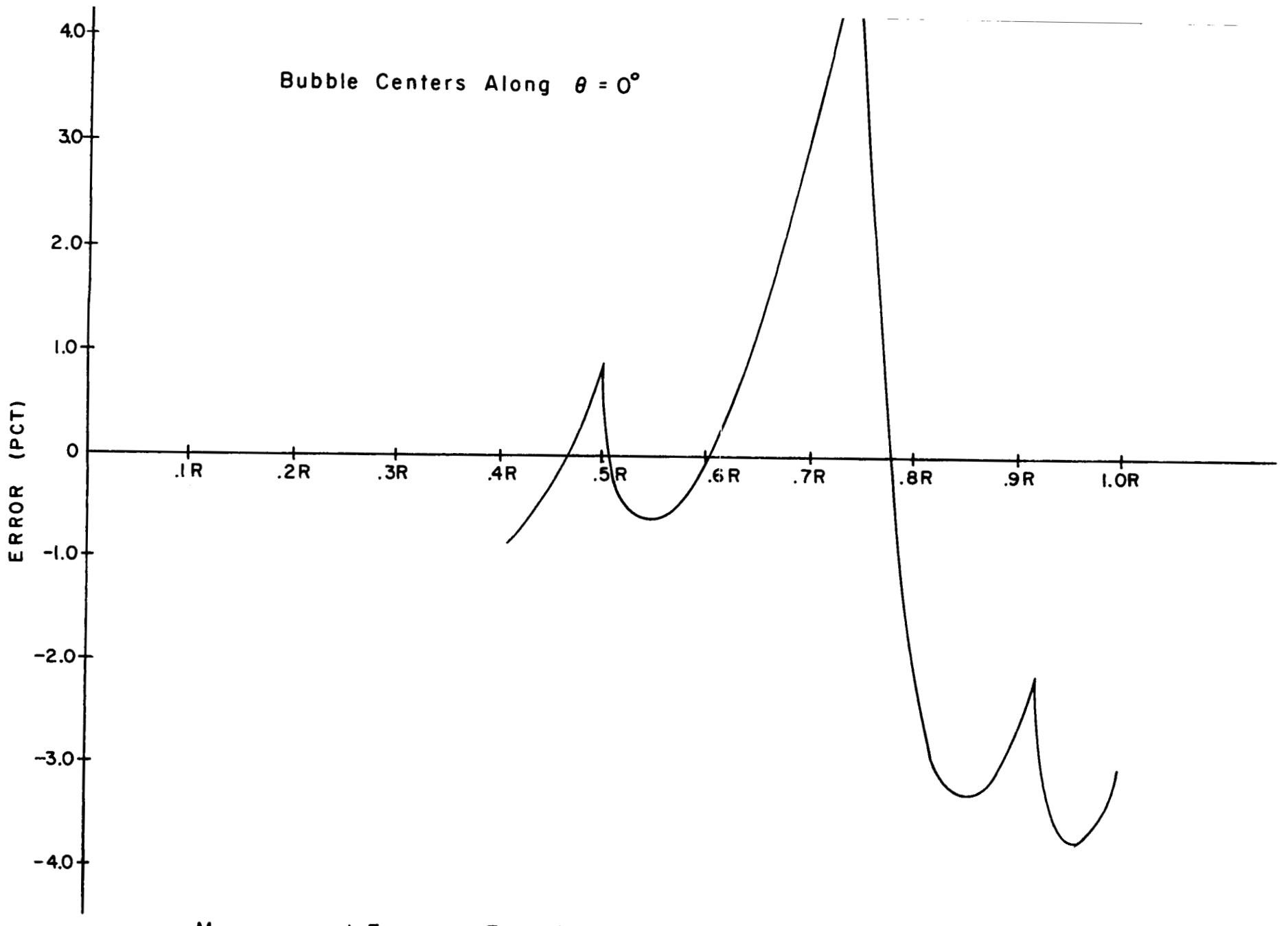

Measurement Error as a Function of Sphere Radius for Tangent Bubble in Optimal Array of Seven Sampling Locations.

Figure B-3

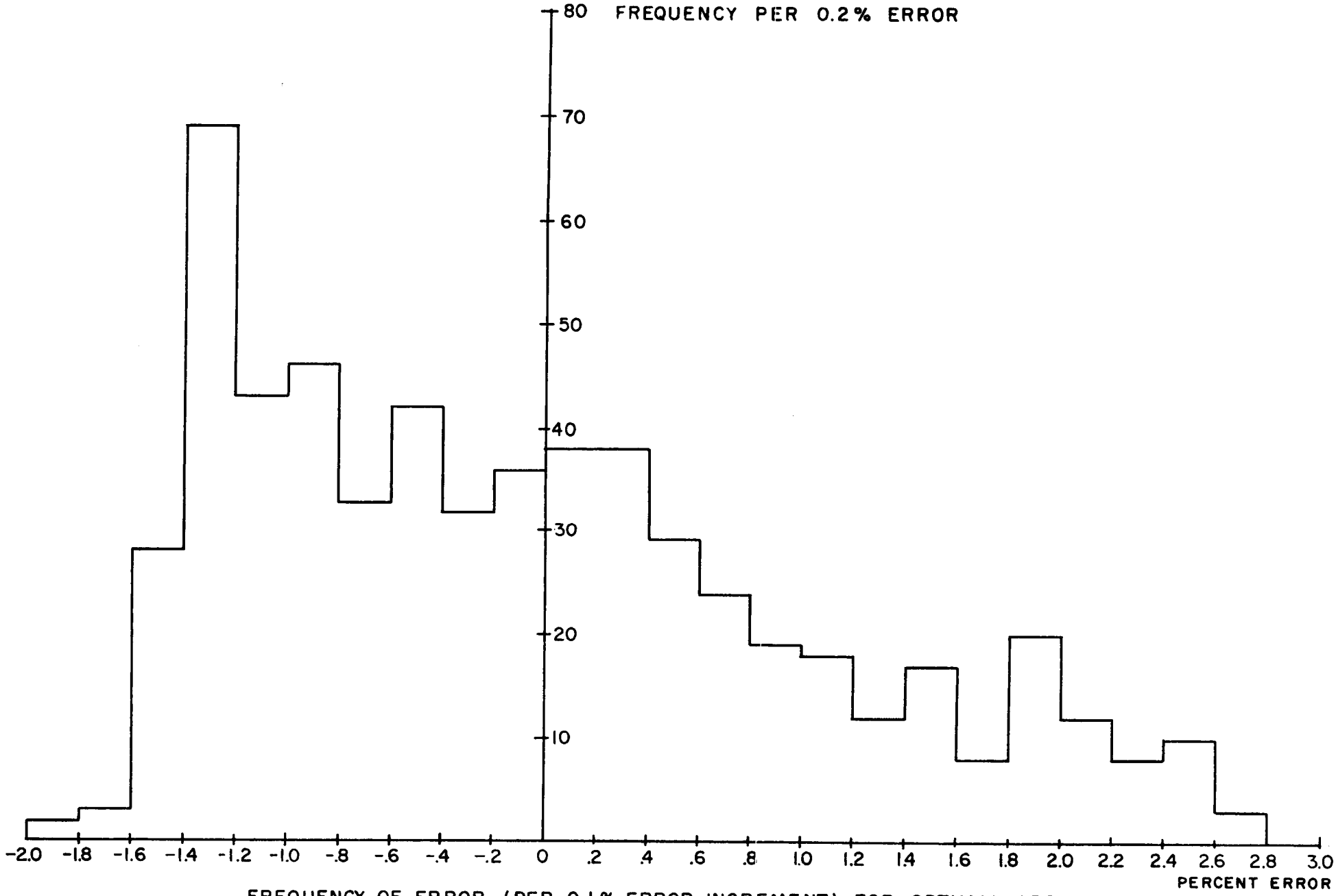

FREQUENCY OF ERROR (PER 0.1% ERROR INCREMENT) FOR OPTIMAL ARRAY OF TEN SAMPLING LOCATIONS, DATA FOR 595 RANDOMLY ORIENTED TANGENT SPHERES OF VOLUME 2% TO 40% OF TANK CAPACITY.

FIGURE B-4

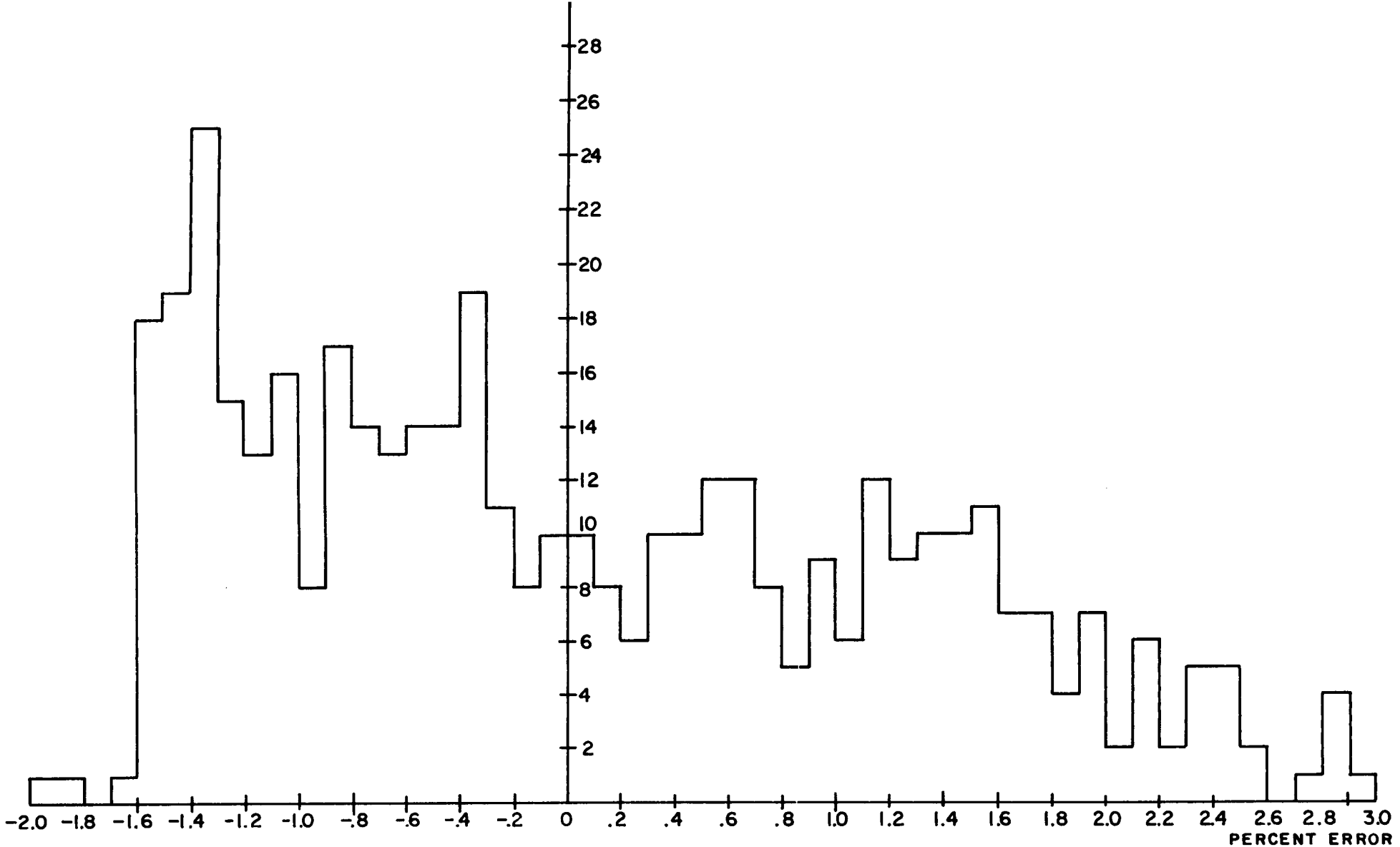

FREQUENCY OF ERROR (PER 0.1% ERROR INCREMENT) FOR OPTIMAL ARRAY OF TWELVE SAMPLING LOCATIONS, DATA FOR 440 RANDOMLY ORIENTED SPHERES OF VOLUME 2% TO 40% OF TANK CAPACITY

FIGURE B-5

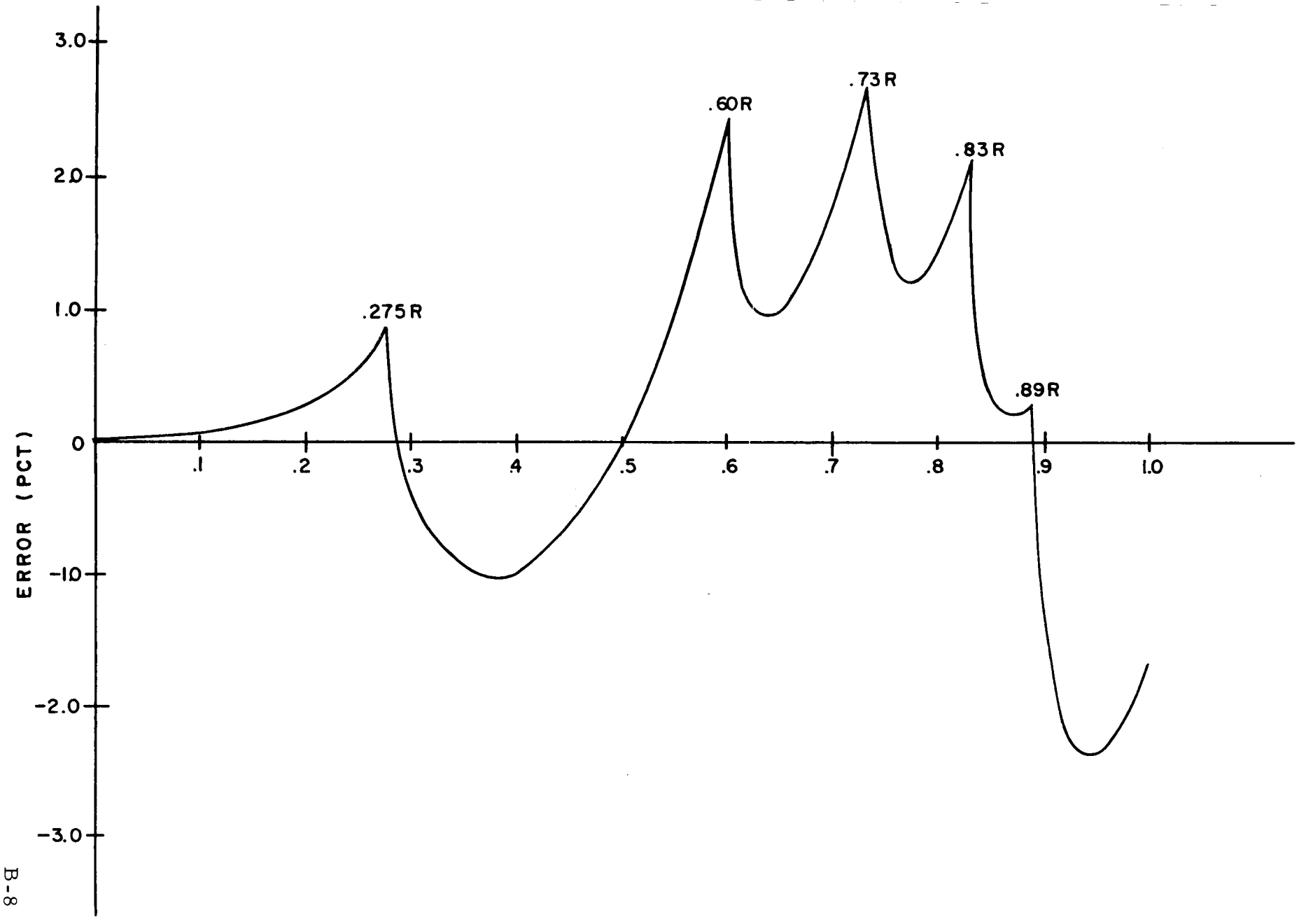

Measurement Error as a Function of Sphere Radius for Centrally Located Bubble in Optimal Array of Ten Sampling Locations

Figure B-6

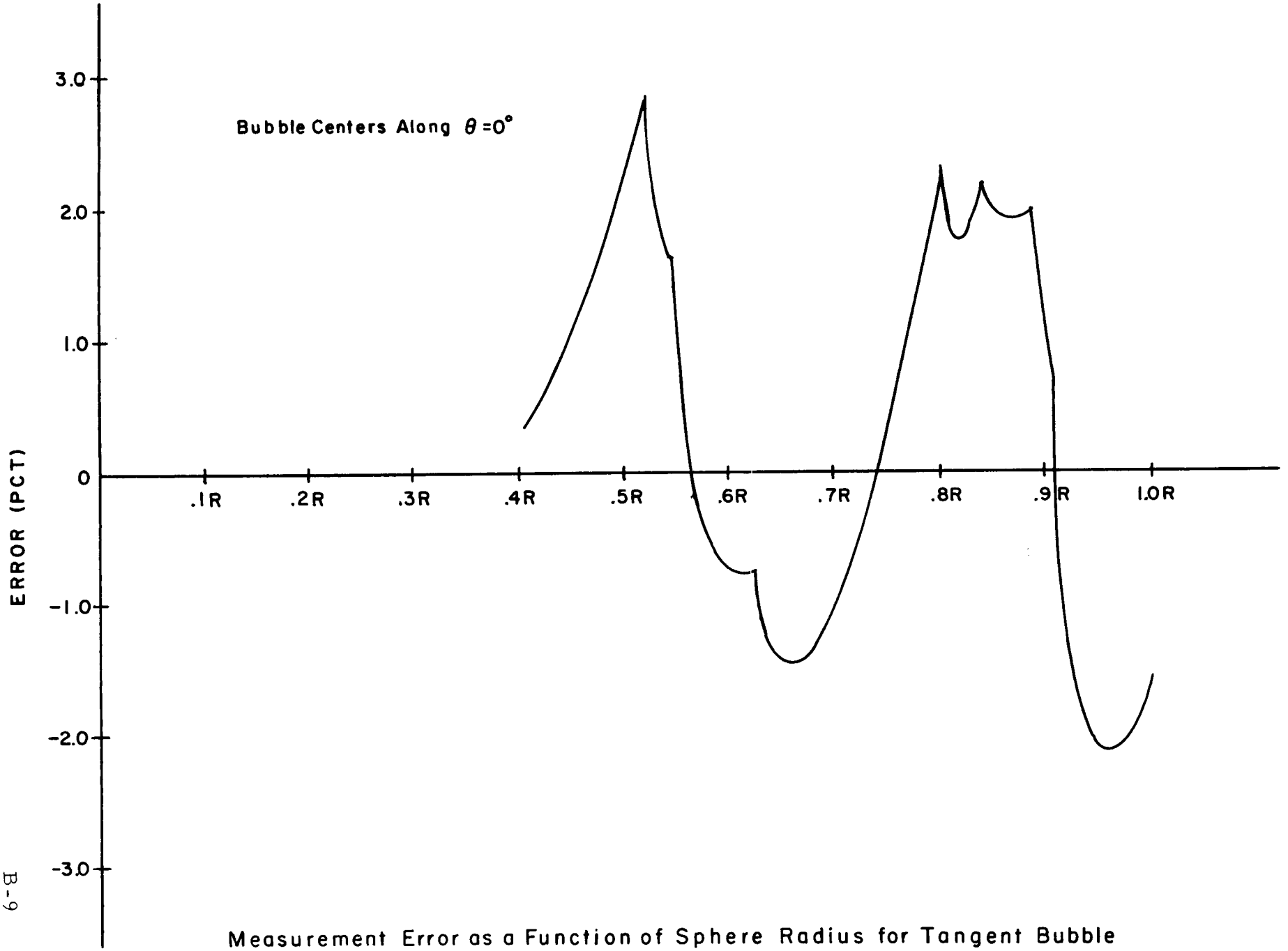

Measurement Error as a Function of Sphere Radius for Tangent Bubble in Optimal Array of Ten Sampling Locations

Figure B-7

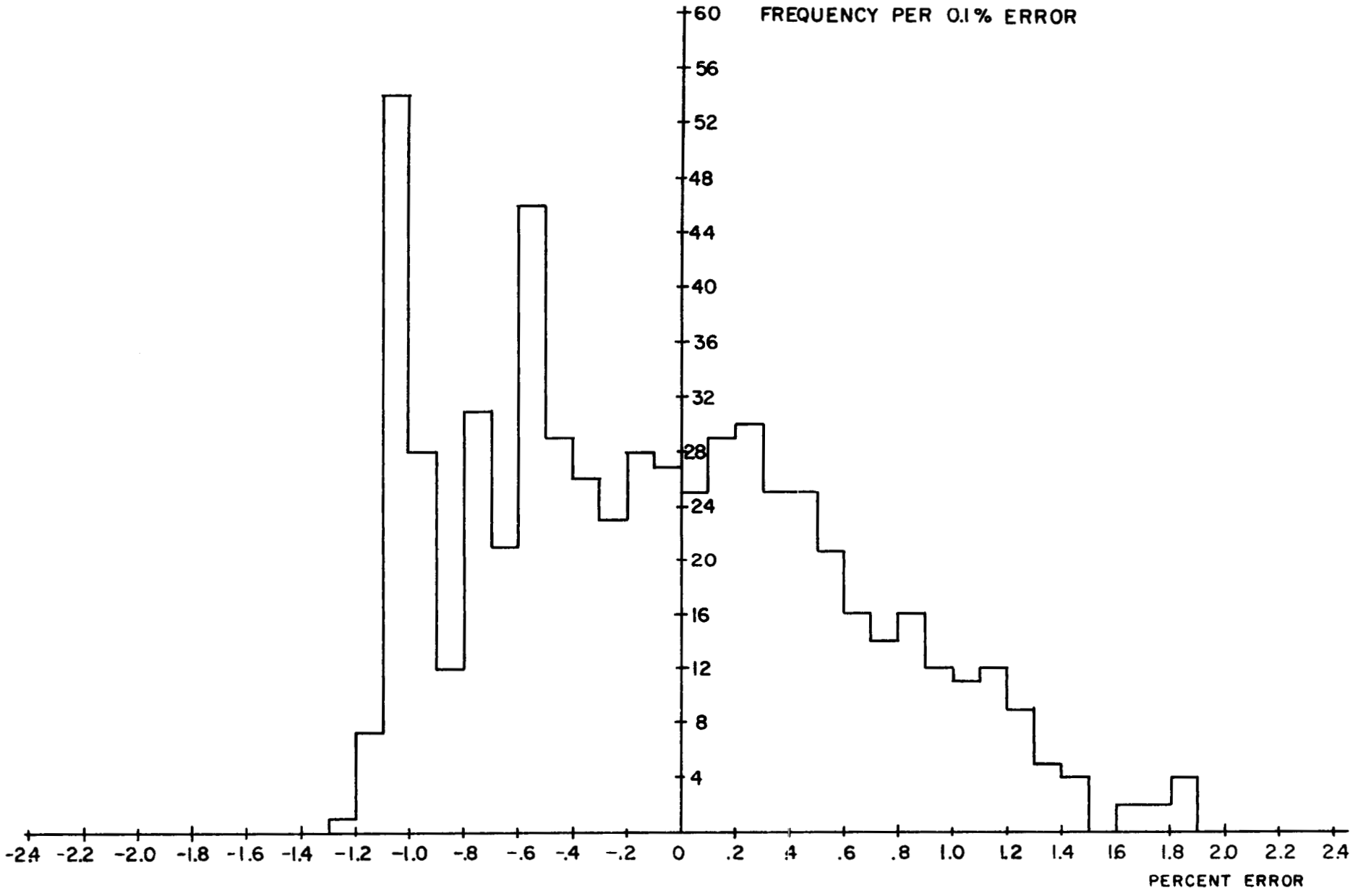

FREQUENCY OF ERROR (PER 0.1% ERROR INCREMENT) FOR OPTIMAL ARRAY OF FIFTEEN SAMPLING LOCATIONS, DATA FOR 595 RANDOMLY ORIENTED TANGENT SPHERES OF VOLUME 2% TO 40% OF TANK CAPACITY

FIGURE B-8

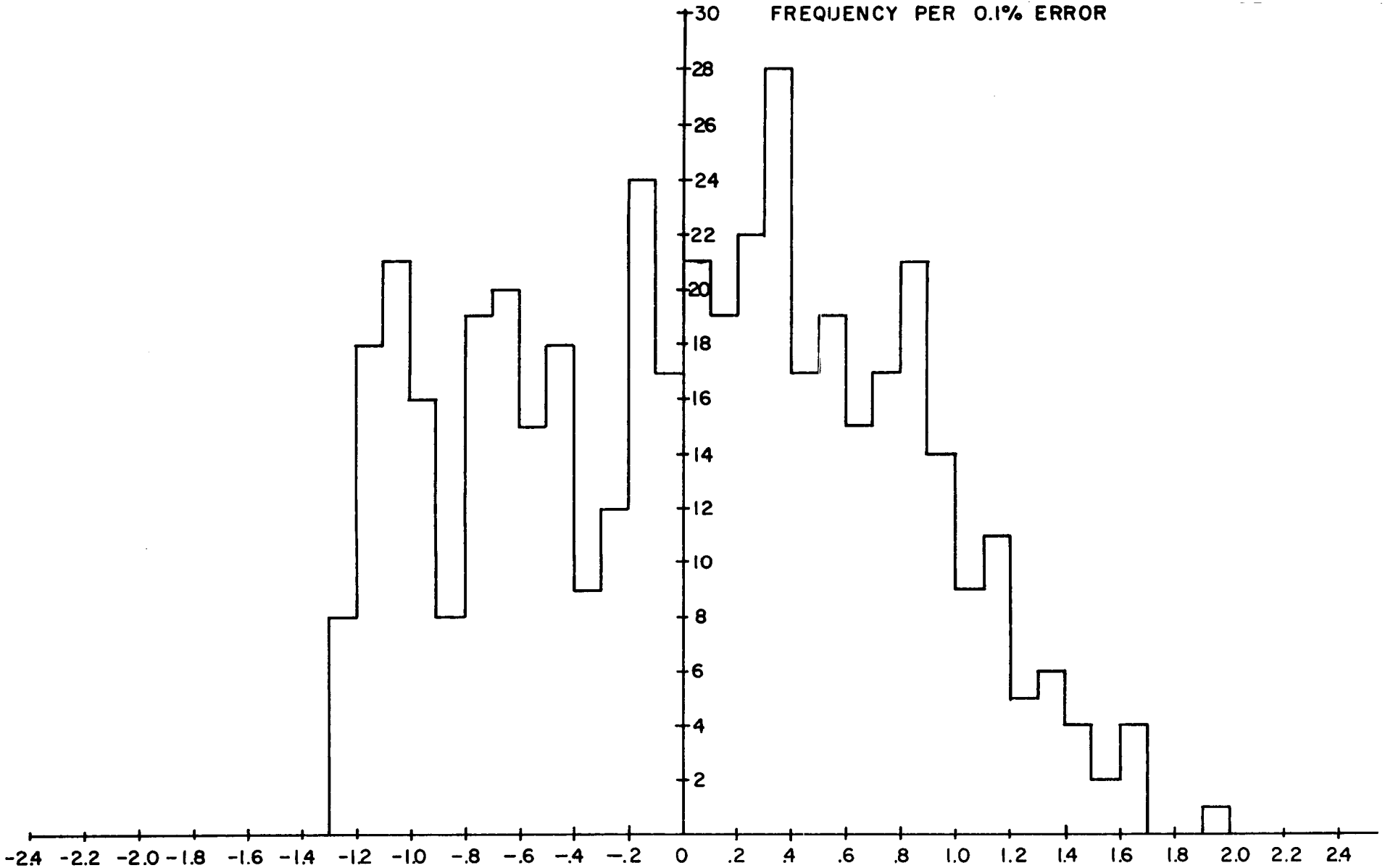

FREQUENCY OF ERROR (PER 0.1% ERROR INCREMENT) FOR OPTIMAL ARRAY OF FIFTEEN SAMPLING LOCATIONS, DATA FOR 440 RANDOMLY ORIENTED SPHERES OF VOLUME 2% TO 40% OF TANK CAPACITY.

FIGURE B-9

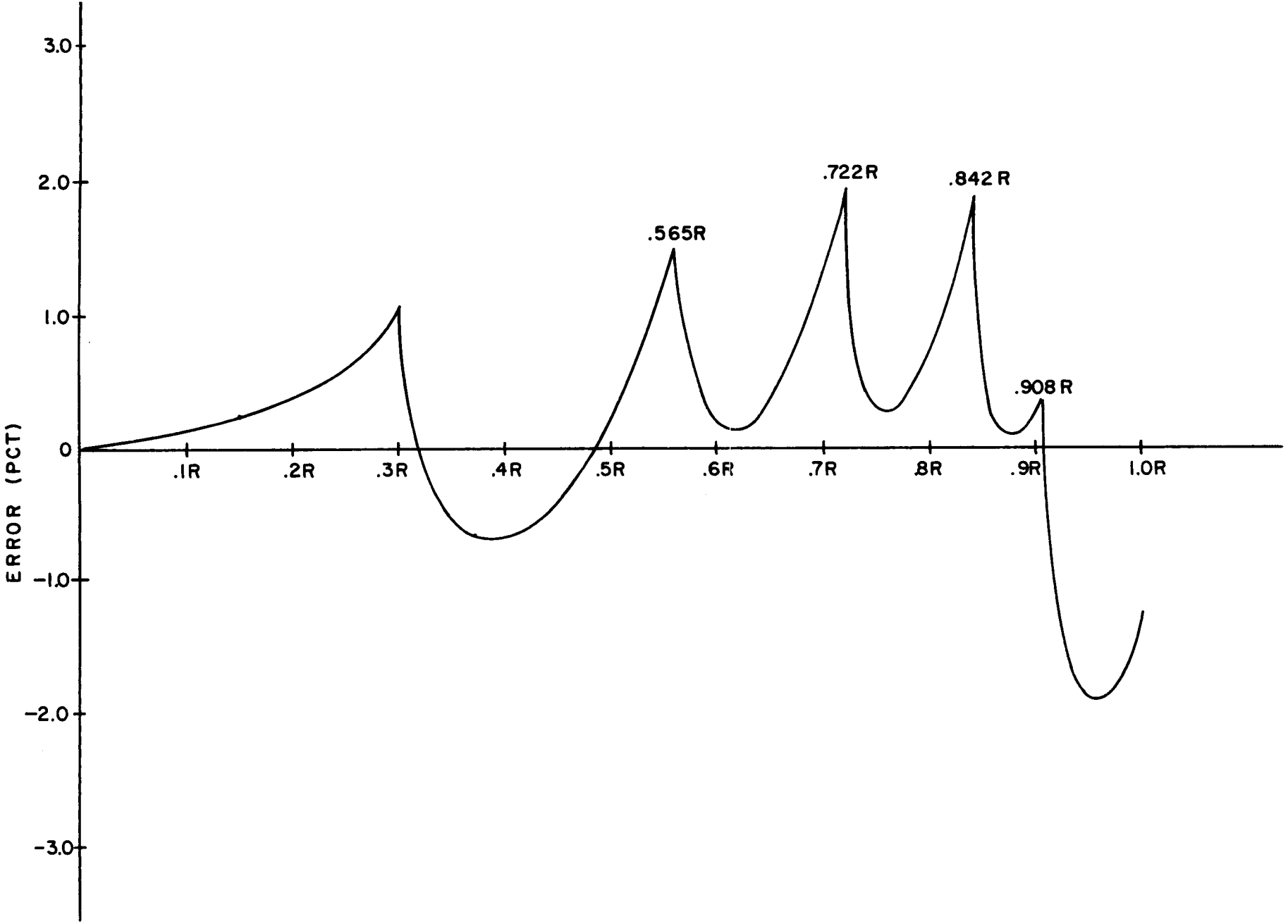

Measurement Error as a Function of Sphere Radius for Centrally Located Bubble in Optimal Array of Fifteen Sampling Locations.

Figure B-10

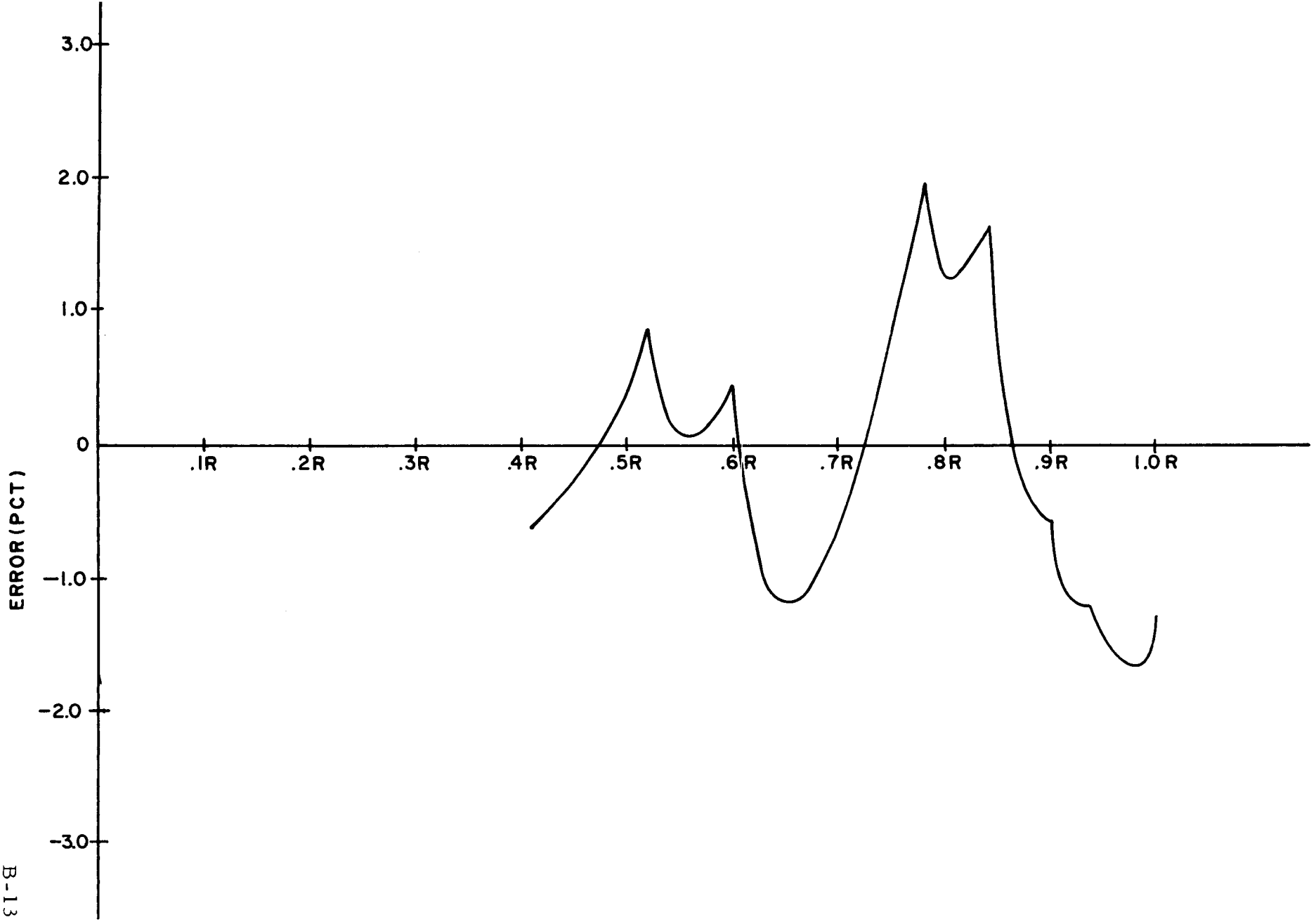

Measurement Error as a Function of Sphere Radius for Tangent Bubble in Optimal Array of Fifteen Sampling Locations.

Figure B-11

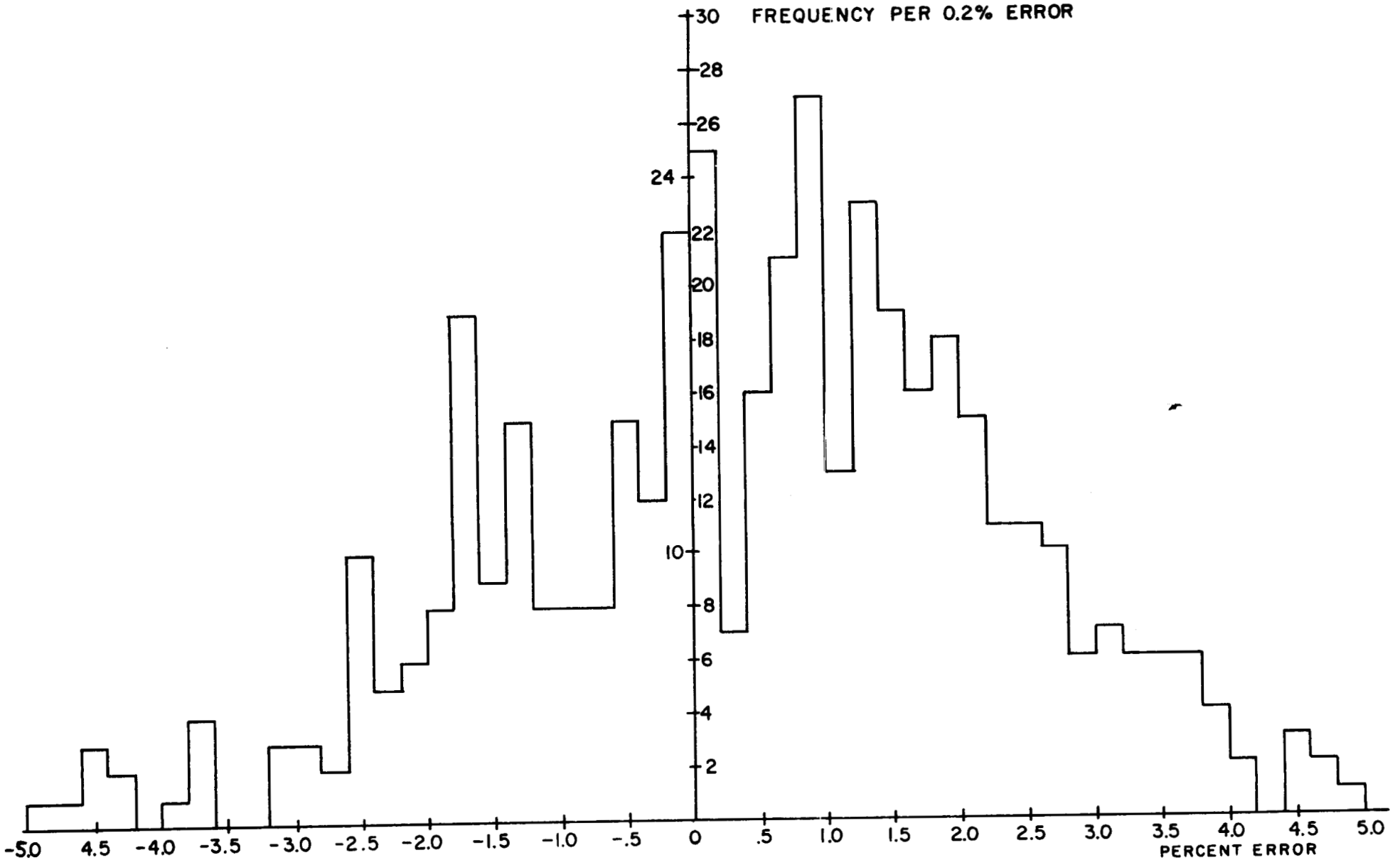

FREQUENCY OF ERROR (PER 0.2% ERROR INCREMENT) FOR ARRAY OF FIFTEEN SAMPLING LOCATIONS PERPENDICULAR TO THE TANK AXIS, DATA FOR 440 RANDOMLY ORIENTED SPHERES OF VOLUME 2% TO 40% OF TANK CAPACITY.

FIGURE B-12

APPENDIX C

Effects of Crosstalk on Uniqueness

For sampling techniques in which radiation from a single source impinges on a number of detectors, it is difficult to establish source-detector positions such that a function of the detector outputs is independent of the position of the propellant within the tank. The magnitude of crosstalk errors encountered in a half filled tank with a single flat liquid-vapor interface is indicated by a typical example. The crosstalk problem is illustrated by the simplified situation of Figure C-1 in which the liquid surface of a tank half filled with LH_2 is perpendicular to or slanted with respect to the tank axis. (The numbers used in the example are approximations.) The count rate at a detector due to a single source is

$$N = N_o e^{-x/\lambda}$$

Typically (for LH_2), $N_o = 10^5$ cps, $\lambda = 3$ feet; the vapor has negligible absorption. For the perpendicular orientation of the liquid surface, the count rate at detector A is due to photons arriving from both of the sources indicated in Figure 1:

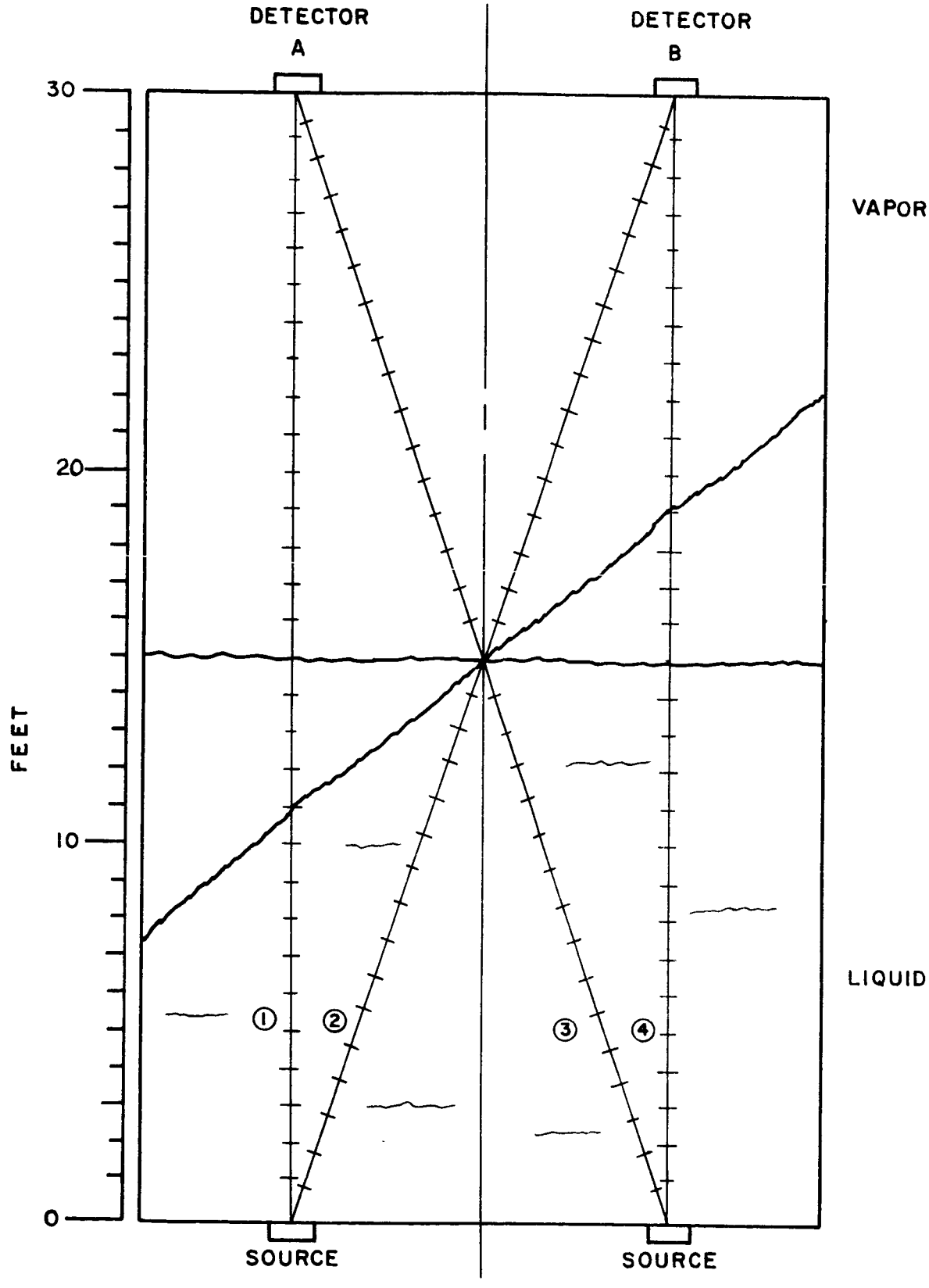

EFFECTS OF CROSS TALK ON MASS MEASUREMENT

FIGURE C-1

$$N_A^{(P)} = N_1 + N_3 = 10^5 e^{-15/3} + 10^5 e^{-16/3}$$

$$= 10^5 (.0067 + .0048) \text{ cps}$$

$$= 1.15 \times 10^3 \text{ cps.}$$

From symmetry, the count rate at detector B is the same:

$$N_B^{(P)} = 1.15 \times 10^3 \text{ cps.}$$

For the slanted orientation of the liquid surface, the count rate at detector A is

$$N_A^{(S)} = N_1 + N_3 = 10^5 (c^{-11/3} + e^{-16/3})$$

$$= 10^5 (.0256 + .0048) \text{ cps}$$

$$= 3.04 \times 10^3 \text{ cps.}$$

The count rate at detector B is

$$N_B^{(S)} = N_2 + N_4 = 10^5 (e^{-16/3} + e^{-19/3})$$

$$= 10^5 (.0048 + .0018) \text{ cps}$$

$$= 0.66 \times 10^3 \text{ cps.}$$

Clearly, the sums of the count rates are not the same for the two surface orientations. Furthermore, neither the logarithms of the sums nor the sums of the logarithms agree:

Sums: $N_A^{(P)} + N_B^{(P)} = (1.15 + 1.15) \times 10^3 \text{ cps} = 2.30 \times 10^3 \text{ cps}$

$N_A^{(S)} + N_B^{(S)} = (3.04 + 0.66) \times 10^3 \text{ cps} = 3.70 \times 10^3 \text{ cps}$

Logarithms of Sums:

$$\log_{10}\left[N_A^{(P)} + N_B^{(P)}\right] = \log_{10} 2.30 \times 10^3 = 3.36$$

$$\log_{10}\left[N_A^{(S)} + N_B^{(S)}\right] = \log_{10} 3.70 \times 10^3 = 3.57$$

Sums of Logarithms:

$$\log_{10} N_A^{(P)} + \log_{10} N_B^{(S)} = \log_{10} 1.15 \times 10^3 + \log_{10} 1.15 \times 10^3$$

$$= 3.062 + 3.062 = 6.12$$

$$\log_{10} N_A^{(S)} + \log_{10} N_B^{(S)} = \log_{10} 3.04 \times 10^3 + \log_{10} 6.6 \times 10^2$$

$$= 3.484 + 2.820 = 6.30 .$$

Indeed, it is doubtful that any function of the count rates can produce a unique answer for all degrees of slant of the liquid surface when a practical number of sources and detectors is employed.

In contrast, if crosstalk in the system is eliminated (as in a transmission system through collimation of both source and detector so that crosstalk beams 2 and 3 in the example do not exist), the situation is satisfactory since a function of the count rate (sum of the logarithms) is a unique function of the mass, independent of surface orientation. For the perpendicular orientation of the liquid surface, the count rate at detector A is

$$N_A^{(P)} = 10^5 e^{-15/3} \text{ cps}$$

$$= 0.67 \times 10^3 \text{ cps} .$$

From symmetry, the count rate at detector B is the same.

$$N_B^{(P)} = 0.67 \times 10^3 \text{ cps} .$$

For the slanted orientation of the liquid surface, the count rate at detector A is

$$N_A^{(\grave{S})} = 10^5 e^{-11/3} \text{ cps}$$

$$= 2.56 \times 10^3 \text{ cps} .$$

The count rate at detector B is

$$N_B^{(S)} = 10^5 e^{-19/3} \text{ cps}$$

$$= 0.18 \times 10^3 \text{ cps} .$$

The sum of the logarithms is identical:

$$\log_{10} N_A^{(P)} + \log_{10} N_B^{(P)} = \log_{10} 6.7 \times 10^2 + \log_{10} 6.7 \times 10^2$$

$$= 2.83 + 2.83$$

$$= 5.66$$

$$\log_{10} N_A^{(S)} + \log_{10} N_B^{(S)} = \log_{10} 2.56 \times 10^3 + \log_{10} 1.8 \times 10^2$$

$$= 3.41 + 2.25$$

$$= 5.66 .$$

Therefore, crosstalk introduces measurement technique errors on the order of 2 to 5% of tank capacity, errors which are eliminated in transmission systems through collimation and energy discrimination.

APPENDIX D

Some Features of Similitude Scaling

A number of types of scaling exist, but the type of most importance with regard to the analysis of large systems through the behavior of scale models is called similitude scaling. All pertinent features of large system behavior are preserved through similitude scaling, all features except geometrical features, which are uniformly reduced by the scaling factor R_{model}/R_{system}, where R is a characteristic dimension of the model and the actual system.

For radiation absorption simulations, the pertinent features which must be preserved are the count information at the tank surface, this information comprising count rate, photon energy, and photon direction information. The count rate at a detector is

$$N = \frac{S \eta A}{4 \pi R^2} e^{-x/\lambda} B(x/\lambda) \qquad \text{(D-1)}$$

where S is the source strength in emissions/second, η is the detector efficiency, A is the detector area, R is the distance from the source to the detector, λ is the characteristic length of radiation in the medium, $B(x/\lambda)$ is the geometry-dependent build-up factor, and x is the thickness of absorber through which the radiation is directed. For a circular detector of radius r, Equation (D-1) can be written

$$N = \frac{S \eta}{4} \left(\frac{r}{R}\right)^2 e^{-x/\lambda} B(x/\lambda) \qquad \text{(D-2)}$$

Equation (D-2) is written such that three of the factors, the radius ratio (r/R), the attenuation factor $e^{-x/\lambda}$, and the build-up factor $B(x/\lambda)$, are in dimensionless form. Hence, a similitude scale model of a large system can be achieved by a small system in which the dimensionless factors have the same values as in the large system. Since the radii r and R can be written as constant multipliers of the characteristic length ($r = k_1 \lambda$, $R = k_2 \lambda$), the similitude model is completely determined by the ratio of characteristic lengths:

$$r_{model} = \frac{\lambda_{model}}{\lambda_{system}} r_{system} ,$$

$$R_{model} = \frac{\lambda_{model}}{\lambda_{system}} r_{system} , \text{ etc.}$$

For liquid systems, the characteristic length is easily changed by changing materials. The difficulty with scaling λ by changing materials is the fact that λ is energy-dependent. Thus, if a material is chosen to scale λ at one photon energy, it may not represent the desired scaled value for λ at another energy. Even for a monoenergetic source, this is a problem because of the diverse photon energies in the build-up. The reason that changing materials does not scale λ correctly at all energies is that the scattering cross sections of dissimilar atoms differ from each other by more than a simple scale factor.

There is, however, one very important exception to the scaling problem, namely, Compton scattering. When the binding energy of electrons

is small compared to the impinging photon energy, then the Compton scattering of materials depends on their electron density but is otherwise independent of their composition. Thus, λ scales correctly for all energies when Compton scattering dominates. This is true in LH_2 at all energies above 1 keV (and even below) and for LOX above about 28 keV. This includes virtually the whole range of photon energies which are of significant effect on detector outputs, particularly if there is any tank-wall shielding of detectors.

If it were possible to photograph the actual tracks of the photons as they scatter their way through the propellant in the large system, then the tracks in the similitude model would look just like a reduced photograph of this original. Since angles are preserved under this transformation, and since in Compton scattering, angle and energy are uniquely related for low atomic number materials, the actual energies as well as the paths of the multiple-scattered photons are correctly represented in the similitude model.

With a similitude model, one may practically and accurately take into account all the build-up spectral shifts and multiple-scattered radiations, and all the baffles and irregular geometry which are so hard to represent in a finite computer program. Digital computer programs are not easily extended to very many multiple scatterings in the case of large tanks nor to very complex tank shapes. The scale model is essentially an analog computer.

The scaling of metal baffles, tank walls, and other high-atomic number materials is more complex because here the photoelectric effect dominates over Compton scattering out to 50 keV (aluminum) or 90 keV (iron). Substituting other materials may give erroneous results in a model. Fortunately for scale modeling of space vehicles, these higher atomic number materials are also relatively heavy and, thus, are normally used as pipe walls, tank walls, or other thin-walled shapes rather than large solid three-dimensional bodies. Thus, if one scales the other dimensions of these heavy materials while keeping their thin dimension constant, the correct scattering intensity at all energies outside the structures is preserved. In other words, one scales down tank diameter but not thickness of metal used in tank wall, a pipe diameter but not pipe wall thickness, baffle size but not the gauge of the metal used to make the baffle.

The only error introduced by this two-dimensional scaling comes from the fact that the geometry of the model is no longer a photographically reduced model of the original--certain metal items seem to be of proportionately heavier gauge. However, since the correct scattering intensity and transmission is maintained, the representation is very good for reasonable scale factors. Of course, if the scale is so reduced that a sheet becomes a bar, then the geometry of the model is no longer a good representation of the original. For scale factors of interest, say linear dimensions reduced by a factor of five, this geometric distortion should be negligible. The scattering and transmission intensity is preserved by

this approach and that is the important factor. Also, great reduction in size is not desired since even the scale model must be large compared to the physical size of the sources and detectors used in the experiment--in order to observe intensities at different points on the model separately.

Actually, there is no need in the presently used technique to consider similitude scaling for build-up and extraneous scatter from structures since these contributions are removed by collimation and energy discrimination. Thus, these terms in the expressions are effectively deleted.

APPENDIX E

Calculation of Mass from Raw Experimental Data

Throughout the experimental program, emphasis was devoted to studies of the optimal array of twelve sampling locations. A total of 16 individual cases were examined for the array of twelve, various-sized foam voids being located randomly within the cylindrical and hemispherically-capped cylindrical tanks. As a result of the number of cases studied for the array of twelve, reasonable statistical confidence can be placed in the results.

Additional cases were studied for non-optimal arrays of seven, ten, and fifteen sampling locations. The studies were exploratory and comparative in nature. Since relatively few cases were studied for these individual arrays, a low statistical confidence level is associated with the results. A summary of experimental results is given in Table E-1; reasonable statistical confidence exists only for the optimal array of twelve.

Table E-1. Summary of Experimental Results

Number of Sampling Locations	Number of Cases Investigated	Average Absolute System Error	Maximum Absolute System Error
7	7	3.6%	7.8%
10	4	4.7	7.7
12*	16	1.3	2.7
15	1	1.5	1.5

*Optimal array of twelve sampling locations, as given by Table 4 and Figure 14c.

A sample calculation is presented in which the measured mass and the measurement system error are computed from the raw data. The calculation is given for Experiment Number 3 (Table 7) for a cylindrical tank of radius 18 inches. The coordinates of the twelve sampling locations were determined from Table 4 (cylindrical coordinates) and are presented in Table E-2 in rectangular coordinate form. The count rate at each sampling location was correlated with a thickness of absorbing medium through the experimental calibration curve presented in Figure E-1. The total mass in the tank is computed by considering that the thickness sensed at each sampling location represents that of an associated cylinder with one-twelfth the cross sectional area of the tank. Expressed mathematically,

$$M_{meas} = \frac{A}{12} \rho_{H_2O} \sum_{i=1}^{12} \ell_i$$

where A is the cross sectional area of the tank, ρ_{H_2O} is the water density, and the twelve values of ℓ_i are determined from the calibration curve. The photon counts detected after one minute of counting at each location and the values of ℓ_i determined for each detector are presented in Table E-3. Hence, the measured mass is

$$M_{meas} = (1/12)(6.55 \times 10^3 cm^2)(1\ gm/cm^3)(742.5\ cm)$$
$$= 4.07 \times 10^5\ gm\ .$$

The actual mass in the tank was determined as the sum of the mass of water remaining in the tank after the foam sphere was removed and the mass of

Table E-2. Experimental Sampling Locations for 18" Radius Cylindrical Tank

Sampling Location	X (inches)	Y (inches)
1	6 1/4	0
2	- 3 1/8	5 3/8
3	- 3 1/8	- 5 3/8
4	5 1/2	9 1/2
5	- 11	0
6	5 1/2	- 9 1/2
7	13	6 1/16
8	-11 3/4	8 1/4
9	- 1 1/4	-14 5/16
10	0	16 3/8
11	-14 3/16	- 8 3/16
12	14 3/16	- 8 3/16

X = 0, Y = 0 at center of tank

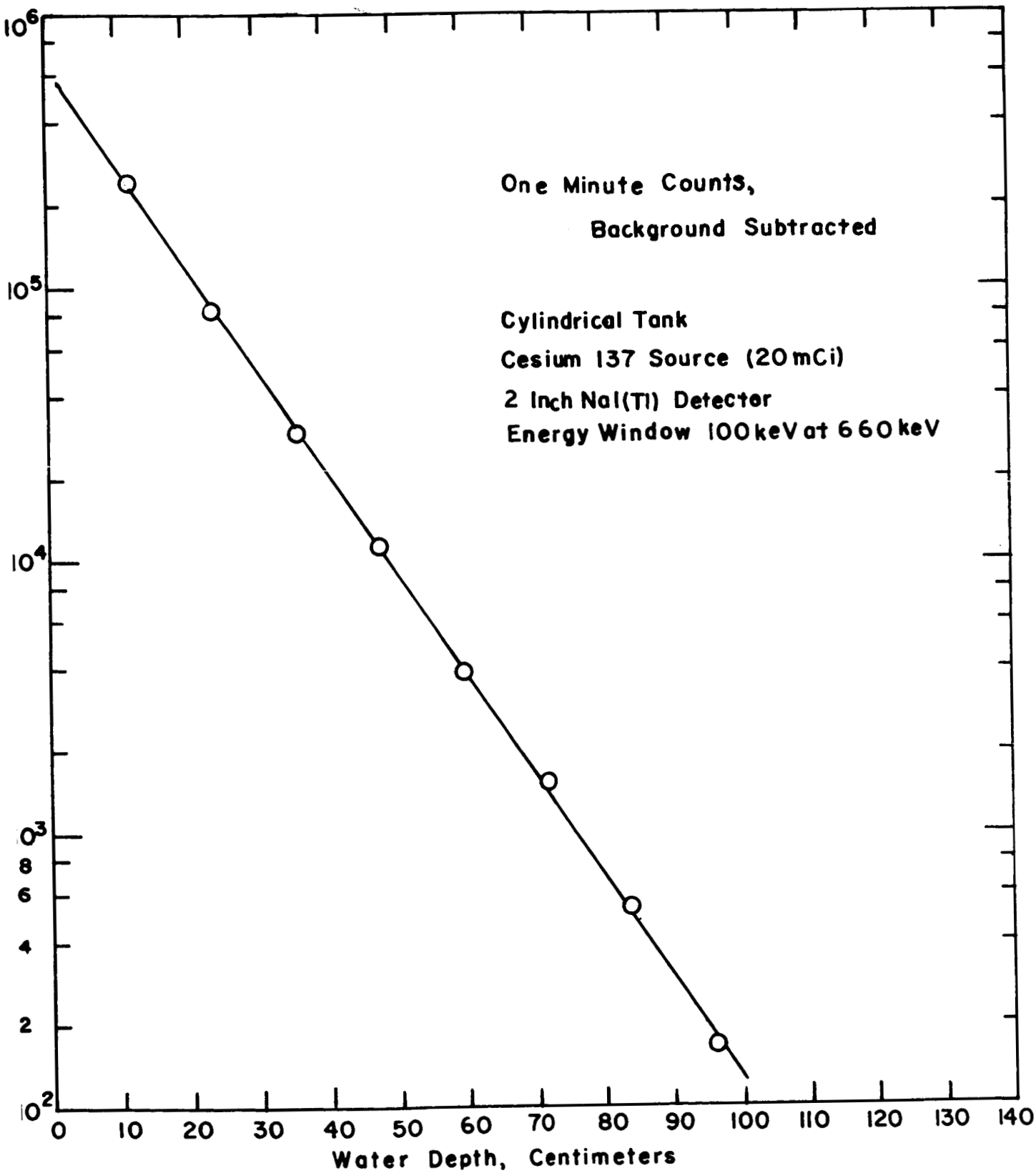

Figure E-1 Calibration Curve. Count Rate as a Function of Water Depth

Table E-3. Raw Count Data for Experiment #3

Sampling Location	Count	Equivalent Absorber Thickness (cm)
1	45, 593	31.5
2	24, 755	38.5
3	48, 800	30.5
4	1, 573	71.0
5	1, 527	71.0
6	1, 166	74.0
7	1, 489	71.0
8	1, 501	71.0
9	1, 441	71.5
10	1, 466	71.5
11	1, 510	71.0
12	1, 623	70.0
	Sum	742.5 cm

the sphere. The wet foam sphere weighed 8 pounds 6 ounces after the test, and the tank contained 23 7/8 inches of water with the sphere removed. Hence, the actual mass within the tank was

$$M_{act} = M_{H_2O} + M_{Foam}$$

$$= (23.87 \text{ in})(2.54 \text{ cm/in})(6.55 \times 10^3 \text{ cm}^2)$$

$$+ (8.37 \text{ lb})(454 \text{ gm/lb})$$

$$= 3.97 \times 10^5 \text{ gm} + .038 \times 10^5 \text{ gm}$$

$$= 4.01 \times 10^5 \text{ gm}.$$

The system error percentage is

$$E = \frac{M_{meas} - M_{act}}{M_{act}} \times 100$$

$$= \frac{4.07 - 4.01}{4.01} \times 100 = 1.5\% .$$

Similar techniques for comparing measured mass with actual mass were employed for all the arrays, foam voids, and tanks that were used.

REFERENCES

1. Reynolds, W. C. and H. M. Satterlee, "Liquid Propellant Behavior at Low and Zero G", The Dynamic Behavior of Liquids in Moving Containers, edited by H. N. Abramson, NASA SP-106, p. 387, (1966).

2. Neiner, J. J., "The Effect of Zero Gravity on Fluid Behavior and System Design", Wright Air Development Center Technical Note 59-149, Wright-Patterson Air Force Base, Ohio, (1959).

3. Evans, R. D., The Atomic Nucleus, McGraw-Hill, New York, Chapter 21, (1955).

4. Leighton, R. B., Principles of Modern Physics, McGraw-Hill, New York, Chapter 12, (1959).

5. Price, B. T., C. C. Horton, and K. T. Spinney, Radiation Shielding, Pergamon Press, New York, p. 50, (1957).

6. Data from "Harshaw Scintillation Phosphors", catalog of Harshaw Chemical Company, Cleveland, Ohio, p. 19, (1966).

* * * * *

Blincow, D. W., K. V. Pearson, and R. A. Ray, "Nucleonic Fuel Gauging Systems for Spacecraft", Radioisotopes for Aerospace, edited by J. C. Dempsey and P. Polishuk, Vol. 2, p. 132, Plenum Press, New York, (1966).

Bradley, C. M., M. A. Dewar, and J. F. Hauck, "Design and Performance Evaluation of Aircraft Nucleonic Fuel Gauging System by Computer Techniques", Radioisotopes for Aerospace, edited by J. C. Dempsey and P. Polishuk, Vol. 2, p. 228, Plenum Press, New York, (1966).

"Large Storage Tank Mass Determination Study", Final Report on NASA Contract NAS8-11311, performed by Giannini Controls Corp., Duante, California, (1966).